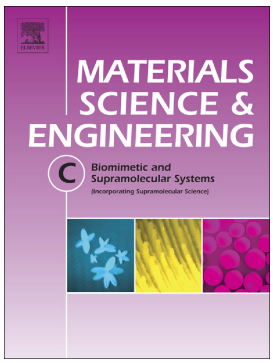


# Recent advances in the modification of carbon-based quantum dots for biomedical applications

Amirhossein Alaghmandfard, Omid Sedighi, Nima Tabatabaei Rezaei, Amir Abbas Abedini, Adrine Malek Khachatourian, Muhammet S. Toprak, Alexander Seifalian

PII: S0928-4931(20)33675-4

DOI: https://doi.org/10.1016/j.msec.2020.111756

Reference: MSC 111756

To appear in: *Materials Science & Engineering C*

Received date: 20 September 2020

Revised date: 18 November 2020

Accepted date: 21 November 2020

Please cite this article as: A. Alaghmandfard, O. Sedighi, N.T. Rezaei, et al., Recent advances in the modification of carbon-based quantum dots for biomedical applications, *Materials Science & Engineering C* (2020), https://doi.org/10.1016/j.msec.2020.111756

# Recent advances in the modification of carbon-based quantum dots for biomedical applications

Amirhossein Alaghmandfard[1*], Omid Sedighi[1*], Nima Tabatabaei Rezaei[1*], Amir Abbas Abedini[1*], Adrine Malek Khachatourian[1§], Muhammet S. Toprak[2], Alexander Seifalian[3,4§]

1. Department of Materials Science and Engineering, Sharif University of Technology, Tehran, Iran
2. Department of Applied Physics, KTH-Royal Institute of Technology, SE10691 Stockholm, Sweden
3. Centre for Nanotechnology & Regenerative Medicine, UCL Division of Surgery & Interventional Science, University College London, London, UK
4. Royal Free Hampstead NHS Trust Hospital, London, UK

* Authors contributed equally at this work.

§ Corresponding authors: Adrine Malek Khachatourian; e-mail: khachatourian@sharif.edu, Alexander Seifalian; email: a.seifalian@UanoRegMed.com



## Abstract

Carbon-based quantum dots (CDs) are mainly divided into two sub-groups; carbon quantum dots (CQDs) and graphene quantum dots (GQDs), which exhibit outstanding photoluminescence (PL) properties, low toxicity, superior biocompatibility and facile functionalization. Regarding these features, they have been promising candidates for biomedical science and engineering applications. In this work, we reviewed the efforts made to modify these zero-dimensional nano-materials to obtain the best properties for bio-imaging, drug and gene delivery, cancer therapy, and bio-sensor applications. Five main surface modification techniques with outstanding results are investigated, including doping, surface functionalization, polymer capping, nano-composite and core-shell structures, and the drawbacks and challenges in each of these methods are discussed.

**Keywords:** carbon-based quantum dots, surface modification, biomedical application

# Contents

# 1. Introduction

Nowadays, human beings are facing some new emerging diseases like various kinds of cancer that are extremely difficult to cure. At the first step, distinguishing tumor cells from normal cells has a key role in the diagnosis and treatment of cancer. Targeted cancer therapies are less harmful to healthy cells and reduce side effects, which was the main restriction for utilizing chemotherapy as principal therapeutic way for most cancers.

Nanomaterials have been developed and used in biomedical applications such as imaging, drug delivery, gene therapy, sensing and photothermal therapy (PTT) [1, 2]. The primary-used nanomaterials that were utilized in this field were gold nanoparticles (Au NPs) for imaging and PTT [3], magnetic NPs (MNPs) for imaging and sensing [4, 5], polymeric NPs [6] and liposomes [7] for drug delivery, and so on. Semiconductor quantum dots (QDs) known as theranostics invented in 1980 were also one of the modern types of nanomaterials that showed appropriate properties for diagnosis and treatment. Their optical and electronic properties could be easily tuned through controlling size and distribution of QDs [8]. Their advantages over conventional materials like organic dyes are high quantum yield (QY), superior photostability, and stable photoluminescence (PL) turn them into a promising material for biomedical applications. However, semiconductor QDs have some drawbacks such as toxicity issues since some of them are composed of toxic elements including cadmium, arsenic, selenium, and mercury. Therefore, these QDs are not subsumed under the category of biodegradable nor environment friendly materials [6, 7]. As a result, scientists tried to replace semiconductor QDs with other nanomaterials that could overcome these shortcomings.

In recent years, carbon-based quantum dots (CDs) that are mainly divided into two subgroups, as carbon quantum dots (CQDs) and graphene quantum dots (GQDs) gained extensive considerations in scientific areas [9]. CQDs were first reported in 2004 by purification of single-walled carbon nanotubes [10]. Possessing superior properties such as low toxicity, large surface area, high photostability, high resistance to photobleaching, and easy modification, compared to traditional nanomaterials, makes them promising materials for biomedical applications [1, 2, 11, 12].

Although CDs have favorable properties, making them proper nanomaterials for biomedical applications, scientists are extensively investigating the possible methods to improve their

properties. Several modification techniques can be applied for this goal which is the main focus of this review and to the best of our knowledge there are few reports in the literature with this perspective. In this review, first, we explain synthesis methods and structure of these unique NPs. Then we take a look at their application in biomedical engineering. In the end, we categorize some important ways of their surface modification including doping, surface functionalization, polymer capping, making composite materials, and core-shell structures, based on the latest researches and discuss the drawbacks and challenges in each method.

## 2. Synthesis methods

CQDs and GQDs synthesis techniques are classified into two main groups as "top-down" and "bottom-up" [13-17]. Through the former one, QDs are prepared by breaking down carbonaceous materials (such as carbon nanotubes, graphene oxide (GO), graphene, graphite powder, coal, etc.) through physical, chemical or electrochemical methods [2, 13, 15-19]. The later techniques lie in chemical synthesis and employ pyrolysis and some chemical reactions in order to carburize small organic molecules [12, 13, 15-18]. Utilizing harsh conditions like combustion, thermal treatment, chemical carbonization, and alkali/acid-assisted oxidation reactions for initiating the process is necessary in these methods [16]. Each of these methods has some pros and cons which can be chosen regarding to the application. Taken together, the synthesis of CDs encounters three main obstacles, which are *i*) agglomeration and aggregation during carbonization, *ii*) controlling size distribution, and *iii*) surface properties that are precarious for solubility and specific applications [1, 13]. These issues can be addressed by some tuning within the synthesis process or some post-treatments [14]. Herein, we introduce some of the most commonly used methods in detail and Figure 1 briefly summarizes the advantages and disadvantages of these synthesis methods.

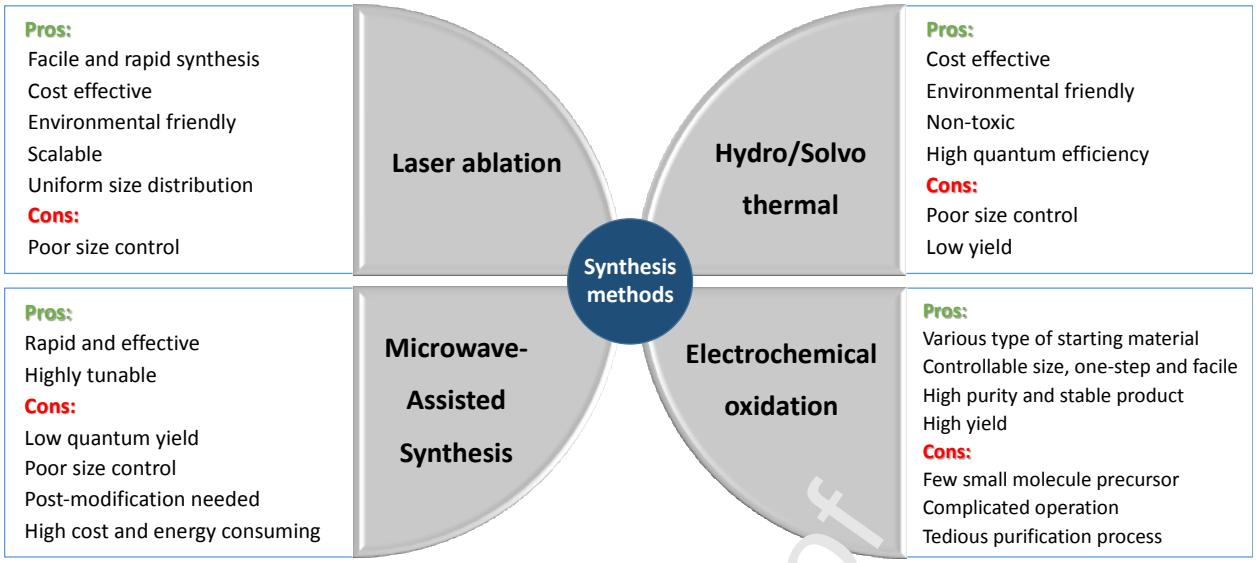


Figure 1. Pros and cons of four main synthesis methods of CDs.

## 2.1. Hydro/Solvothermal

Hydrothermal carbonization (HTC) is a facile technique, extensively used to fabricate carbon-based nanomaterials including CDs and GQDs. It is a cheap, environmentally friendly and non-toxic method [12-14, 20], which is performed by using various precursors such as glucose [21, 22], sucrose [22], maltol [22], chitosan [23, 24], citric acid [25, 26] and also banana juice [27] and orange juice [28]. Nevertheless, there is a poor control over the size of the particles in this method [14]. In general, a water solution of an organic precursor is sealed in a hydrothermal reactor and is reacted under high-temperature [13, 14, 18, 20]. Reaction temperature and time are the most significant parameters, which straightly influence the optical properties and luminescence efficiency of carbon-based NPs [18]. Pan et al. [29] introduced the synthesis of fluorescent GQDs through hydrothermal route for the first time. They used thermally reduced GO (rGO) as the precursor and then treated them by an oxidizing agent like $HNO_3$ in $H_2SO_4$ solution under ultrasonication to induce epoxy groups on the carbon layers as cleavage sites. At last, GQDs were obtained by chemically cutting and deoxidation under hydrothermal condition at 200 °C for 10 h in weakly alkaline medium (pH=8) [15, 29]. Figure 2 represents the mechanism of hydrothermal cutting of rGO to GQDs.

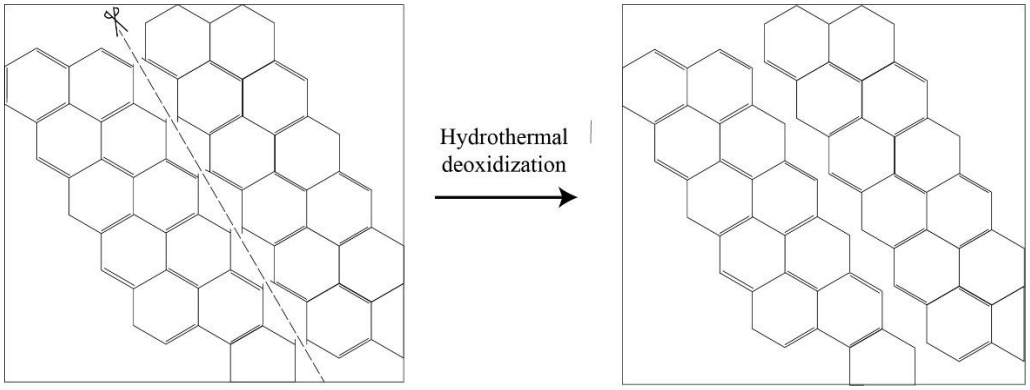


Figure 2. Mechanism for the hydrothermal cutting of rGOs into GQDs: a mixed epoxy chain composed of epoxy and carbonyl pair groups (left) is converted into a complete cut (right) under the hydrothermal treatment [29]. Copyright 2010 Wiley.

In the solvothermal method, other organic solvents with higher boiling points (i.e., benzene, DMF, and DMSO) are used instead of water. Typically, carbon sources are solved in such solvents, then subjected to heat treatment at elevated temperatures following by extraction and concentration [20, 30].

### 2.2. Electrochemical oxidation

The electrochemical approach is one of the widely used methods to obtain CQDs and GQDs by utilizing different bulk carbon materials such as carbon fiber, graphene and graphite as precursor [13, 20]. Generally, two carbon-based electrodes are immersed in a water-based electrolyte. By applying redox potential, water electrolysis and $H^{\bullet}$ and $OH^{\bullet}$ radicals initiate at the edges and the defects of electrodes act as electrochemical scissors to form CQDs and GQDs [12, 15, 31, 32], Low-cost, mass production, absence of highly hazardous chemicals and ease of operation are some advantages of this technique [1, 12, 13, 20, 31]. Although size control of CDs was difficult in traditional electrochemical synthesis, further separation through filtration or chromatography was inevitable in order to achieve a narrow size distribution of CDs [1, 19, 33-35]. However, it is also possible to produce monodispersed carbon-based NPs through this method by tuning parameters like the applied potential or starting material. Bao et al. [35] synthesized luminescent CDs with narrow size distribution by tuning the applied potentials, which eliminates need for further separation. They showed that the voltage enhancement results in CDs with a narrow size distribution.

In another work, Deng et al. [34] prepared monodispersed CDs directly from low-molecular-weight alcohols as the precursor of the electrochemical method, for the first time. The only major disadvantage of this method is the existence of many oxygen-containing groups on the

surface of dots due to electrochemical oxidation, which causes further tedious purification process [1, 18].

### 2.3. Laser ablation

Laser ablation is one of the most popular synthesis techniques of carbon-derived nanomaterials, using laser as an energy source in order to ablate solid target materials. During this process, a significant amount of energy is concentrated at a particular point on a solid surface to evaporate the material. Due to the fact that the purity of the final product is basically depended on the purity of target and ambient media (either liquid or vapor), highly pure particles can be produced by using this method. Cao et al. [36-38] used laser ablation to prepare CQDs. The laser ablation of carbon target was carried out in the presence of water vapor and a carrier gas (Ar) at 900 °C and 75 kPa. After refluxing in $HNO_3$ for 12 hours and surface passivation by organic polymers, CQDs with bright luminescence were obtained. Hu et al. [39] found that tuning the laser pulse-width alters the nucleation and growth processes and results in different size distribution. They demonstrated long-pulse-width laser to be a better option for the synthesis of various nanostructures. They observed that when the laser pulse width increased, CDs' size and crystalline grains increased.

It was reported that CQDs with different surface modifications and tunable light emission could be obtained by selecting appropriate solvents [40]. Santiago et al. [41] developed a method to dope nitrogen (N) into GQDs via pulsed laser ablation, which augmented the PL intensity of GQDs. One of the challenges in this method is the amount of energy, which is lost via scattering and absorption, as well as its non-uniform distribution on the surface of samples. It was observed that by using continuous flow jet, CQDs with the smaller size would be produced and this strategy minimized the losses of energy [42].

### 2.4. Microwave-Assisted Synthesis

Varieties of approaches adapted to synthesize CDs are mostly time-consuming and require sophisticated apparatus [43-45]. Therefore, it is essential to develop a simple, rapid, and selective method with homogeneous heating, which can be used for large-scale synthesis. Microwave (MW)-assisted method fulfills all these goals, allowing rapid production as well as producing in large quantities. One of the limitations of using this method is the small penetration depth of MW radiation in some substances, while carbon-based materials could easily interact with MW radiation, which causes fast heating rate as well as localized heating

[46]. Zhu et al. [47] firstly presented an economical, and facile MW pyrolysis approach, which was used to synthesize bright, and stable luminescent CQDs. Later on, many researches have attempted to improve this method. For instance, Li et al. [48] developed an ultra-fast strategy that produces GQDs with high QYs (up to 35%) in just three minutes under MW irradiation. Moreover, Nguyen et al. [49] introduced a method of fabricating N-doped GQDs (N-GQDs) using MW combined with hydrothermal processes. They successfully prepared GQDs and N-GQDs from citric acid by hydrothermal pyrolysis with the help of MW in a reducing medium.

## 3. Structure

There is a wide range of CDs grounded in the structure from fully amorphous to crystalline. Their structure shaped by $sp^2$ and $sp^3$ carbons and could be turbostratic (where basal planes have slipped out of alignment) or graphitic [50, 51]. The structure depends on the method of synthesis and the carbon source [51] Figure 3(a-c) displays the different structures of these materials. The morphology of CQDs is mostly spherical and can be crystalline or amorphous [15]. GQDs are entirely crystalline and involve pieces of single or a few layered graphenes [52]. The edge of GQDs can be zigzag or armchair. Zigzag and armchair edges could be found in circular or elliptical GQDs, while the polygonal structure only has armchair edges (Figure 3(d-h)). In linear regions, the armchair edge is dominant, while in curved regions the armchair and zigzag edges are mixed. [53]. Additionally, some functional groups also exist on the surface of both CQDs and GQDs [54].

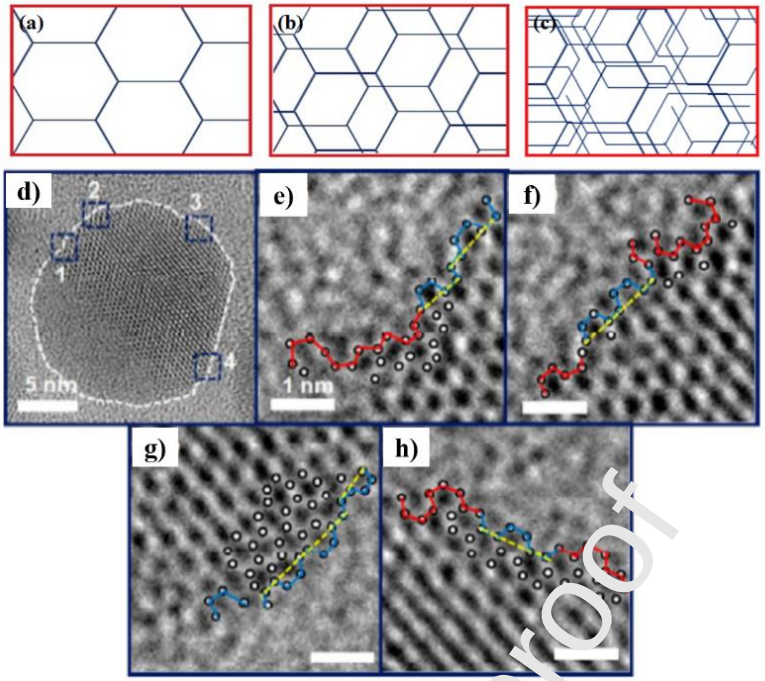


Figure 3. The structure of a) GQD, b) crystalline CQD, and c) amorphous CQD. d) HRTEM image of a typical GQD with partially curved and linear regions at the edge with mixed edges of zigzag and armchair at four different edge positions (1-4), (e-h) magnified HRTEM images corresponding to the four edge positions in d. Red and blue lines show zigzag and armchair edges, respectively. The scale bars in (e-h) are all 1 nm [53]. Copyright 2012 American Chemical Society.

# 4. Properties

## 4.1. Adsorption

Regarding the $\pi$-$\pi^*$ transition of the C=C bonds in the short-wavelength region, both CQDs and GQDs have potential in photon-harvesting. CQDs typically exhibit strong optical adsorption in the UV region (230-320 nm), with a tail extending into the visible region [15, 55]. However, GQDs might show some adsorption shoulders in the range of 270-390 nm [56]. This phenomenon is associated with the $\pi$-$\pi^*$ transition of the C=C bonds or the n-$\pi^*$ transition of C=O bonds. When it comes to comparison, CQDs are generally more efficient in the adsorption of long-wavelength. It is also reported that adsorption properties depend on various parameters like the size of CDs. Ritter et al. [57] monitored that the bandgap energy is proportional to the approximately $\frac{1}{L}$, where $L$ is GQDs average size.

## 4.2. Photoluminescence

The main appealing characteristic of both CQDs and GQDs is their tunable PL properties. Owing to the emissive traps on the surface of CDs, these NPs have low PL quantum yield (PL QY) (approximately <10%). In comparison, due to the layered structure and better

crystallinity of GQDs, they show higher QY. The exact PL mechanism is still unclear, but it can be derived from intrinsic state emission and defect state emission [58], which might be due to aromatic structures, emissive traps, quantum confinement effect (QCE), free zigzag sites, edge defects, and oxygen-containing groups [59-61]. The PL of CQDs and GQDs are affected by a number of parameters, including size, excitation wavelength, pH, solvent polarity, surface oxidation degree, surface functionalization, and heteroatom doping. Kim et al. [53] investigated the effect of GQDs size on the shape, absorption characteristics, and PL properties. Figure 4a, illustrates when the size of the GQDs increase from 5 nm to 35 nm, the GQDs shape changes from circular and elliptical with zigzag and armchair edges to hexagonal and parallelogram-types rectangular with mostly armchair edges. Figure 4b, illustrates by increasing the GQDs average size in the mentioned range, the absorption peak energy decreases from 6.2 eV to 4.6 eV, and this is related to the QCE. Moreover, it is observed that size of the GQDs also influences the PL spectra, owing to the presence of the oxygen-functional groups (OFGs) like C-O, C=O, and COOH. While increasing the size does not alter the OFGs amount on the GQDs surface, yet the negligible changes in the PL spectra can be observed. In some curves, the PL spectra peaks resolved into two PL bands, and this comes from the absence of the unique shape and size (Figure 4c). In the particular excitation wavelength, by increasing the GQDs size up to 17 nm, the PL peak energy decreases and this is attributed to the QCE. When GQDs size gets larger, the QCE no longer holds, and therefore, the PL peak energy increases (Figure 4d) [53].

PL are dependent on excitation wavelength and PL emission peak with a maximum intensity shifted to longer wavelengths when the excitation wavelength is altered to longer wavelengths [29, 60, 62]. Shen et al. [60] showed that for GQDs the strongest peak is detected at 360 nm when the excitation wavelength is altered from 300 nm to 470 nm, emitting bright blue PL.

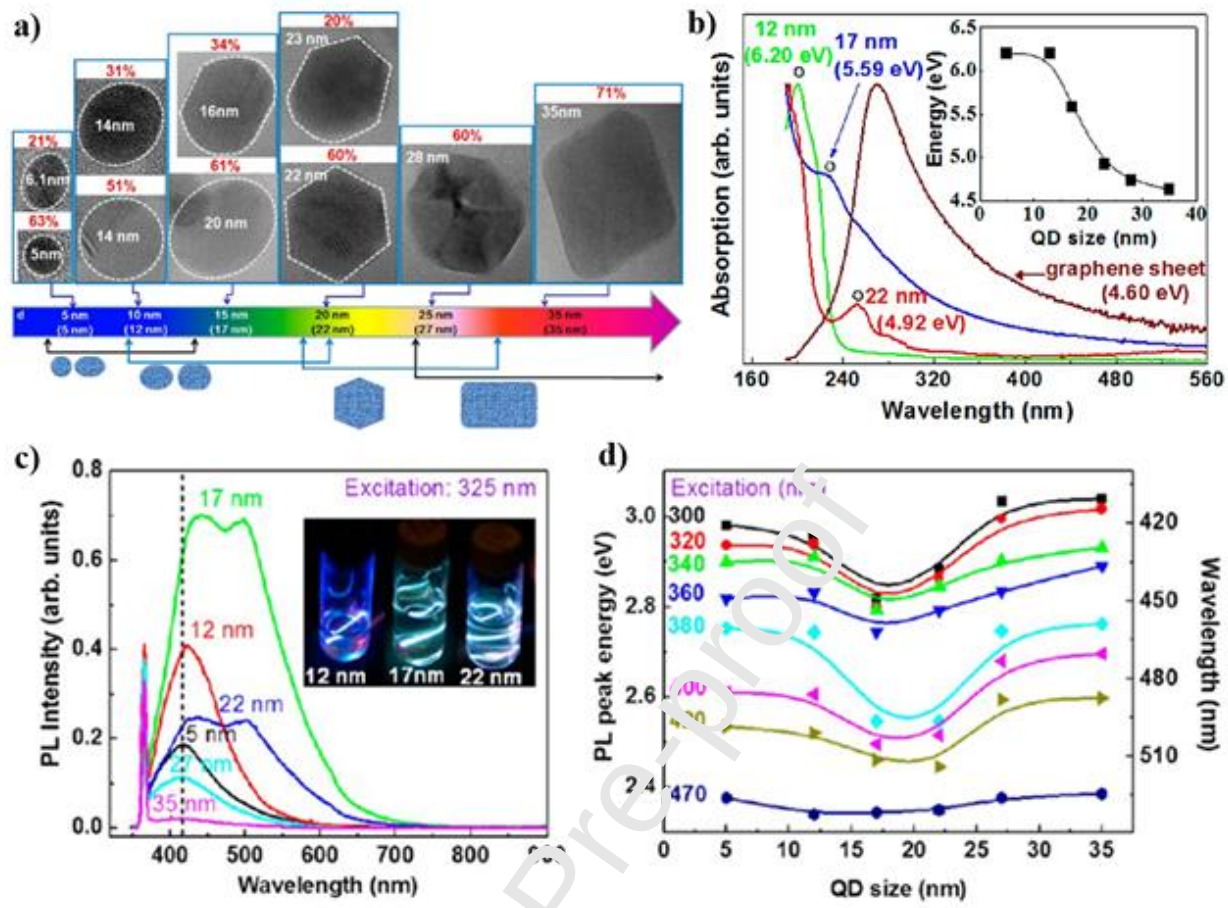


Figure 4. a) GQDs size and shape relation from HR-TEM imaging, b) absorption spectra of GQDs with different size and graphene sheet. c) Size dependent PL spectra for GQD with 325 excitation wavelength, d) effect of GQDs size on PL peak energy when it is excited with 300 to 470 nm. [53]. Copyright 2012 American Chemical Society.

The pH of solution is also a significant parameter, influencing the PL intensity. Pan et al. [29] stated that under alkaline conditions, GQDs emitted strong PL. In contrast, the PL was almost quenched when samples were under acidic conditions. This behavior might constrain the application of GQDs, however it is possible to address this problem with surface modification methods [60]. Gu et al. [63] studied extrinsic factors such as pH of the solvent, solution concentration, and reaction temperature that could play a paramount role in the PL intensity and PL QY of N-GQDs. The optimum pH that conduces to the high PL intensity is the neutral pH. This pH dependent PL behavior is associated with both surface states and functional groups. In addition to the solvent pH, solution concentration is a significant factor too. Additionally, they showed that while increasing the solution concentration enhances the PL intensity, the PL emission wavelength remain stable. The reaction temperature during the synthesis of GQDs is important too. Reaction temperature affects different surface functional

groups, surface, and molecular state and finally, PL properties. As the temperature rises, the more carbonization occurs in the system and more N atoms dope into the system, so PL QY increases. At higher reaction temperatures the extent of carbonization may be reduced, leading to decrease of the PL QY.

### 4.3. Up-conversion photoluminescence

Till the last years, the up-conversion PL (UCPL) properties of CDs were mostly unclear. According to most of the reports, CQDs and GQDs can only exhibit the down-conversion PL (DCPL) emission (emission of light at a shorter wavelength than the excitation wavelength) [64, 65]. The UCPL properties of CDs are considered to be due to the multi-photon activation process (simultaneous absorption of two or more photons). Cao et al. [36] stated that CDs were strongly emissive in the visible range with either the pulsed laser excitation in the near-infrared for two-photon excitation (800 nm) or excitation with Ar-ion laser (458 nm). Moreover, experimental results of luminescence in vitro imaging confirmed that the CDs were internalized into the human breast cancer cells likely through endocytosis which open new opportunities for cell imaging. GQDs showed the DCPL emission as well as the UCPL emission, which means that the same PL emission peak was observed when GQDs were excited with excitation wavelength between 500 to 700 nm [66]. In most of the cases, both down-conversion and up-conversion PL spectra had excitation-independent PL behavior that could not be seen in the other fluorescent carbon-based materials [67].

### 4.4. Aggregation induced emission effects

According to surface thermodynamics, NPs and specially QDs have high surface free energy which is favorable for these QDs to decrease that by aggregation. Aggregation would cause some changes in optical properties of these QDs including aggregation induced emission enhancement (AIEE) effect, aggregation induced red-shift emission (AIRS) effect, and aggregation induced emission quenching (AIEQ) effect [18]. As a sight of view, in AIEE effect the aggregation restricts rotational vibration of surface group and enhances the π-conjugation of fluorescent materials, which increases radiative rate and deceases non-radiative rate [18]. So, this mechanism would be the basis of sensing applications. Chen et al. [68], synthesized single-layered GQDs (s-GQDs) by addition of aluminum ions ($Al^{3+}$), it is observed that because of s-GQDs specific binding with aluminum ions accumulation occurs. This aggregation resulted in improvement of PL intensity thanks to the (AIEE) mechanism. In AIEQ effect, when the fluorescent material aggregates, the excited energy would rapidly

transfer to ground state with non-radiative transition. So that it causes PL emission quenching [18]. Wang et al. [69] employed this characteristic of GQDs for detection of $Co^{2+}$. Due to the high affinity between N-related group of GQDs and $Co^{2+}$ ions, GQDs aggregated and obvious PL quenching occurred (AIEQ). Finally, due to the relation of PL peak position and the fluorescent material size which affects the band-gap energy, by aggregation there would be some red-shift in emission spectra (AIRS) which is rarely used for sensing applications. Li et al. [70], showed that the PL emission of phosphorous (P)-doped carbon dots (P-CDs) shifted from blue to orange yellow (AIRS) by increasing the concentration of P-CDs.

### 4.5. Electrochemiluminescence

Electrochemiluminescence (ECL) is a kind of luminescence phenomenon that occurs during the electrical reactions. The applied voltage transfers an electron to the exciting state and causes the stable luminescence emission [71]. The ECL behavior of GQDs is similar to that of QDs, as they have similar ECL mechanism. For instance, the ECL mechanism of GQDs occurs by introducing $K_2S_2O_8$ as a co-reactant. According to the electrochemical reaction, GQDs and $S_2O_8^{2-}$ are reduced to $GQDs^{\cdot-}$ and $SO_4^{\cdot-}$ radicals. Afterward, $SO_4^{\cdot-}$ radicals and $GQDs^{\cdot-}$ radicals might react by injecting the hole into the highest occupied molecular orbital (HOMO) of $GQDs^{\cdot-}$, producing an excited state of $GQDs^{*}$ which could emit light as the electrons relax back to their ground-state (equation 1 to 4) [72, 73].

$$GQDs + e^- \rightarrow GQDs^{\cdot-} \quad (1)$$

$$S_2O_8^{2-} + e^- \rightarrow S_2O_8^{\cdot 2-} \rightarrow SO_4^{2-} + SO_4^{\cdot-} \quad (2)$$

$$GQDs^{\cdot-} + SO_4^{\cdot-} \rightarrow GQDs + SO_4^{2-} \quad (3)$$

$$GQDs^{*} \rightarrow GQDs + h\nu \quad (4)$$

Several parameters affect ECL properties and may cause enhancement of this feature. The surface state is an adequate site for some chemical reactions. Thus, the higher the density of functional groups and defects, the higher the solubility and the stronger the ECL becomes [72-74]. Liang et al. [75] observed a slight decrease in ECL signal, when peptides conjugated to the GQDs/Chitosan(CS) electrode surface, and this was owing to decrease in transferring electrons. Accordingly, by assembly Ab-GO (anti-phosphoserine antibody conjugated GO) to the Peptide/GQDs/CS modified electrode a negligible decrease could be observed in the ECL

signals and this was due to the slight binding interaction in the existence of adenosine 5'-triphosphate (ATP) and casein kinase II (CK2) (Figure 5a). They also confirmed that the ECL intensity was a CK2 concentration dependence and had linear behavior in the range of 0.5-5 U/ml with the detection limit of 0.023 U/ml (Figure 5b,c). This detection range was much higher than other carbon-based nanocomposites.

There are few reports on the ECL bio-sensing and especially, cytosensing behavior of CDs. Wu et al. [76] fabricated CDs@Ag based ECL cytosensor. The cell capture abilities had a linear response range from 10 to $1\times10^5$ HeLa cell per ml with a low detection limit (Figure 5d). ECL intensity of three cancer cells was investigated when they were incubated with the fabricated electrode (Figure 5e). The results showed a negligible decrease for normal NIH-3T3 cell. While in contrast, the high differences were monitored for both HeLa and MCF-7 cells. In addition, when Folic acid (FA) treated HeLa cells (FA-HeLa), fewer changes were detected. As seen in Figure 5f-i, FL microscopy also provides changeable behavior in different conditions. HeLa and MCF-7 cells showed more PL spots than NIH 3T3 and FA-HeLa. When HeLa cell treated with FA, fewer binding sites were available on the fabricated surface, as a result, fewer PL spots could be detected.

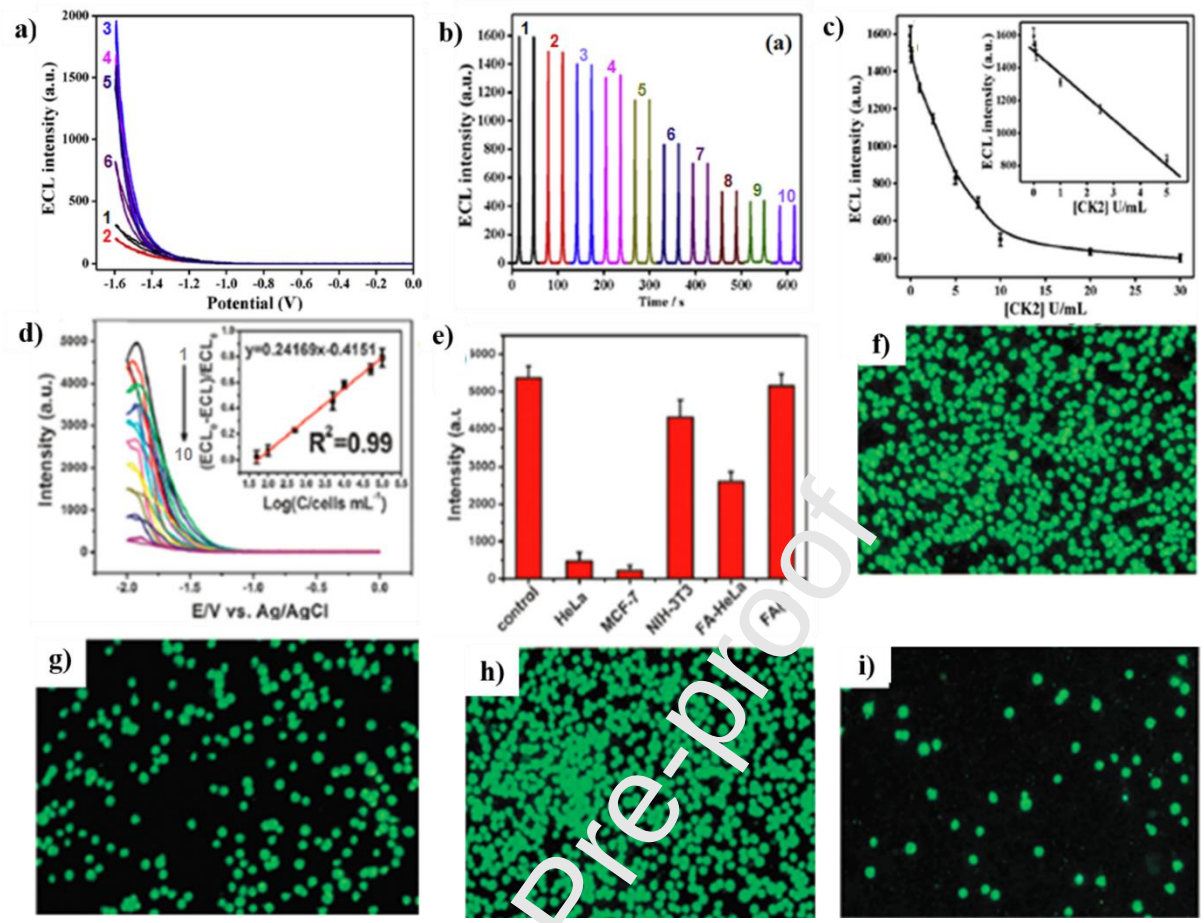


Figure 5. ECL-potential curve of bare electrode (a1), CS (a2), GQDs/CS (a3), peptide covalently conjugated GQDs/CS electrode surface (a4), assembly of Ab-GO onto the peptide/GQDs/CS modified electrode surface in presence of (a5) 0 U/mL and (a6) 5 U/mL CK2 and 50 mM ATP in 0.1 M phosphate buffer saline (PBS) containing, 0.1 M KCl and 0.1 M $K_2SO_4$. (b) ECL-time curve of bio-sensor in presence of (b1) 0, (b2) 0.05, (b3) 0.1, (b4) 1.0, (b5) 2.5, (b6) 5.0, (b7) 7.5, (b8) 10.0, (b9) 20.0 and (b10) 30.0 U/mL of CK2, (c) ECL intensity and CK2 concentration relation [75]. [Copyright 2016 Elsevier.] (d) Cyclic ECL curves of the as-prepared electrodes tested by culturing with different concentrations of HeLa cell suspension: (d1) blank control, (d2) 10, (d3) 100, (d4) 500, (d5) 1000, (d6) 3000, (d7) 5000, (d8) $1\times10^4$, (d9) $5\times10^4$, (d10) $1\times10^5$ cells per mL; inset: the linear relationship between the degree of ECL intensity change and logarithm of HeLa cell concentration. (e) Selectivity analysis for cancer cell detection by monitoring the ECL intensity between three types of cancer cell lines (HeLa cells, MCF-7 cells and a normal cell line, NIH-3T3 cells), FA-pretreated HeLa cells (FA-HeLa), and HeLa cells not immobilized with FA (FA (-)). FL microscopic images of different cell lines with the concentration of $1\times10^5$ cells per mL cultivated on the modified glass slides (the same modification procession as the electrode): (f) HeLa, (g) FA-HeLa, (h) MCF-7 and (i) NIH-3T3 cells. [76] Copyright 2013 Royal Society of Chemistry.

# 5. Current limitations

## 5.1. Toxicity

According to the specific bio-applications of carbon-based nanomaterials such as bio-imaging, drug delivery, cancer therapy, etc., studying the toxicity of these nanomaterials is very important. Its importance leads to deeper research in this part and investigating different

effective parameters to reduce this behavior compared with the other nanomaterials. In this section, we review some up to date research working on toxicity of CQDs and GQDs.

The in vitro toxicity tests measure the viability of the cells and are carried out with some special tests as Lactate dehydrogenase (LDH), 3-(4,5-Dimethylthiazol-2-yl)-2,5-diphenyltetrazolium bromidefor (MTT), and Adenosine tri phosphate (ATP). In vitro toxicity depends on several parameters such as cell type or dosage [77-80]. Wu et al. [79] demonstrated that the cytotoxicity of GQDs had better performance on MGC-803 and MCF-7 cells compared with the GO. They indicate that in the same time and culturing environment, by increasing the concentration of GQDs, the viability of MCF-7 and MGC-803 cells reaches 70%. While in contrast, significant decrease in cell viability can be observed for GO, especially on the MGC-803 which reaches to 40%. Senel et al. [80] showed that N-GQDs had varying impacts on different cells, which NIH-3T3 cells are highly affected as compared to A549 and MDA cells when the concentration of GQDs increased. Ko et al. [77], developed GQDs nanocarriers comprising Herceptin (HER), which acted to enhance targeting and accumulation in the breast cancer cell, and β-cyclodextrin, providing a proper chemical surrounding for loading doxorubicin (DOX) as a hydrophobic anticancer drug. Their study revealed that both cell viability and chemical release were dose-dependent, and in most cases, BT-474 cell viability decreased and chemical release increased by increasing GQDs concentration. Bagheri et al. [78] also confirmed dose-dependent toxicity of CQDs. They investigated effect of CQDs concentration on yeast cell and realized that increasing concentration results in higher toxicity.

It is well known that cells and dots interaction, and shrinkage of cells and holes on their surface are main reasons of toxicity. Therefore, surface charges are essential in toxicity evaluations. Yuan et al. [81] revealed that GQDs with different surface exposed groups (COOH, $NH_2$, and CO-N$(CH_3)_2$) had little influence on human A549 lung carcinoma cells. In all cases, GQDs exhibited greater cytotoxicity, and more than 80% of cells remain. Polymer coatings can also modify toxicity of CDs which will be discussed later (see section 7-3). Additionally, reactive oxygen species (ROS) is one of main drawbacks of NPs that may harm cell signaling, hurt DNA, causing toxicity and even promoting cancer. Large surface area of nanomaterials results in high level of ROS. Chemical nature of NPs indicates the level of ROS production. Number of parameters like QDs size, morphology, solubility, surface functional groups, interaction with cells, and pH or environmental factors like light, strongly

influences the level of ROS. NPs with smaller size can enter the cells more easily but they are more toxic too. Nanoparticle morphology is not as important as size, however, as the contact area increases the biocompatibility increases [82, 83]. Hoskins et al. [84] showed that coating of NPs influenced ROS generation, for instance neutral polyethylene glycol (PEG) coating had lower level of ROS compered to positively charged polyethylenimine (PEI).

Nurunnabi et al. [85] investigated the targeting efficiency, distribution, in vivo toxicity, and interaction of GQDs in biological systems. First, GQDs were incubated with three different cancer cells, KB (human epidermal cancer cell), MDA-MB231 (breast cancer cells), and A549 (human epithelial cancer cell) to illustrate the MTT assay and LDH release profile. This research showed that LDH release and cell mortality of KB cell were much higher than MDA-MB231, A549, and MDCK normal cell and this exhibited that A549 and MDA-MB231 had less sensitivity compared with KB. In other work, Goreham et al. [86] did a research about the interaction between GOQDs and J774A.1 (macrophage cells of mouse) and investigated toxicity by LDH assay which help better understanding of the in vivo cytotoxicity of these nanomaterials. The detailed cytotoxicity effect of GQDs and GOQDs is shown in Table 1.

Table 1. Cytotoxity effect of GQDs and GOQDs

| QDs | Cell Type | C ($\mu g/ml$) | Cell Viability (%) | | QDs | Cell Type | C ($\mu g/ml$) | Cell Viability (%) | | Ref |
|---|---|---|---|---|---|---|---|---|---|---|
| | | | 24 h | 48 h | | | | 24 h | 48 h | |
| MTT assay (cell viability) | | | | | | | | | | |
| GQDS | MCF7 | 50 | 99 | | GQDS | MGC-803 | 50 | 90 | | [79] |
| | | 100 | 85 | | | | 100 | 80 | | |
| | | 200 | 83 | | | | 200 | 80 | | |
| | | 400 | 72 | | | | 400 | 70 | | |
| N-GQDs | NIH-3T3 | 1 | 100 | 96 | N-GQDs | A549 | 1 | 96 | 100 | [80] |
| | | 5 | 90 | 80 | | | 5 | 94 | 100 | |
| | | 10 | 80 | 73 | | | 10 | 94 | 100 | |
| | | 15 | 73 | 66 | | | 15 | 75 | 98 | |
| | | 20 | 49 | 63 | | | 20 | 75 | 71 | |
| | | 50 | 10 | 8 | | | 50 | 47 | 44 | |
| GQDs | BT-474 | 20 | | 93 | GQDs | MCF7 | 20 | | 99 | [77] |
| | | 100 | | 94 | | | 100 | | 100 | |
| | | 200 | | 85 | | | 200 | | 93 | |
| | | 300 | | 78 | | | 300 | | 76 | |
| | | 500 | | 60 | | | 500 | | 60 | |
| Alamar blue assay (LDH release) | | | | | | | | | | |
| GOQDs | macrophage cells | 15.6 | 59 | 140 | FA-GOQDs | macrophage cells | 15.6 | 59 | 136 | [86] |
| | | 31.3 | 55 | 131 | | | 31.3 | 56 | 129 | |
| | | 62.5 | 48 | 128 | | | 62.5 | 47 | 125 | |
| | | 125 | 47 | 105 | | | 125 | 43 | 122 | |
| | | 250 | 45 | 80 | | | 250 | 45 | 117 | |
| | | 500 | 62 | 75 | | | 500 | 66 | 1 | |

### 5.2. Biodistribution and circulation time

Biodistribution of CDs is crucial parameter since it helps to determine the circulation time of nanoparticles in vivo. There are two vital systems in our body that clear the NPs from the blood. First, the mononuclear phagocyte system (MPS), which attacks and eliminates NPs by covering them with proteins making them easy to be seen by macrophage. Quick clearance of NPs by this system leads to their disappearance in a few hours. However, MPS assessment needs more research about macrophage uptake. Second, the reticuloendothelial system (RES) that can be investigated by measuring the half-life of NPs and observing their bio-distribution in the target tissue and RES organs. This system is an impediment for gathering of foreign particles in body and eliminate them [87]. The size of NPs would be an important feature from the sight of biodistribution. Zhang et al. [88] demonstrated that smaller NPs were more stable in the body and their circulation time is longer. They compared Au NPs with 20, 40, and 80 nm diameters and stated that 20 nm diameter NPs had less uptake by liver and spleen, so its stability was higher in the body. Licciardello et al. [89] evaluated the bio-distribution of Silicon NPs and CQDs with average size less than 5 nm. According to their results, most of the NPs cleared via the renal pathway with very little liver uptake. On the other hand, the surface charge of NPs can affect their bio-distribution. Negatively and positively charged NPs are more capable of protein adsorption (corona effect), so they accumulate in organs like liver. Conversely, the neutral and zwitterionic NPs have almost no protein adsorption and mostly placed in the kidney and removed by renal filtration. As a result CQDs have short circulation time due to their small size and surface charge, Therefore, finding a solution to increase their circulation time is necessary [89, 90].

### 5.3. Photobleaching

One of the most important properties of GQDs and CQDs is their excellent photostability. The stable structural morphology of CDs leads to resistance to photobleaching, which has deteriorated impacts on optical properties during the time, and is an essential drawback of nanomaterials for bio-imaging [91]. Malina et al. [92] examined the Quaternized Carbon Dots (QCDs) by confocal microscopy. It was found that QCDs had stable PL for even two weeks. Then, their photobleaching was observed, and it was reported that red PL only decreased about 4.2%. Additionally, Hu et al. [93] manifested that the CQDs were fluorescently stable in different pH values. They altered the pH from 1 to 13 and observed that the NPs were resistant to photobleaching. Nevertheless, some factors have effects on photobleaching of

CQDs. Wang et al. [94] investigated the photobleaching of CQDs synthesized by the bottom-up method. They showed that the light exposure time, the concentration of CQDs, and the presence of oxygen were the parameters that influenced the photobleaching of CQDs.

# 6. Bio-applications

## 6.1. Bio-imaging and labeling

The first priority of biological studies and cancer medicine is to achieve an efficient method, which enables scientists to target cancer cells and tumors and then deliver the drugs to specific locations. Nowadays, one of the ways to monitor cancer cells is FL imaging. When it comes to bio-imaging of cancer cells, robust fluorescent probes are required. Recently, a wide variety of fluorescent probes have been used for cell imaging, including up-conversion NPs (UC NPs) [95], QDs [96], silica NPs [97], Au NPs [98], and metallic nanoclusters [99]. However, these fluorescent nanomaterials have some weaknesses of organic fluorophores like poor photostability in long-term bio-imaging. Owing to the unique optical properties, favorable cellular permeability and uptake feature, low toxicity, and photobleaching, carbon-based nanomaterials have been developed for bio-imaging and labeling applications [100]. Firstly, Yang et al. [101], observed the feasibility of CDs as a PL contrast agent in mice. They injected PEGylated CDs (in an aqueous solution) into mice and collected FL images at different wavelengths. They experienced sufficient contrast for the images, which were in both red and green emission. Nurunnabi et al. [85] studied in vivo imaging of mice after GQDs injection. Figure 6a illustrates that at 12 h post injection, the GQDs accumulate around the tumor which is located on the skin, and these QDs could not reach to the deep organs at this period. Due to the circulation system, after 12 h GQDs move inside the body. Primarily, GQDs spread in the liver and heart, then after 2 h while the effect of GQDs disappears from the liver, the presence of GQDs increases in other organs such as the kidney. Finally, after 24 h of GQDs injection, the sign of GQDs is less detected in both tumor and organs. Figure 6b reveals that PL intensity at 24 h was lower than 12 h post injection. Figure 6c demonstrates the PL intensity of GQDs at different dosages form isolated organs at 2 h post injection.

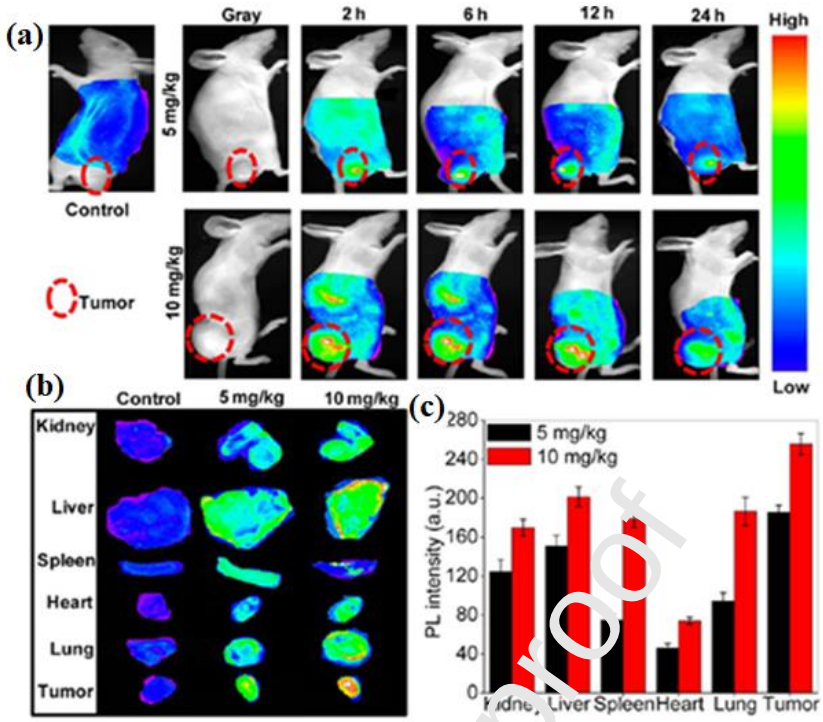


Figure 6. In vivo imaging and biodistribution of the carboxylated GQDs. (a) The in vivo imaging of KB tumor bearing mice after intravenous injection of GQDs (5 and 10 mg/kg), (b) ex vivo images of isolated organs of mice at 24 h after injection of each carboxylated GQDs, and (c) PL intensities of the carboxylated GQDs from isolated organs at different dosages (5 and 10 mg/kg). The data represent mean SEM (n = 3) ($p < 0.05$, one-way ANOVA). [85]. Copyright 2013 American Chemical Society.

Besides in vivo targeted, and diagnostic imaging, CDs also revealed a good ability for cell imaging [102]. Xue et al. [103] synthesized lignin hybridized CDs with different molar ratios of ethanediamine and citric acid. They reported that the L-CDs in HeLa cells showed the excitation-dependent PL behavior and the fact that L-CDs are advantageous to be used in bio-imaging and bio-labeling. Feng et al. [104] developed a charge-convertible cis-platin (IV) prodrug-loaded (CDs-Pt(IV)@PEG-(PAH/DMMA)), which responded to tumor extracellular microenvironment for imaging-guided delivery. The final product had a charge-changing property, which means that it had positive charge at tumor extracellular microenvironment (pH = 6.8) and negative charge at normal physiological condition (pH =7.4). These extraordinary properties caused a number of characteristics such as multicolor bio-imaging, long circulation time, convenient endosome escape, superior internalization by cancer cells, effective accumulation at the tumor site, and controlled drug release. The charge of CDs-Pt(IV)@PEG-(PAH/DMMA) at mildly acidic tumor extracellular microenvironment was positive. Since the charge of cell membrane was negative, this feature helped the product to easily enter into the cancer cells and significantly increased the efficiency of internalization.

### 6.2. Cancer therapy

Cancer is one of the most lethal diseases for human beings [105]. For this reason, researchers are searching methods for diagnosis and treatment. In the previous section we focused on the diagnosis of cancer cells using carbon-based nanomaterials. Next step is to eliminate these cells from the body. There were progresses on the treatment techniques of cancer tumors which the traditional, and most common ones are surgery and chemo/radio therapy used for a wide variety of cancers [106]. For most anticancer agents, there is no selectivity between cancer and non-cancer cells leading to poor targeting for the drug to show its influence. Also, toxicity of these agents would cause harmful effects on the healthy cells and limits the maximum dose of drugs [107]. Therefore, nanotechnology emerges as a key area in biotechnology field in order to enhance specificity and eliminate undesired side effects [107]. Three well-known nano-technological methods for cancer therapy are illustrated in Figure 7.

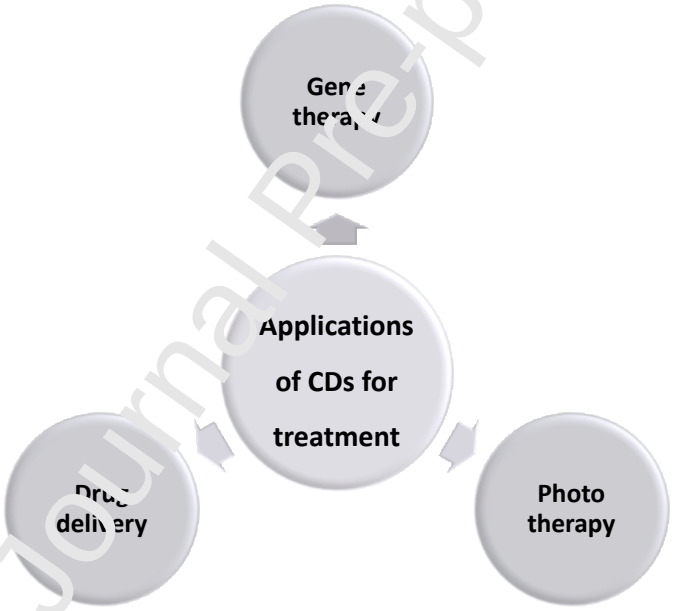


Figure 7. Three main nano-technological methods for cancer therapy.

Grounded in low toxicity, and good biocompatibility, CQDs are suitable choices for treatment of diseases like cancer. They are advantageous for reducing the side effects of drugs through sustained drug delivery, and their PL properties assist scientists in tracking NPs and targeting the specific site which the drug would influence [108, 109]. In this section, we introduced the bio-applications of CQDs/GQDs for photo therapy, drug delivery and gene therapy.

#### 6.2.1. Photo therapy

In recent decades, photo-thermal therapy (PTT) and photo-dynamic therapy (PDT), which are two main types of cancer phototherapies, attract attentions because of their superiorities over traditional curing methods. These treatments are non-invasive, have less side effects, possess low systemic toxicity and additionally, would be a targeted way to influence cancer cells [106].

#### 6.2.1.1. Photo-thermal therapy (PTT)

Increasing the temperature in cancer cells would results in denaturation of proteins and have therapeutic functions [106]. By this way, phototherapeutic nano-agents upon irradiation of specific wavelength of light would convert it to thermal energy which abolish tumor cells [105, 106]. Typically, near-infrared (NIR) light-adsorbing agents are used for this conversion and therapeutic technique [110]. The first carbon-based nanomaterials applied for PTT were single walled nanotubes (SWNTs) [111]. But beyond nanotubes, nanohorns, graphene, and CDs gained attention to be used in PTT. For example, Wang et al. [102] has prepared CQDs by using polythiophene benzoic acid as carbon source which had light absorption in the range of 400-700 nm and emitted bright red PL with a peak between 640-680 nm at different excitations. Its photo-thermal conversion efficiency was 36.2% and it was used for both PDT and PTT. They showed that CQDs had relatively no cytotoxicity in dark condition unlike under irradiation of 635 nm laser. Also, lower cell viabilities were observed in higher concentrations of CQDs for PDT and PTT.

The poor NIR absorption of CDs is a restriction in PTT applications. There are several ways to overcome this challenge such as: 1) using CDs with metal NPs, 2) synthesis of CDs using precursors with NIR adsorption, 3) assembling CDs with metal ions or some dyes with NIR absorption [112]. Zheng et al. [113], synthesized NIR CDs with solvothermal process by the reaction of hydrophobic cyanine dye [2-((E)-2-((E)-2-chloro-3-((E)-2-(1-(2-hydroxyethyl)-3,3dimethylindolin-2-ylidene)ethylidene)cyclohex-1-en-1-yl)vinyl)-1-(2-hydroxyethyl)-3,3dimethyl-3H-indol-1-ium iodide, CyOH] and PEG800 which resulted in emission within the range of 600 nm to 900 nm and PTT conversion efficiency of $\eta$ = 38.7%. Figure 8a illustrates cancer cell count as function of time. Also, as it is apparent in Figure 8b-n, successful accumulation of CDs in tumor region is observed within 6 h and maintained good retention of PL signal at the tumor even at 240 h.

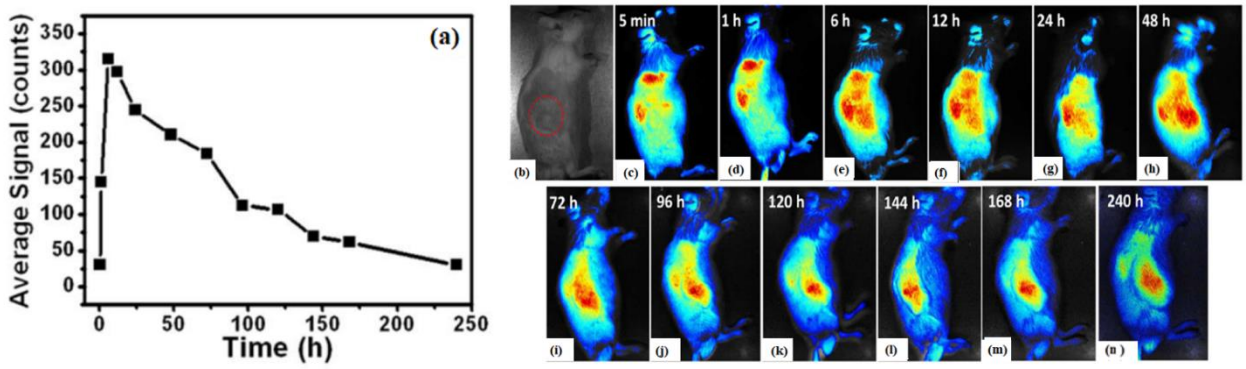


Figure 8. (a) Average PL intensity of the tumor area as a function of time. Time based in vivo red FL images of BALB/c mouse bearing CT26 tumors after the intravenous (i.v.) injection of CyCD (the tumor is circled with a red dotted line). (b) 0 min (taken under natural light; the red circle marks the position of tumor), (c) 5 min, (d) 1 h, (e) 6 h, (f) 12 h, (g) 24 h, (h) 48 h, (i) 72 h, (j) 96 h, (k) 120 h, (l) 144 h, (m) 168 h, and (n) 240 h. [113]. Copyright 2016 American Chemical Society

### 6.2.1.2. Photodynamic therapy (PDT)

Different from PTT, PDT's function is relying on ROS utilizing photosensitized (PS) agents to convert photonic energy to ROS, like $O_2$ or OH radicals which are toxic for cancer cells, in order to eliminate abnormal cancer cells [63, 114]. For the first time, Markovic et al. [115], reported that GQDs had the ability to be used for PDT applications. They synthesized PEGylated GQDs which produced $^1O_2$ under blue light irradiation. Using U251 human glioma cells as a model system, they investigated cytotoxicity of aforementioned agents and showed that by increasing the exposure time, cell viability would decrease in comparison with the condition which they had no exposure and cell viability remained constant. Additionally, Ge et al. [116] prepared large-scale GQDs using polythiophenes as the precursors by hydrothermal method. As prepared GQDs exhibited a wide-ranging absorption from the visible to NIR, deep-red emission, great photo and pH stability, excellent aqueous dispersibility, and favorable biocompatibility. GQDs had great $^1O_2$ generation yield, higher than 1.3, making them favorable agents for PDT applications. They also showed that by injecting GQDs into the back of the nude mice with breast cancer, the injected sites had much higher PL with a high signal-to-noise ratio (Figure 9a). Three groups of treatments were also investigated. For the PDT group, mice were injected with GQDs and irradiated twice, while the C1 group only got the GQDs without any irradiation, and the last group was C2 group that only irradiated, without any GQDs injection. As depicted in Figure 9c, in PDT group, the tumor grew and turned black, and after several days, this tumor began to decompose and was destroyed totally. In contrast, the tumor grows similarly in the two other groups. This shows the fact that both GQDs and radiation are necessary for removing tumors.

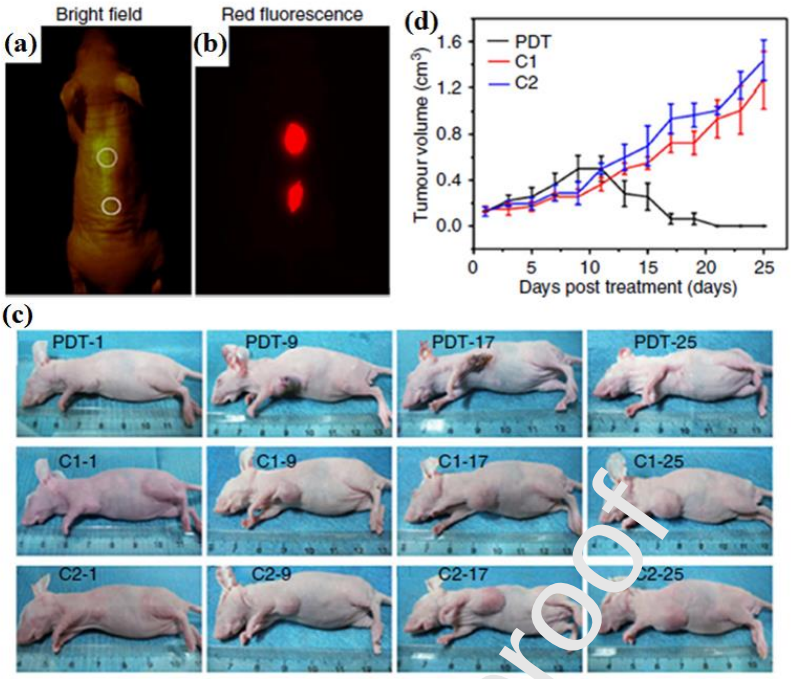


Figure 9. In vivo imaging and PDT. (a) Bright-field image and (b) red-FL image after subcutaneous injection of GQDs in different areas. The excitation wavelength was 502–540 nm, and the collected PL channel was 695–775 nm. (c) Photographs of mice after various treatments on the 1st, 9th, 17th and 25th day. (PDT: GQDs light irradiation; C1: GQDs only; C2: light irradiation only.) (d) Time-dependent tumor growth curves (n¼5) after different treatments. Po0.05 for each group. [116]. Copyright 2014 Nature.

### 6.2.2. Drug delivery

DOX is an anticancer drug that is used in so many research as a model to show the capability of different systems for drug delivery. It have been utilized to evaluate targeted drug delivery of CQDs as well. Ding et al. [117] demonstrated that DNA-CQDs was worthy for DOX and rhodamine 6G (Rh 6G) delivery. DNA-CQDs not only made electrostatic interactions with drugs for better loading but also its stability in neutral pH and drug release in lower pH was useful for proper drug delivery. The N and P that existed in DNA structure improved the PL of CQDs and had the benefit of imaging. Samantara et al. [118] used heteroatom doped CQDs for imaging and drug delivery. They revealed that DOX drug loaded in this system had non-covalent interaction with CQDs. Their investigation confirmed the increasing drug release of CQDs in acidic conditions. After 46 hours, the release in pH 5 was 97% and in pH 7.4 was 78%. Additionally, they proved that the amount of drug which entered the cells increased compared to free DOX. Bao et al. [119] used NPs consist of N- doped CQDs (N-CQDs), D-biotin and methoxy polyethylene glycol amine (mPEG- $NH_2$) with oxidized sodium alginate (OAL) for DOX delivery. N- CQDs which had so many amine groups were the crosslinking agent of OAL. D-biotin caused efficient targeting of the system in

comparison to free DOX. Therefore, this system reduced the side effect of DOX as lower amount of drug can be used for treatment. Moreover, this system inhibited cancer cell proliferation without toxicity for healthy cells. Their observations illustrated that the NPs remained in cytoplasm and membrane, while the drug could enter the nucleus (Figure 10). Wang et al. [120] utilized GQDs coated by PEG for DOX drug delivery. The results showed that in the acidic condition like a tumor environment, the hydrophobic bond between DOX and GQD/PEG weakened and NPs released the drug. It is caused by protonation of $NH_2$ group of DOX in lower pH (acidic condition). Even in the alkaline condition the release of drug was higher than the neutral condition.

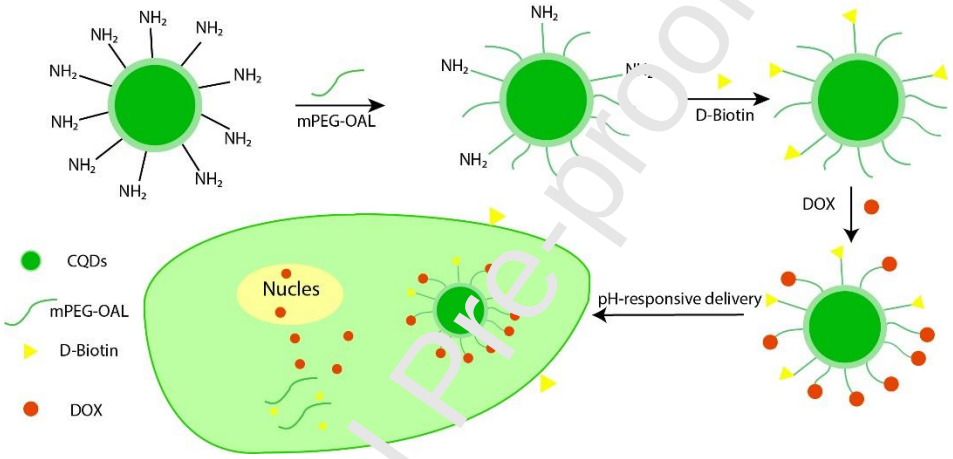


Figure 10. Assay of working protocol of the pH- sensitive CQDs−DOX NPs for tumor cellular targeted drug delivery. [119]. Copyright 2019 Wiley.

### 6.2.3. Gene therapy

On the other hand, The CDs are convenient as a vector for gene delivery. Gene therapy is one of the important ways to treat diseases like cancer. Some critical factors are involved in the gene delivery by NPs. The DNA structure includes phosphates that are the source of negative charge, so positive charge on the surface of NPs is needed to create a complex. Furthermore, the transfection of NPs is another challenge that limits non-viral gene delivery systems. Nevertheless, CDs has advantages like tracking the vectors through PL properties of dots. Therefore, the CDs are applicable gene vectors if the problems of their usage would be solved [121].

One of the essential modifications that applied to non-viral vectors for gene therapy is coating by polymers. Chitosan and PEG coated graphene were examined for their capability for gene delivery. Positively charged chitosan successfully condensed DNA. Moreover, PEG protects

the vector against agents in the body like proteins [122]. Ghosh et al. [123] exploited CDs conjugated with polyamidoamine (PAMAM) to cure Triple negative breast cancer (TNBC) that is the worst type of breast cancer. They found that electrostatic interaction between positively charged polymer and negatively charged DNA leads to effective complexation. By increasing the PAMAM polymer, the density of amine groups increased leading to its enhanced complexation capability. Additionally, RGD peptide improved the ability of creating complex as well as enhancing the cellular uptake of NPs. Cheng et al. [124] applied cationic poly-[2-(dimethylamino)ethylmethacrylate] (PDMAEMA) and zwitterionic poly[N-(3-(methacryloylamino)propyl)-N,N-dimethyl-N-(3-sulfopropyl) ammonium hydroxide] (PMPDSAH) polymers by atom transfer radical polymerization (ATRP) on the surface of CDs. The PDMAEMA used for making a complex with DNA and condensed it to NPs with size about 50 nm. PMPDSAH not only protected the CDs against proteins, but it was also helpful for efficient transfection.

### 6.3. Bio-sensors

CDs have revealed great potential for bio-sensing applications. The non-standard levels or variation of biomarkers in the body, such as peptides, glucose, UA, DA, DNAs, enzymes, proteins, antigens and hormones can be related to diseases [125]. Garcia et al. [126] utilized CQDs modified by gold for making a DNA bio-sensor. They attached 25mer or 100mer DNA probes for sensing cystic fibrosis transmembrane regulator (CFTR) gene. They could create a sensor with high selectivity and detection limit of 0.16 nM. In another research, Huang et al. [127] synthesized a nanocomposite bio-sensor based on CQDs, Au, and Pd for colitoxin gene detecting. Mechanism of sensing grounded in immobilization of single stranded DNA through carboxyl ammonia between carboxyl group of nanocomposite and amino group of (S1) probe DNA. Pd-Au@CQDs was ultrasensitive and its detection limit was $1.82\times10^{-17}$ $molL^{-1}$. Ji et al. [128] investigated application of N-CQDs to determine glucose in blood. They prepared a compound of N-CQDs and chitosan (Figure 11). The amino-carboxyl reactions brought about immobilization of glucose oxidase ($GO_x$) and it showed the amount of glucose in blood efficiently with detection limit of 0.25 mM. Table 2 shows some other bio-sensing applications of CDs.

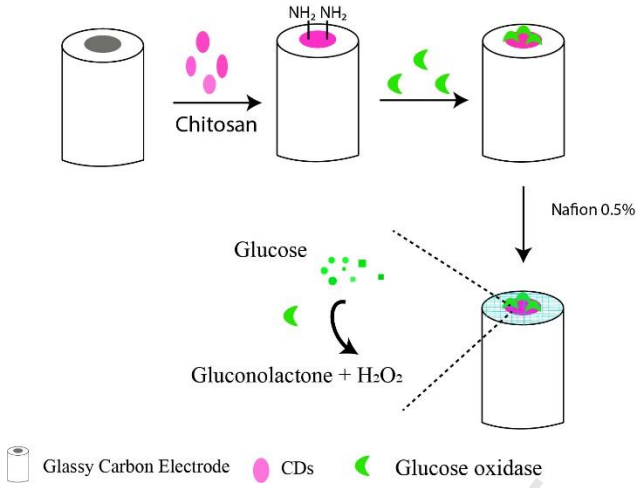


Figure 11. Schematic of the N-CDs based electrochemical glucose bio-sensor. [128]. Copyright 2016 Multidiciplinary Digital Publishing Institute.

Table 2. Bio-sensing applications of CDs

| Probe | Application | Linear range | Detection limit | Ref. |
|---|---|---|---|---|
| BSA/Ab-Vd2/CD-CH/ITO | Vitamin $D_2$ sensing | 10–50 $ng.mL^{-1}$ | 1.35 $ng.mL^{-1}$ | [129] |
| CDs/Boh | determination of DOX | 1-500 $ng.mL^{-1}$ | 0.2 $ng.mL^{-1}$ | [130] |
| $Cu_2O$–CDs/NF | Dopamine sensing | 0.05–45.0 µM | 1.1 nM | [131] |
| N-GQDs | Glucose sensing | 25 – 375 µM | 16 µM | [132] |

# 7. Modifications of CDs for bio-applications

One of the most important methods for improvement of CDs for bio-applications is modification. Some drawbacks like dose-dependent toxicity and photobleaching will be reduced in this way. Moreover, properties like PL is enhanced, and biological properties like cell transfection improves. Usual techniques of modification are doping, surface functionalization, polymer capping, making a composite, and core-shell structure. In this section, these methods will be discussed.

## 7.1. Doping

Chemical doping is considered as one of the methods to alter the optical properties of the CDs. Zhang et al. [133] reported that doping of larger particles showed higher red-shift than

smaller particles due to their surface status and size effects. N firstly doped into the structure of GQDs in 2012 [134]. Owing to the constant size and emission site of the $sp^2$ cluster, N-GQDs reveal excitation-independent PL properties [135]. Hu et al. [136] found a facile fabrication method of N-GQDs by hydrothermal treatment of GO in the presence of ammonia with no further surface modification. The synthesized N-GQDs presented highly blue luminescence and maximum QY of 24.6%. They also used cervical cancer cells to show that N-GQDs did not exhibit toxicity in the MTT assay. N was also doped into GQD's structure by using plasma pulsed laser ablation (PLA) and showed a strong blue luminescence [137]. Ju et al. [138] studied the impact of N concentration on the PL characteristics. It was reported that due to the strong electron affinity of N atoms in the GQDs, after doping N, the emission wavelength exposes a blue shift and when the dopant concentration reaches to 16.7 M, the PL intensity augmented 25-fold compares to GQDs. Ren et al. [139] recently synthesized N-doped microporous carbon quantum dots (NM-CQDs) with a high QY and dual-wavelength PL emission from biomass. Two co-existing PL emissions in the indigo–blue wavelength region were reported. This phenomenon was explained by the fact that excited electrons were transported from the intrinsic $\pi^*$ orbital to the surface state. The QY of NM-CQDs was 32.4%, which significantly surpassed the QY of non-doped CDs. Further studies indicate that the PL emissions of NM-CQDs are independent in various conditions, including pH, irradiation time, excitation wavelength and temperature. All these features lead to the enormous potential of this material in biomedical imaging. For the first time, Travlou et al. [140] studied the antibacterial activity of sulfur doped CQDs (S-CQDs) and N-doped CQDs (N-CQDs) by the disk diffusion method and MIC test. The S and N-CQDs, which were produced by a hydrothermal approach, could act as bactericides against B. subtilis and E. coli bacterial strains. This study showed that N-CQDs were more effective than S-CQDs. The abnormal amount of hydrogen sulfide ($H_2S$) in tissue could easily affect cellular functions and might lead to some dangerous diseases like Alzheimer [141]. In a research, copper was doped into CQDs (Cu-CQDs) for living cell imaging of $H_2S$. In order to assess the practicability, H3122 lung cancer cells were selected as a model system. A major intracellular PL quenching was noticed when 100 μM NaHS is incubated with Cu-CQDs. With the further addition of NaHS, the intracellular PL reduced significantly. The provided results concluded that the as-prepared Cu-CQDs had an excellent potential in in-situ dynamic monitoring the distributions and variations of cellular $H_2S$ levels [142]. Jin et al. [143] showed that S-doped GQDs (S-GQDs) performed in a high-quality cell imaging with low cytotoxicity that

penetrated into the cell membrane. A slight decrease was reported in cell viability when the S-GQDs concentration was increased two orders of magnitude, from 10 to 1000 μg/ml. Moreover, they demonstrated when HeLa cells were incubated with S-GQDs, no morphological changes in the cell were observed and the S-GQDs can easily penetrate into the cytoplasm of the cell membrane (Figure 12a,b). In addition to N and S doping, several investigations have been done on other elements doping such as boron (B) [144], P [145], Cl [146], and fluorine (F) [147]. Feng et al. [148] studied the effect of B on the optical properties of the pristine GQDs. The red-shift absorption of the GQD-B2 ($C_{40}B_2H_{18}$) with the $BC_3$ bonding configuration could be observed. Moreover, when GQD-B2 covalently bonds with $BC_2O$ or $BCO_2$, the blue shift in $\lambda_{max}$ were detected compared with the GQD-B2. These shifts in absorption peaks occurred both for surface and edge doping

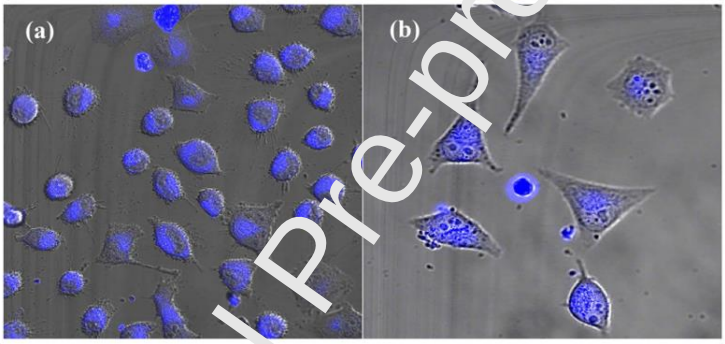


Figure 12. (a) FL images of HeLa cell after incubation with S-GQDs for 24 h. (b) Partial enlarged drawing of FL images of HeLa cell after incubation with S-GQDs for 24 h [143]. Copyright 2018 Elsevier.

Some research group also investigated the co-doped GQD or CQDs which means that the combination of heteroatoms doped to these materials such as N-P [149], F-N [150], N-Cl [151], etc. This kind of doping provided more opportunities to modify the structure and optical and electrical properties. For example, ECL of GCDs was modified by co-doping. Zhang et al. [72] showed that N and S doped GQDs (NS-GQDs) with $K_2S_2O_8$ had ECL 5.8-fold more than the ECL of the GQDs. Kundu et al. [152] introduced a single-step synthesis of S, N, F co-doped GQDs from CNTs by using MW treatment. They succeed to reach a high QY of 70%. It was asserted that this high QY might be attributed to the interaction of defect clusters and dopants. Nafiujjaman et al. [151] developed chlorine (Cl) and N-doped GQDs (Cl-GQDs-N) via a simple hydrothermal technique with the size of 30 nm. Significant increase in the PL intensity is observed when Cl and N were doped to GQDs and Cl-GQDs-N exhibited powerful blue PL emission under the UV excitation with PL QY of 20.39%. The excitation dependent emission of Cl-GQDs-N was also investigated, when the wavelength

increases from 350 nm to 380 nm, the emission peaks become stronger. By further increase of wavelength from 390 nm to 450 nm, the emission intensity shows a decrease. The mechanism of excitation dependent emission profile is still debated. It might be caused by bandgap transition or because of unique energy trap structure [154]. In vitro cell uptake studies showed that the Cl-GQDs-N successfully diffused into the cells. Cytotoxicity of Cl-GQDs-N in high concentration (1 mg/mL) in madin derby canine kidney (MDCK) cells and cancer cells (MDA-MB231) had been also studied. Results confirmed that Cl-GQDs-N were biocompatible and promising for bio-imaging.

### 7.2. Surface functionalization

Due to the presence of reaction sites on the surface of GQDs and CQDs, other species can be used to functionalize them. Several groups were used as functionalizing agents, and especially amino-modifications attracted great attention [153]. Functional species can result in altering the band gap, and tuning the optical properties. In addition, functionalization of NPs with antibodies, small molecules, peptides, aptamers, etc. is a suitable way that can be used for specific targeting. They are helpful to prevent the accumulation of NPs in normal cells and assist in higher concentration in tumor cells. The expression of some markers on the surface of tumor and cancer cells and their interaction with functionalized CDs is the main reason of targeting.

Surface functionalization processes are divided into the two main covalent and non-covalent methods [154, 155]. In this section, we introduce some of the recent reports about functionalization. Tam et al. [156] synthesized cysteine-functionalized GQDs (cys-GQDs) and showed that the amine groups of the cysteine react with the carboxylate groups of GQDs. Figure 13a,b shows optical properties of synthesized GQDs and reveals that the UV-vis spectrum of cyst- GQDs shift from 321 nm to 331 nm, and shoulder from 452 nm to 503 nm compared with the pristine GQDs. Moreover, by increasing the cysteine concentration, the red shift could be observed when it is excited with 365 nm laser. Figure 13c demonstrates the excitation wavelength dependence of the cyst-GQDs. Due to the electron-donating amine groups of cysteine on the surface of the GQDs, the prepared GQDs has a higher QY of about 28% compared with the bare GQDs QY of about 8.8%. These synthesized nanomaterials were also used to investigate the sensing ability. Figure 13d,e shows that prepared GQDs higher selectivity to $Hg^{2+}$ as compared to other ions and the green PL solution quenched in

the presence of $Hg^{2+}$. The $Hg^{2+}$ concentration-dependent PL intensity is shown in Figure 13f, and finally, a high quench from a low concentration of $Hg^{2+}$ to 100 μM was reported.

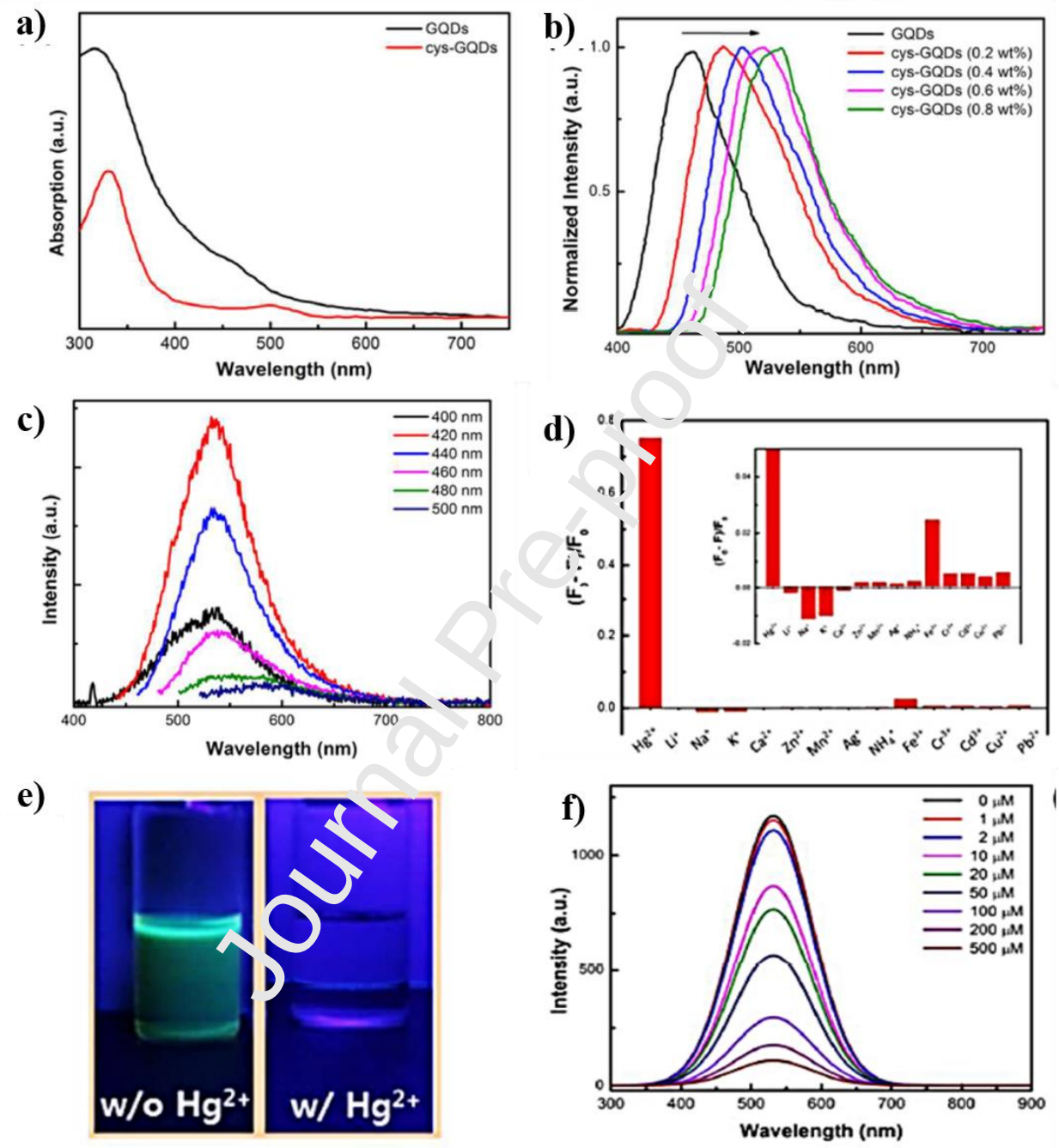


Figure 13. (a). UV-vis absorption of GQDs and cys-GQDs. (b) PL spectra of cys-GQDs with various amounts of L-cysteine. (c) The PL spectra of cyst-GQDs at different excitation wavelengths ranging from 400 nm to 500 nm. (d) The PL enhancement factors [(F-F0)/F0] of cys-GQDs for the various metal ions (100.0 μM). (e) The photo image of the cys-GQDs solutions in the presence (right) and absence of $Hg^{2+}$(left) under the 365nm UV light irradiation. (f) The PL change of cys–GQDs with the various $Hg^{2+}$ concentrations [156]. Copyright 2015 Royal Society of Chemistry.

Wang et al. [157] revealed some enhancement in optical properties that occurred during GQDs functionalization. They reported that the QY of GQDs increased from 4.7% to 13.8%. Furthermore, af-GQDs showed five-time stronger PL intensity than pristine GQDs (Figure 14a). GQDs have two major peaks at 450 nm, and 510 nm which attribute to the $sp^2$ domains π-π* transition and the n-π* transition of surface functional group, respectively. However, the af-GQDs second peak shifted from 510 nm to 520 nm which were related to the surface functional groups (Figure 14b,c).

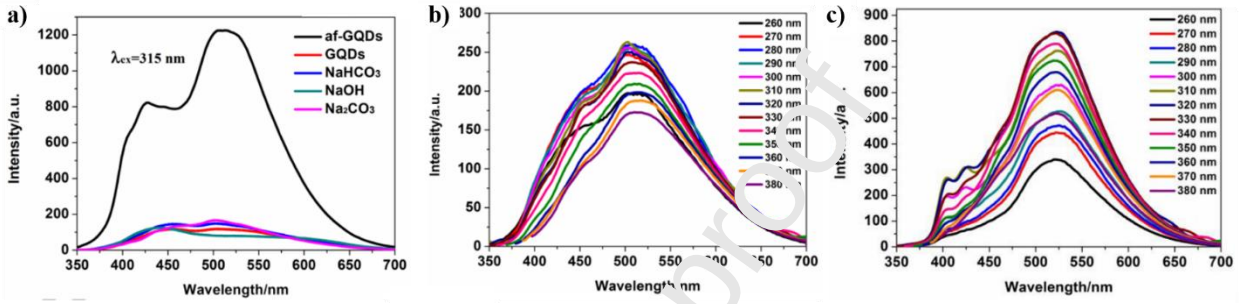


Figure 14. (a) Emission spectra of GQDs solutions neutralized with different reagents before and after the hydrothermal treatment. PL spectra of GQDs, (b) and af-GQDs, (c) in aqueous solution under shifted excitation wavelengths. The mass concentrations of GQDs and af-GQDs were both 0.1 mg/mL. [157]. Copyright 2019 Elsevier.

Fu et al. [158] modified CQDs by thiosemicarbazide (TSC) that were sensitive molecule to copper ions. They conjugated TSC on the surface of CQDs through amide bonds between the carboxyl group of CQDs and the amine group of TSC, and obtained NPs with the size about 2.38 nm. Optical properties of NPs illustrated by UV-Vis analysis indicated that a new peak appeared in 289 nm after conjugation. Another benefit of functionalization was the stability of PL of CQDs in various pH (from 3 to 10) due to high pKa value of TSC and its undisrupted form. Moreover, TSC-CQDs were stable in solutions with different concentrations of NaCl. The primary approach of functionalized NPs to detecting Cu ions was PL quenching that was a result of forming a complex of Cu ions and modified NPs. Deka et al. [159] manipulated the hydrophobicity and the optical properties of GQDs through functionalization. In their research, firstly GQDs were functionalized by dodecyl amine (DDA), and then were reduced by glycine. The long-chain alkyl groups ($C_{12}H_{27}$) that were covalently bonded with GQDs were hydrophobic. They resulted from modification by dodecyl, and were crucial factors of hydrophobicity. The oxygen functional groups on the surface of GQDs caused green PL. After functionalization, those groups were diminished, and blue PL was observed.

Aptamers are essential agents for modifying NPs aimed at targeting. Liu et al. [160] used an anti-VEGF aptamer to functionalize CDs for tumor targeting. They firstly covered the surface of CDs with $NH_2$-PEG-$NH_2$ by an interaction between the amine group of PEG and the carboxyl group of CDs. Then, the aptamers were placed on the surface of CDs through the reaction of the carboxyl group with the amine group of PEG-coated CDs. Aptamer addition increased the ability to target tumor cells as the PL of cells treated by aptamer-conjugated CDs is higher than CDs without aptamers. Moreover, CDs targeted mitochondria since they were positively charged and tend to go to the negatively charged membrane of mitochondria. Additionally, aptamers were used for diagnosis. Motaghi et al. [161] demonstrated a new technique for sensing cancer cells by modification of CDs through AS1411 aptamer. This method was based on the expression of nucleolin on the surface of cells. The CDs without aptamer had no specific targeting because the PL intensity of both human foreskin fibroblast cells (HFFF) and cancer cells (4T1) quenched similarly. Conversely, the aptamer conjugated CDs indicated different PL intensity because of variation of nucleolin expression on the cancer cells.

FA is another molecule that is useful for surface modification. It makes the ability of interaction with cancer cells because of folate receptors on their surface. Mewada et al. [162] functionalized CDs with bovine serum albumin (BSA) and FA for drug delivery. The former not only improved biocompatibility of CDs but also increased the drug loading capacity, and the later used as targeting molecule. The BSA covered on the surface through interactions between the carboxyl group of CDs and functional groups of BSA. By using the FA as a targeting agent for the folate receptor of tumor cells, the toxicity of the system for healthy cells declined. Moreover, the FA-modified CDs were applied for cancer diagnosis. Zhao et al. [163] used CDs from ethanediamine (EDA) as the resource. So the surface of CDs had enough amino groups to covalently bond to the carboxyl group of FA. Their results showed that the folate receptor that mostly exists on the membrane of cell caused adsorption of functionalized CDs. Figure 15 shows the process of functionalization. Hai et al. [164] demonstrated cancer cell imaging capability of folic acid encapsulated GQDs (FA-GQDs). They provide the pH sensing probe and cell imaging systems by using FA-GQDs and successfully applied for detection in the cell culture. In this research, the FA-GQDs-loaded HeLa cells were used to investigate cell FL imaging, which was treated with different pH (5, 6, 7, 8). The results showed the green channel of PL intensity in HeLa cell was becoming brighter as the pH rose to 8 while the blue channel was almost identical. As mentioned

before, GQDs exhibit a pH-independent PL excitation wavelength and just the PL emission intensity changes [63].

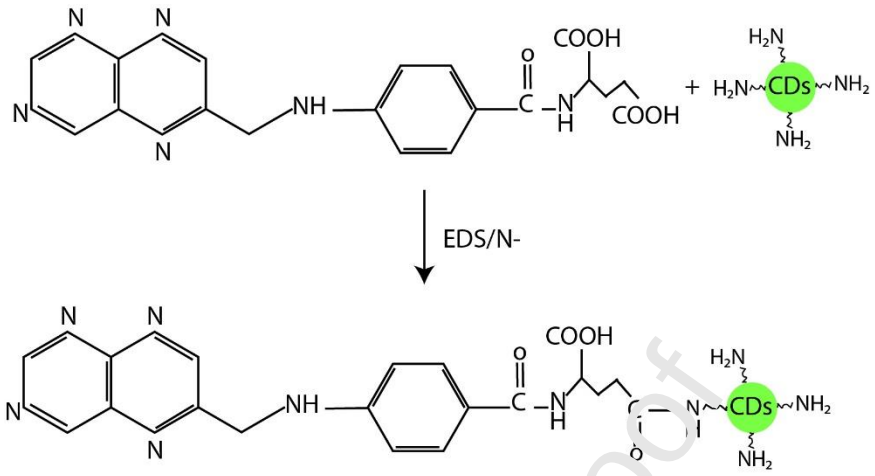


Figure 15 The covalent conjugation of FA to the green PL CDs [163]. Copyright 2017 Royal Society of Chemistry.

### 7.3. Polymer Capping

There are plenty of defects on the surface of CDs make them suffering from non-radiative re-combination, which would cause decrease in PL QY [165]. Presence of these traps is due to the synthesis and surface passivation techniques like capping these QDs with polymer chains, or other organic molecules would be inevitable to eliminate these imperfections [166]. Also, this adjustment will enhance optical properties as well [166]. Shen et al. [60] addressed PL quenching problem under acidic conditions by introducing a GQDs surface passivated by PEG. They reported a bright PL in water solution of neutral pH while the PL peaks dropped by only 25% under both alkaline and acidic conditions. Therefore, capping them with polymers also is beneficial from this point of view. Sun et al. [55] utilized diamine-terminated oligomeric poly-(ethylene glycol) $H_2NCH_2(CH_2CH_2O)_nCH_2CH_2CH_2NH_2$ (average n ≅ 35, PEG1500N) for surface passivation. They mixed PEG1500N with acid-treated particles and heated to 120 °C for 72 h. By this means, surface energy traps decreased, and the QY ranged from 4% up to 10% due to the effectiveness of surface passivation. Gonçalves et al. [167], fabricated CQDs by laser ablation and functionalized them with $PEG_{200}$ and mercaptosuccinic acid (MSS). Their results showed that by increasing the reaction time, surface defects decrease, and PL intensity increases. Milosavljevic et al. [168] compared the influence of PEG, polyvinylpyrrolidone (PVP), and bovine serum albumin protein (BSA) as capping chemicals on the PL intensity of CQDs. They concluded that the highest PL was for CDs capped by BSA.

In the case of biological applications, cytotoxicity and environmental threat of these materials are vital factors which researchers are concerned about [55]. Some researchers investigated the influence of capping of QDs on their toxicity. Chandra et al. [169], mitigated the toxicity of GQDs by embedding them in PEG matrix. After synthesizing GQDs from multi-walled carbon nanotubes (C-GQDs), they PEGylated them to form P-GQDs and performed hydrothermal protocol to produce hydrothermally treated-GQDs (H-GQDs) as a control sample. Figure 16a,b illustrates the impact of each treatment on cell viability. The influence of PEGylation on decreasing the toxicity of GQDs in high concentrations was significant. As side effects, PEGylation improved drug delivery ability and dropped ROS as it is comparable in Figure 16c,d and Figure 16e,f, respectively [169]. Chong et al. [170] reported that PEG-GQD had almost no toxicity on Hela cells. Yang et al. [171] used CQDs modified with cresyl violet (one of organic dyes) and coated with PEG for tumor imaging in vivo in mice. Non-toxic behavior of these CQDs demonstrates their potential for bio-imaging.

Except for PEG, other polymers and molecules were used as passivation agents. Sachdev et al. [172] opted PEI as passivation agent and compared its properties with PEG. Although the starting precursor, chitosan, was the same for two batches, the PL properties of CD-PEI was significantly better than CD-PEG in terms of high QY, strong PL intensity, and prolonged lifetime. Additionally, A549 and BHK-21 cells viability were higher for CD-PEI and their difference is tremendous for higher concentrations. Moreover, Gao et al. [114] showed that in the GQDs coated by PEI with various molecular weights, different PL emissions was detected. In this research U-87 cells were incubated with bare GQDs, $PEI_{1800}$GQDs, and $PEI_{600}$GQDs. After 18 h incubation, the yellow, blue, and red color of U-87 cells were indicated which were related to the GQDs, $PEI_{1800}$GQDs, and $PEI_{600}$GQDs, respectively (Figure 17a,d,g). The penetration capability of GQDs into the cells is also reported (Figure 17c,f,i).

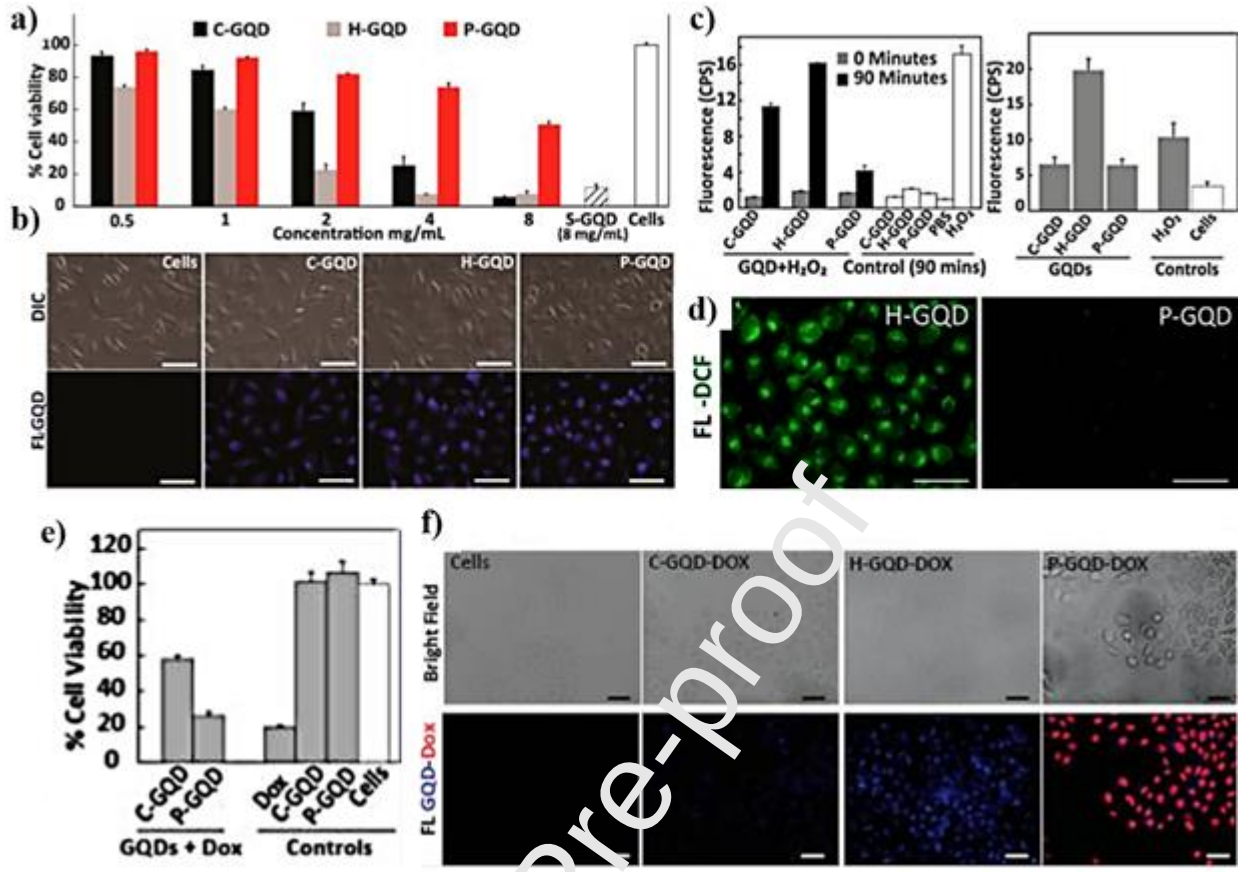


Figure 16. (a) Cell viability for C-GQD, H-GQD, and P-GQDs, as assessed by MTT. Controls: S-GQD (8 mg/mL); Only cells. (b) Cellular labeling of HeLa cells with GQDs. Blue: GQDs. Scale bar is 50 µm. (c) ROS production in a solution containing samples with 20 µM $H_2O_2$ at 0 and 90 min (left image) and Intracellular ROS in HeLa cells (right image). (d) Intracellular ROS image in HeLa cells. Green: DCF. Scale bar is 50 µm. (e) HeLa cell viability after incubation with P-GQD-Dox and C-GQD-Dox. (f) Intracellular delivery of DOX with P-GQD-DOX; red: DOX; blue: GQDs. Scale bar is 50 µm [169]. Copyright 2014 American Chemical Society.

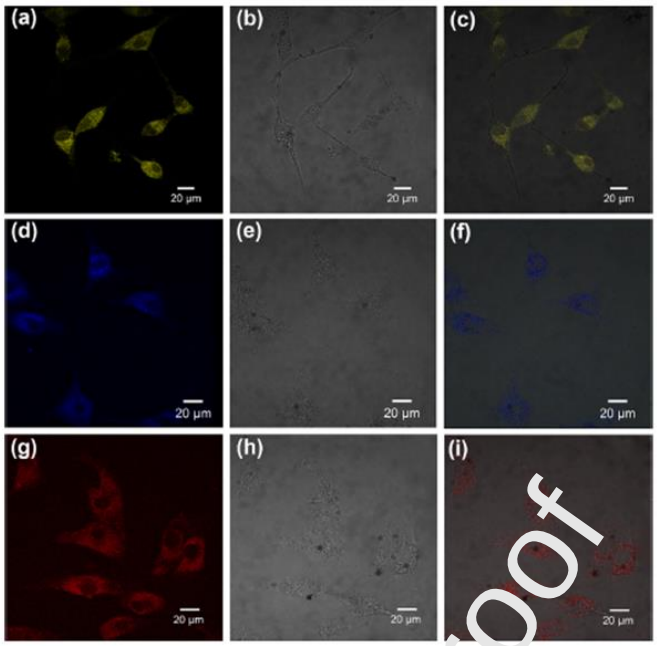


Figure 17. Confocal FL images of U-87 cells incubated with 50 μg $mL^{-1}$ GQDs (a−c), PEI1800 GQDs (d−f), and PEI600 GQDs (g−i) for 18 h. (a), (d), and (g) are the FL images of U-87 cells labeled with these three GQDs, with excitation at 405 nm. (b), (e), and (h) are the bright-field images of U-87 cells. (c), (f), and (i) are the merged images of U-87 cells incubated with three GQDs. [114]. Copyright 2017 American Chemical Society.

In another work, Havrdova et al. [173] used PEI, pristine and PEG coatings to find out the effect of surface charge on toxicity. They manifested that positively charged PEI was the most toxic coating, and even could enter the cell nucleus. In contrast, negatively charged pristine made some abnormalities because of interaction with cells and finally neutral PEG almost had no destructive effect on cells. In order to evaluate antibacterial properties, Liu et al. [174], prepared PEI-modified GQD and ZnO NPs nanocomposites by sol-gel method and compared its antibacterial characteristics with PEI-free ZnO/GQD. They realized that ZnO/GQD−PEI nanocomposites had egregious antibacterial properties toward E coli. compared with ZnO/GQD nanocomposites. This was due to PEI, which improved dispersion and adsorption of nanocomposite on bacterial cells. E.coli that treated with ZnO/GQD−PEI nanocomposite had lower survival rate than ZnO/GQD nanocomposite.

### 7.4. CDs composite-based nanomaterials

CQDs and GQDs have tremendous applications in different areas like optoelectronic, photovoltaic, sensors, and electronic devices. These applications are not only because of their excellent properties, but also for their interaction ability with other materials like MNPs [175, 176], silver NPs (Ag NPs) [177], and Au NPs [178, 179]. In addition, interaction of carbon-based nanomaterials with other nanomaterials can lead to tuning of some of the pristine

features and introduce novel properties. Several investigations have been performed on the combination of metal-organic frameworks (MOFs) and carbon-based nanomaterials [180, 181]. This combination leads to high surface area and microporosity, regarding the MOFs, and desirable optical and electronic properties of CDs and GQDs that can be used in different applications like photocatalysis, energy storage, and sensing [182]. Wang et al. [183] prepared CQDs@ZIF-8 nanocomposites at room temperature. The CQDs@ZIF-8 morphology was a regular diamond dodecahedral unit with porosity and revealed very strong orange-red PL emission. This emission also showed the success in CQDs coating on the ZIF-8.

CDs composite based nanomaterials can also be used in bio-applications. Ju et al. [184] designed a novel colorimetric sensor to detect glutathione (GSH) based on the intrinsic peroxidase-like activity of Ag NPs introduced on the N-doped GQDs. This nanocomposite provided a naked catalytic surface which could catalyze the oxidation of 3,3 5,5 - tetramethylbenzidine (TMB) in the presence of $H_2O_2$ accompanied by a visual color variation. Then, GSH could reduce oxidized TMB (oxTMB), and showed GSH concentration dependent UV-vis spectra. Consequently, the novel nanocomposite could detect GSH with a lower detection limit of 31 nM and a wide detection linear range of 0.1-157.6 µM.

Su et al. [185] fabricated the ECL detection based on the CQDs coated mesoporous silica NPs (MSNs) to detect MCF-7 cancer cells. Figure 18(a, b) shows FL imaging of the MCF-7 cancer cells after 8 hours incubation with CQDs@MSNs in the cell culture, and on the modified indium tin oxide electrode. Moreover, several factors affect the ECL intensity. Incubation time, for example, has a direct impact on the ECL intensity, which means that the higher the incubation time, the higher the ECL response and it started to have a slight increase after 50-min incubation as shown Figure 18c. Apart from the incubation time, the optimum ratio of the CQDs@MSNs to MUC1 aptamers that are used for nanoprobe fabrication is reported (Figure 18d). These nanocomposites showed not only desirable ECL behavior but also large surface areas and porous structure that provided the opportunities for electrons to move inside the structure, and additionally, provided more active site to immobilize the CQDs surface. An efficient film, 3D-GR@AuNPs, that induced suitable biocompatibility and conductivity is also used. Therefore, the ratio of about 4:1 of CQDs@MSNs to MUC1 aptamers, is the ideal ratio for the ECL nanoprobes fabrication. It is also shown that an increase in the amount of MCF-7 cancer cells also had an effect on the

ECL curve. The same condition for detection of the other cancer cells such as SKBr-3 or K562 is investigated, and is found that the ECL weak signal was the same as the background. While in contrast, it is demonstrated that MCF-7 cancer cells detection was significantly higher than K562 or SKBr-3 cancer cells (Figure 18e,f) [185].

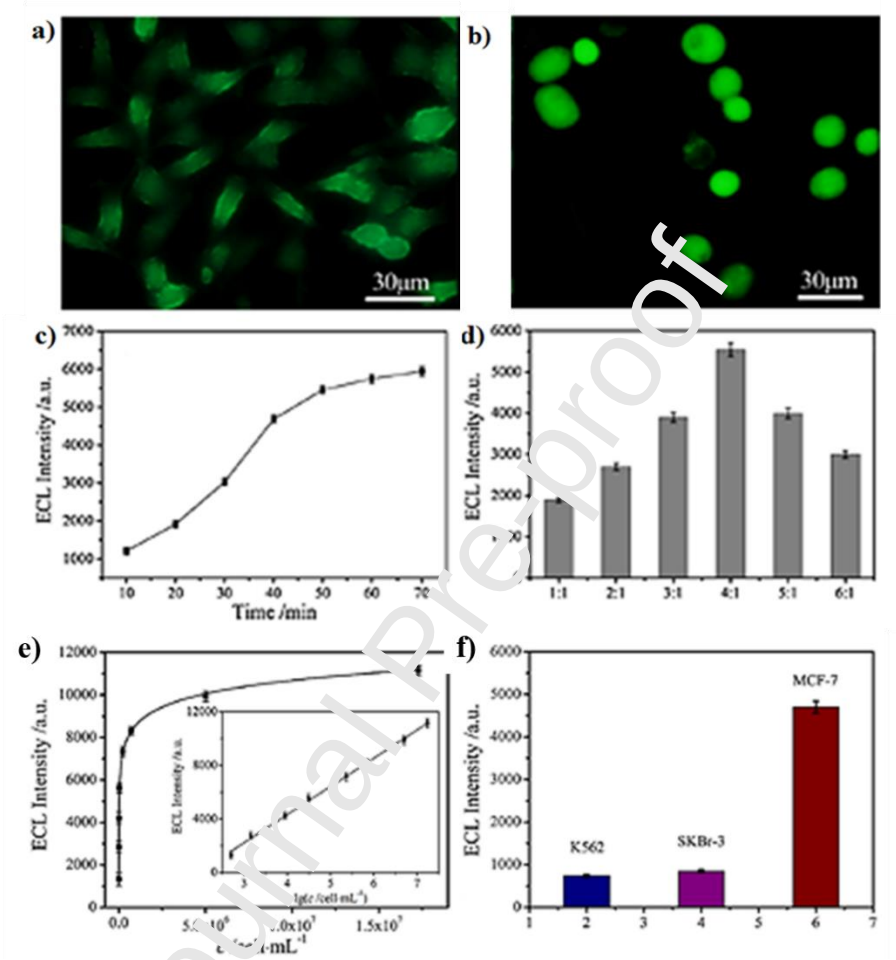


Figure 18. (a) FL imaging of the MCF-7 cancer cells after the incubation with CQDs@MSNs in the culture dish for 8h; (b) FL imaging of the MCF-7 cancer cells after cell capture onto the modified indium tin oxide electrode; (c) Effect of incubation time on ECL intensity; (d) Effect of the volume ratio of CQDs@MSNs (0.2gmL$^{-1}$) to muc1aptamers (0.2mg mL$^{-1}$) on ECL intensity. (e) Relationship between ECL intensity and cell concentration, each point was the average of ten measurements. Insert: logarithmic calibration curve for MCF-7 cancer cell. (f) Histograms for the specificity of the proposed ECL cyto-sensor. From left to right: 3.0×104 cell·mL$^{-1}$ K562 cancer cells; 3.0×104 cell·mL$^{-1}$ SKBr-3 cancer cells; 1.5×104 cell·mL$^{-1}$ MCF-7 cancer cells. [185]. Copyright 2014 Elsevier.

Nozaki et al. [186] revealed that N-doped CQDs acted as a suitable photosensitizer to generate $O_2$ under visible light using 9,10-anthracendipropionic acid (ADBA) as the trapping agent. Figure 19a,b shows that the white LED light irradiation decreases in the presence of N-doped CQDs within first 30 min. It was also demonstrated that the amounts of $O_2$ generation are highly dependent on the TA:PEI ratio. The most effective ratio of the TA:PEI that

produced the highest amount of oxygen was TA:PEI = 1. Au NPs with N-doped CQDs is also synthesized to enhance the $O_2$ generation and improve the photostability. CQDs were used to reduce Chloroauric acid ($HAuCl_4$ for Au NPs formation. The value of the $O_2$ generations of the synthesized nanocomposite were 2.3 times larger than N-CQDs, which revealed that adding Au NPs to the N-doped CQDs could boost the amounts of $O_2$ production. The PL decay (τ) of the N-CQDs and N-CQDs–Au NPs nanocomposite at 485 nm from 365 nm excitation is also investigated, and it was reported that the PL decay of the N-CQDs-Au NPs nanocomposites (ca. 2.3 ns) was larger than PL decay of N-CQDs (ca.1.5 ns) (Figure 19c).

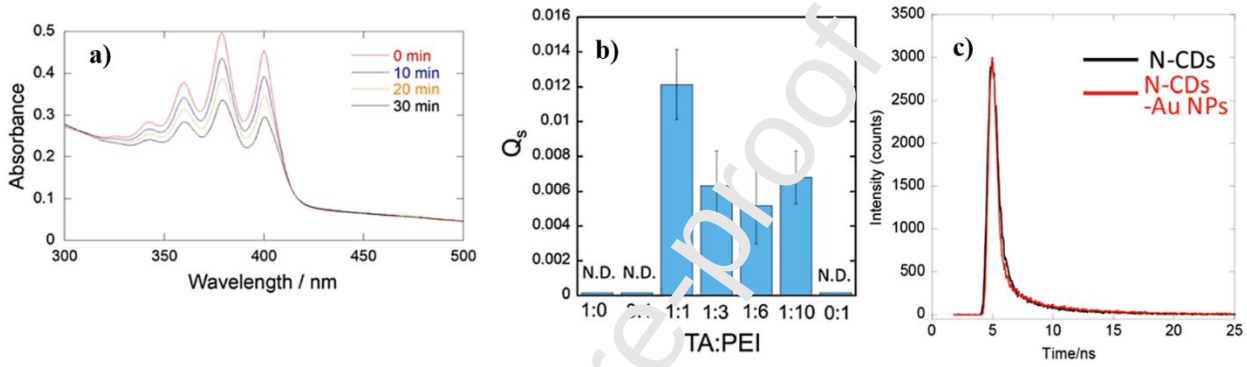


Figure 19. (a) UV-Vis spectra of ADBA aqueous solution in the presence of N-CDs (TA : PEI = 1 : 1). (b) The 1O2 generation efficiency, Qs, of N-CDs with different TA:PEI. N.D denotes an undetectable 1O2. (c) PL decay curves for N-CDs. [186]. Copyright 2019 Royal Society of Chemistry.

### 7.5. Core-shell structures

Core-shell architecture is another convenient way to modify NPs like QDs for biomedical applications [187]. Researchers mostly used this modification of CDs for bio-sensors. Bhogal et al. [188] made a core shell structure based on CDs as core and a molecularly imprinted polymer (MIP) as shell by sol-gel method. They used this product for sensing ketoprofen. The MIP has the capability of specific detection, and the CDs showed suitable PL properties, therefore their core-shell structure is useful for accurate sensing. The CDs obtained by pyrolysis of citric acid. The carboxyl group of CDs and amine group of N-β-(aminoethyl)-γ-aminopropyltrimethoxysilane (AEAP) reacted and CDs bonded to AEAP. AEAP had the role of both functionalizing agent and monomer for polymerization. The quenching of PL of CDs in presence of ketoprofen was the key of sensing. The quenching strongly depended on concentration of the drug.

Some metallic NPs like Ag have been used in number of research to making a core-shell with CDs. Confinement of electrons and holes on the surface of CDs is the main reason of their PL

properties. So the interaction between metallic ions and the CDs leads to entrapment of electrons and holes, and lower radiative recombination and results in quenching of PL [189]. Kong et al. [190] produced the GQDs@Ag core-shell which was applied for sensing uric acid. Ag shell covered the GQDs and quenched the PL of GQDs. The method of sensing was based on the etching of Ag shell with $H_2O_2$ of uric acid. After the removal of the shell the PL recovered. By increasing the amount of uric acid, the $H_2O_2$ rose up and the PL intensity was enhanced. Another research used a core-shell structure that included Ag NPs, and GQDs for sensing prostate specific antigen (PSA). The synthesis of this product was based on the electrostatic interactions between carboxyl and hydroxyl groups of GQDs and the $Ag(NH_3)_2^+$ cation that is adsorbed on their surface. Afterwards, the agglomeration of $Ag°(NH_3)_2$ resulted in making clusters and they finally turned to Ag NPs. The Ag NPs that quenched PL of GQDs would be etched by $H_2O_2$ and reestablished the PL GQDs. The PL intensity enhancement was observed by increasing the concentration of PSA [191]. Ma et al. [192] applied the CDs@AgNPs core-shell structure for detection of glucose. They demonstrated that Ag ions of $AgNO_3$ solution interacted with functional groups on the surface of CDs such as the carboxyl group and the amine group. At that time, the combination of CDs and $Ag^+$ ions reduced to Ag NPs by $NaBH_4$ and core-shell was made. They reported that the Ag NPs quenched the PL and the $H_2O_2$ which was generated during the oxidation of glucose to gluconic acid, eliminated the Ag shell released the CDs and re-established PL. So, this CD@AgNPs is useful as a sensor for glucose (Figure 20).

Table 3 shows a brief summary about some selected research on CD modification methods.

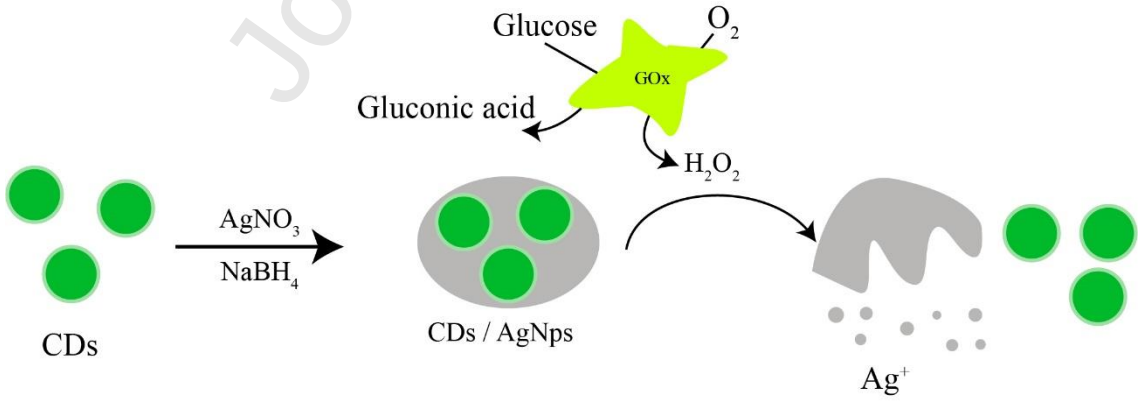


Figure 20. PL turn-on strategy for glucose detection based on combination of CDs supported on Ag NPs and GOx-mediated oxidation of glucose.[192]. Copyright 2016 American Chemical Society.

Table 3. A brief listing of selected works on GQD/CQD surface modification methods

| Material | Agent for Modification | Application | Goal | Ref. |
|---|---|---|---|---|
| Doping | | | | |
| GQDs | Nitrogen | Biomedical imaging and optoelectronic applications | superior luminescence characteristic | [134] |
| GQDs | Nitrogen | Bio-imaging | A high QY of maximum 24.6%, bright luminescence and excellent biocompatibility | [136] |
| CQDs | Nitrogen | Biomedical imaging | Independent emission behaviors, QY: 32.4%, and PL:6.56 ns | [139] |
| GQDs | Nitrogen | Increased biocompatibility for biomedical uses | Increase the GQDs QY to 24.62% | [193, 194] |
| GQDs | Nitrogen, and sulfur | Light emitting devices and bioanalytical applications. | PL QY is 9.3-fold higher than undoped GQDs and ECL efficiency is 5.8-fold higher than undoped GQDs. | [72] |
| GQDs | Nitrogen, and sulfur | Improving PL applications | photoconversion efficiency $(\eta)$~1.46% and incident-photon-to-current conversion efficiency (IPCE) ~ 92.48% at 340 nm. | [195] |
| GQDs | Nitrogen and Chlorine-doped | Bio-imaging | No Toxicity, QY: 20.39%, Cell Viability: 90–100%, | [151] |

| | | | | |
|---|---|---|---|---|
| CQDs | Cu | Bio-imaging and Bio-sensing | QY: 56% | [142] |
| GQDs | Sulfur | Cell-imaging | Low Cytotoxicity, easily penetrated into the cell membranes of HeLa cell | [143] |
| GQDs | Nitrogen | Sensing and Cell-imaging | ideal ionic stability, hydrophilicity and antiphotobcleaching properties, PL QY ≅ 29% | [196] |
| GQDs | Nitrogen | Sensing and Cell-imaging | high QY of 64.2%, efficient fluorescent probe for detecting Cr(VI) | [197] |
| GQDs | Boron | Bio-imaging (as MRI contrast agent) | Improved magnetic properties, improved stability, increased contrast capability | [198] |
| Surface functionalization | | | | |
| GQDs | Arginine | Bio-sensor | QY: 28.3%, Low Cytotoxicity, | [153] |
| GQDs | Cysteine | Bio-sensor | QY: 28%, highly selective for $Hg^{2+}$, High crystallinity | [156] |
| GQDs | Amino | Bio-sensor | -- | [199] |
| GQDs | Amino | Bio-sensor | QY: 13.8%, $Fe^{3+}$ ion detection | [157] |
| CQDs | Thiosemicarbazide | Bio-sensor | Strong PL Intensity, Highly Sensitive & Selective Detection of Trace $Cu^{2+}$ | [158] |

| | | | | |
|---|---|---|---|---|
| GQDs | D-penicillamine (DPA) | Bio-sensor | great promise as an alternative to previous fluorescent probes for bio-labeling and sensing | [200] |
| GQDs | Diamine | Chelating and Antioxidant activities | QY: 22%, highly sensitive to trap Fe(II), and Cu(II) | [201] |
| CQDs | Carboxyl/Amino | Drug delivery/Bio-imaging | Image guided drug delivery to brain for cancer therapy | [202] |
| CQDs | Carboxyl | Bio-imaging | Better water dispersion | [203] |
| Polymer Capping | | | | |
| GQDs | PPy (polypyrrole) | Dopamine (DA) sensor | High selectivity and sensitivity | [204] |
| CDs | N-Isopropylacrylamide (NIPAAM) | Bio-imaging | QY and stability improvement + reduce toxicity | [205] |
| N-CDs | Polyethylenimine (PEI) | Imaging + crossing blood brain barrier (BBB) | QY increase + low toxicity | [206] |
| CDs | Polyamidoamine (PAMAM) | Bio-sensor | New biocompatibility platform + increasing stability | [207] |
| CDs | Poly(N-vinylcaprolactam) (PVCL) | Bio-sensor<br>Bio-imaging | Enhancement in biocompatibility | [208] |
| GQDs | Polyethylene glycol (PEG) | Accelerating photoactive regen | Photodynamic therapy<br>(PDT) | [209] |
| N-GQDs | Molecularly imprinted polymer (MIPs) | Sensing tetracycline (TC) | High sensitivity and accuracy | [210] |
| CDs composite-based nanomaterials | | | | |

| | | | | |
|---|---|---|---|---|
| GQDs | $Fe_3O_4$ | Bio-sensor | Detection of Amino Acid | [175] |
| GQDs | $Fe_3O_4$/anti IgG/BSA | Bio-imaging | Diagnosis renal disease | [211] |
| GQDs | $Cu_2O$ | Antibacterial | High antibacterial activity against E. Coli, and Staphylococcus aureus. | [212] |
| GQDs | $Gd_2O_3$ | Bio-imaging | dual-modality magnetic resonance imaging and fluorescent probes | [213] |
| GQDs | Carboxymethyl cellulose (CMC) | Anticancer film and drug delivery system | DOX-loaded nanocomposite | [214] |
| CQDs | $MnO_2$ | Bio-sensor | Fluorescent probe for biomolecule detection | [215] |
| GQDs | RGD and DOX | chemo-photothermal combination therapy | - great photothermal efficacy for cancer cells<br>- pH-responsive drug-release behavior<br>- good ability of cellular uptake | [216] |
| S-GQDs | Ag | Antibacterial | Improve cell viability | [217] |
| GQDs | Multiwalled Carbon Nanotubes | Bio-sensor | Increased detection of Dopamine in human serum (from living PC12 cells) | [218] |
| CQDs | Zinc Oxide | Antibacterial | High antibacterial activity against Gram- negative and Gram- positive bacteria (E.coli and | [219] |

| | | | | |
|---|---|---|---|---|
| | | | S.aureus) | |
| CQDs | Chitosan | Bio-sensor | Immobilization of insulin aptamers for accurate insulin detection | [220] |
| Core-shell structures | | | | |
| CQDs | Au | Biosensor | PL turn-off up to 96% | [189] |
| GQDs | Ag | Biosensor | Detection of Uric Acid | [190] |
| GQDs | Ag | Biosensor | Detection of Prostate Specific Antigen | [191] |

# 8. Conclusion and Perspectives

Carbon-based nanomaterials consider as an emerging technology in biomedical applications due to their unique physicochemical properties. This article has discussed the recent progress in the methods of synthesis, optical properties, and toxicity of CDs, focusing on their modification strategies for biomedical applications. The applications highlighted, included; bio-imaging, drug/gene delivery, cancer treatment, and biosensing. The synthesis processes of CDs are facile and can be achieved by using low cost and abundant materials. However, there is still a lack of a standard method for synthesis of CDs, especially under GMP (Good Manufacturing Practice) with a defined morphology, composition, structure, and high quantum yield. This is essential for obtaining FDA (Food and Drug Administration) regulatory approval for clinical trials as well as commercialization of the products for clinical applications. Investigation on the synthesis of CDs with desirable shapes, sizes, and specific targeting characteristics with the modified surfaces and the engineered band gaps are scopes of future investigation. An example of the application of CDs in clinical imaging is the localization of sentinel nodes (SLN). The SLN are the first place that cancer is likely to spread. In breast cancer, the sentinel node is usually located in the axillary nodes, under the arm. The SLN biopsy is a surgical procedure used to determine whether cancer has spread beyond a primary tumor into your lymphatic system. Organic dyes and radiocolloid are currently used for SLN mapping but expose patients to radiation which cause tissue damage. CDs are the ideal technology to be used for live SLN mapping, there have some experimental and preclinical animal tests, however still waiting to move to the clinical setting. The CDs are photostable and have improved deep tissue penetration. Experimental have shown the slow elimination of CDs raises concerns of potential accumulation, including the study effect of CDs on the blood-brain barrier (BBB). Nevertheless, an encouraging outcome with CDs in recent in vivo studies suggest huge potential for cancer diagnostic and therapy. However, in comparison with traditional QDs, CDs show unique properties that extend their applications in the biological field. However, they face many challenges, including biocompatibility, toxicity, a lifetime in applications, pharmacokinetics, and clearance from the body, BBB, and

in vivo targeting efficiency. The latter also depends on the depth of the tissue that requires imaging as well as the color of the tissue. Therefore, it seems crucial to extend investigations of CDs within the biological environment at the preclinical animal model studies before starting clinical trials in humans. Nevertheless, this step also can be enormously challenging, so new techniques should be developed to indicate CDs' behavior in physiological biological matrices. Biosensors are easier to develop for clinical use; this is due to its assessment is carried out outside the body. For example newly emerging diseases such as COVID-19, there is a demand for fast and accurate diagnostics methods, due to the high QY, photo-, chemical-stability, and excellent electro-catalytic activity, CDs have been used to develop highly sensitive biosensors and have shown their potential for clinical use in the future. They still need to be improved for a higher selectivity to avoid auto-fluorescence and background. CDs can be a suitable candidate for drug and gene delivery, though limited research is allocated to this matter. Scientists are using targeted receptors to improve specific targeting of CDs in gene/drug delivery, but more research is still needed. Considering the potential of surface-modified CDs, we believe that in near future, more research will be focused on the progress of modification methods to overcome the limitations of CDs for biological applications as a multifunctional agent, for instance, they can be used as both imaging and sensing probes and delivery agents simultaneously. In summary, the lack of optimal design for CDs and surface functionalization and conjugation to drug and other molecules for delivery to target cells gives plenty of room for the research and development of the ideal CDs, which is indicated for the future of CDs in biomedical applications. Drugs/gene and molecules deliver as well as biomolecular imaging and biosensors are a multi-billion dollar industry with huge interest to clinicians, academia as well as pharmaceutical and medical devices industries.

# References:


1. Farshbaf, M., et al., *Carbon quantum dots: recent progresses on synthesis, surface modification and applications.* Artificial cells, nanomedicine, and biotechnology, 2018. **46**(7): p. 1331-1348.

2. Shen, J., et al., *Graphene quantum dots: emergent nanolights for bioimaging, sensors, catalysis and photovoltaic devices.* Chemical communications, 2012. **48**(31): p. 3686-3699.

3. Divakaran, D., et al., *Dragon fruit extract capped gold nanoparticles: Synthesis and their differential cytotoxicity effect on breast cancer cells.* Materials Letters, 2019. **236**: p. 498-502.

4. Kunzmann, A., et al., *Efficient internalization of silica-coated iron oxide nanoparticles of different sizes by primary human macrophages and dendritic cells.* Toxicology and applied pharmacology, 2011. **253**(2): p. 81-93.

5. Li, S., et al., *Nanocomposites of polymer and inorganic nanoparticles for optical and magnetic applications.* Nano reviews, 2010. **1**(1): p. 5214.

6. Couvreur, P., et al., *Biodegradable polymeric nanoparticles as drug carrier for antitumor agents*, in *Polymeric nanoparticles and microspheres*. 2018, CRC Press. p. 27-94.

7. Dave, V., et al., *Synthesis and characterization of celecoxib loaded PEGylated liposome nanoparticles for biomedical applications.* Nano-Structures & Nano-Objects, 2019. **18**: p. 100288.

8. Wagner, A.M., et al., *Quantum dots in biomedical applications.* Acta Biomaterialia, 2019. **94**: p. 44-63.

9. Zou, X., et al., *Mechanisms of the antimicrobial activities of graphene materials.* Journal of the american chemical society, 2016. **138**(7): p. 2064-2077.

10. Xu, X., et al., *Electrophoretic analysis and purification of fluorescent single-walled carbon nanotube fragments.* Journal of the American Chemical Society, 2004. **126**(40): p. 12736-12737.

11. Dong, J., et al., *Application of graphene quantum dots for simultaneous fluorescence imaging and tumor-targeted drug delivery.* Sensors and Actuators B: Chemical, 2018. **256**: p. 616-623.

12. Li, K., et al., *Technical synthesis and biomedical applications of graphene quantum dots.* Journal of Materials Chemistry B, 2017. **5**(25): p. 4811-4826.

13. Wang, R., et al., *Recent progress in carbon quantum dots: synthesis, properties and applications in photocatalysis.* Journal of Materials Chemistry A, 2017. **5**(8): p. 3717-3734.

14. Namdari, P., B. Negahdari, and A. Eatemadi, *Synthesis, properties and biomedical applications of carbon-based quantum dots: An updated review.* Biomedicine & Pharmacotherapy, 2017. **87**: p. 209-222.

15. Zheng, X.T., et al., *Glowing graphene quantum dots and carbon dots: properties, syntheses, and biological applications.* Small, 2015. **11**(14): p. 1620-1636.

16. Choi, Y., et al., *Microwave-assisted synthesis of luminescent and biocompatible lysine-based carbon quantum dots.* Journal of industrial and engineering chemistry, 2017. **47**: p. 329-335.

17. Wang, Z., H. Zeng, and L. Sun, *Graphene quantum dots: versatile photoluminescence for energy, biomedical, and environmental applications.* Journal of Materials Chemistry C, 2015. **3**(6): p. 1157-1165.

18. Liu, M.-L., et al., *Carbon dots prepared for fluorescence and chemiluminescence sensing.* Science China Chemistry, 2019: p. 1-14.

19. Jegannathan, P., et al., *Enhancement of graphene quantum dots based applications via optimum physical chemistry: A review.* Biocybernetics and Biomedical Engineering, 2018. **38**(3): p. 481-497.

20. Wang, Y. and A. Hu, *Carbon quantum dots: synthesis, properties and applications.* Journal of Materials Chemistry C, 2014. **2**(34): p. 6921-6939.

21. Yang, Z.-C., et al., *Intrinsically fluorescent carbon dots with tunable emission derived from hydrothermal treatment of glucose in the presence of monopotassium phosphate.* Chemical communications, 2011. **47**(42): p. 11615-11617.

22. Tang, Q., et al., *Rapid conversion from carbohydrates to large-scale carbon quantum dots for all-weather solar cells.* ACS nano, 2017. **11**(2): p. 1540-1547.

23. Yang, Y., et al., *One-step synthesis of amino-functionalized fluorescent carbon nanoparticles by hydrothermal carbonization of chitosan.* Chemical Communications, 2012. **48**(3): p. 380-382.

24. Liang, Z., et al., *Probing energy and electron transfer mechanisms in fluorescence quenching of biomass carbon quantum dots.* ACS applied materials & interfaces, 2016. **8**(27): p. 17478-17488.

25. Zhu, S., et al., *Highly photoluminescent carbon dots for multicolor patterning, sensors, and bioimaging.* Angewandte Chemie International Edition, 2013. **52**(14): p. 3953-3957.

26. Dong, Y., et al., *Blue luminescent graphene quantum dots and graphene oxide prepared by tuning the carbonization degree of citric acid.* Carbon, 2012. **50**(12): p. 4738-4743.

27. De, B. and N. Karak, *A green and facile approach for the synthesis of water soluble fluorescent carbon dots from banana juice.* Rsc Advances, 2013. **3**(22): p. 8286-8290.

28. Sahu, S., et al., *Simple one-step synthesis of highly luminescent carbon dots from orange juice: application as excellent bio-imaging agents.* Chemical Communications, 2012. **48**(70): p. 8835-8837.

29. Pan, D., et al., *Hydrothermal route for cutting graphene sheets into blue-luminescent graphene quantum dots.* Advanced materials, 2010. **22**(6): p. 734-738.

30. Xu, M., et al., *Hydrothermal/Solvothermal Synthesis of Graphene Quantum Dots and Their Biological Applications.* Nano Biomedicine & Engineering, 2013. **5**(2): p. 65-71

31. Li, H., et al., *Water-soluble fluorescent carbon quantum dots and photocatalyst design.* Angewandte Chemie International Edition, 2010. **49**(26): p. 4430-4434.

32. Ahirwar, S., S. Mallick, and D. Bahadur, *Electrochemical method to prepare graphene quantum dots and graphene oxide quantum dots.* ACS Omega, 2017. **2**(11): p. 8343-8353.

33. Zhao, Q.-L., et al., *Facile preparation of low cytotoxicity fluorescent carbon nanocrystals by electrooxidation of graphite.* Chemical Communications, 2008(41): p. 5116-5118.

34. Deng, J., et al., *Electrochemical synthesis of carbon nanodots directly from alcohols.* Chemistry–A European Journal, 2014. **20**(17): p. 4993-4999.

35. Bao, L., et al., *Electrochemical tuning of luminescent carbon nanodots: from preparation to luminescence mechanism.* Advanced Materials, 2011. **23**(48): p. 5801-5806.

36. Cao, L., et al., *Carbon dots for multiphoton bioimaging.* Journal of the American Chemical Society, 2007. **129**(37): p. 11318-11319.

37. Yang, S.-T., et al., *Carbon dots for optical imaging in vivo.* Journal of the American Chemical Society, 2009. **131**(32): p. 11308-11309.

38. Wang, X., et al., *Photoinduced electron transfers with carbon dots.* Chemical Communications, 2009(25): p. 3774-3776.

39. Hu, S., et al., *Laser synthesis and size tailor of carbon quantum dots.* Journal of Nanoparticle Research, 2011. **13**(12): p. 7247-7252.

40. Hu, S.-L., et al., *One-step synthesis of fluorescent carbon nanoparticles by laser irradiation.* Journal of Materials Chemistry, 2009. **19**(4): p. 484-488.

41. Santiago, S., et al., *Synthesis of N-doped graphene quantum dots by pulsed laser ablation with diethylenetriamine (DETA) and their photoluminescence.* Physical Chemistry Chemical Physics, 2017. **19**(33): p. 22395-22400.

42. Doñate-Buendia, C., et al., *Fabrication by laser irradiation in a continuous flow jet of carbon quantum dots for fluorescence imaging.* ACS omega, 2018. **3**(3): p. 2735-2742.

43. Dey, S., et al., *New methods of synthesis and varied properties of carbon quantum dots with high nitrogen content.* Journal of Materials Research, 2014. **29**(3): p. 383-391.

44. Tang, Y., et al., *Carbon nitride quantum dots: a novel chemiluminescence system for selective detection of free chlorine in water.* Analytical chemistry, 2014. **86**(9): p. 4528-4535.

45. Zhao, L., et al., *Chemiluminescence of carbon dots under strong alkaline solutions: a novel insight into carbon dot optical properties.* Nanoscale, 2013. **5**(7): p. 2655-2658.

46. Singh, R., et al., *Progress in microwave-assisted synthesis of quantum dots (graphene/carbon/semiconducting) for bioapplications: a review.* Materials Today Chemistry, 2019. **12**: p. 282-314.

47. Zhu, H., et al., *Microwave synthesis of fluorescent carbon nanoparticles with electrochemiluminescence properties.* Chemical Communications, 2009(34): p. 5118-5120.

48. Li, W., et al., *Three Minute Ultrarapid Microwave-Assisted Synthesis of Bright Fluorescent Graphene Quantum Dots for Live Cell Staining and White LEDs.* ACS Applied Nano Materials, 2018. **1**(4): p. 1623-1630.

49. Nguyen, H.Y., et al., *Microwave-assisted synthesis of graphene quantum dots and nitrogen-doped graphene quantum dots: Raman characterization and their optical*

*properties.* Advances in Natural Sciences: Nanoscience and Nanotechnology, 2019. **10**(2): p. 025005.

50. Li, H., et al., *Carbon nanodots: synthesis, properties and applications.* Journal of materials chemistry, 2012. **22**(46): p. 24230-24253.

51. Kelarakis, A., *From highly graphitic to amorphous carbon dots: A critical review.* MRS Energy & Sustainability, 2014. **1**.

52. Zhu, S., et al., *The photoluminescence mechanism in carbon dots (graphene quantum dots, carbon nanodots, and polymer dots): current state and future perspective.* Nano research, 2015. **8**(2): p. 355-381.

53. Kim, S., et al., *Anomalous behaviors of visible luminescence from graphene quantum dots: interplay between size and shape.* ACS nano, 2012. **6**(9): p. 8203-8208.

54. Sciortino, A., A. Cannizzo, and F. Messina, *Carbon Nanodots: A Review—From the Current Understanding of the Fundamental Photophysics to the Full Control of the Optical Response.* C, 2018. **4**(4): p. 67.

55. Sun, Y.-P., et al., *Quantum-sized carbon dots for bright and colorful photoluminescence.* Journal of the American Chemical Society, 2006. **128**(24): p. 7756-7757.

56. Eda, G., et al., *Blue photoluminescence from chemically derived graphene oxide.* Advanced materials, 2010. **22**(4): p. 505-509.

57. Ritter, K.A. and J.W. Lyding, *The influence of edge structure on the electronic properties of graphene quantum dots and nanoribbons.* Nature materials, 2009. **8**(3): p. 235.

58. Zhu, S., et al., *Surface chemistry routes to modulate the photoluminescence of graphene quantum dots: from fluorescence mechanism to up-conversion bioimaging applications.* Advanced Functional Materials, 2012. **22**(22): p. 4732-4740.

59. Fan, L., et al., *Fluorescence resonance energy transfer quenching at the surface of graphene quantum dots for ultrasensitive detection of TNT.* Talanta, 2012. **101**: p. 192-197.

60. Shen, J., et al., *Facile preparation and upconversion luminescence of graphene quantum dots.* Chemical communications, 2011. **47**(9): p. 2580-2582.

61. Chen, S., et al., *Full-range intracellular pH sensing by an aggregation-induced emission-active two-channel ratiometric fluorogen.* Journal of the American Chemical Society, 2013. **135**(13): p. 4926-4929.

62. Shen, J., et al., *One-pot hydrothermal synthesis of graphene quantum dots surface-passivated by polyethylene glycol and their photoelectric conversion under near-infrared light.* New Journal of Chemistry, 2012. **36**(1): p. 97-101.

63. Gu, J., et al., *Facile synthesis and photoluminescence characteristics of blue-emitting nitrogen-doped graphene quantum dots.* Nanotechnology, 2016. **27**(16): p. 165704.

64. Khan, F. and J.H. Kim, *Emission-wavelength-dependent photoluminescence decay lifetime of N-functionalized graphene quantum dot downconverters: Impact on conversion efficiency of Cu (In, Ga) Se 2 solar cells.* Scientific reports, 2019. **9**(1): p. 10803.

65. Dai, Y., et al., *Tailoring of ammonia reduced graphene oxide into amine functionalized graphene quantum dots through a Hofmann rearrangement.* Rsc Advances, 2016. **6**(41): p. 34514-34520.

66. Zhuo, S., M. Shao, and S.-T. Lee, *Upconversion and downconversion fluorescent graphene quantum dots: ultrasonic preparation and photocatalysis.* ACS nano, 2012. **6**(2): p. 1059-1064.

67. Gan, Z., H. Xu, and Y. Hao, *Mechanism for excitation-dependent photoluminescence from graphene quantum dots and other graphene oxide derivates: consensus, debates and challenges.* Nanoscale, 2016. **8**(15): p. 7794-7807.

68. Chen, B.B., et al., *Self-exothermic reaction prompted synthesis of single-layered graphene quantum dots at room temperature.* Chemical Communications, 2017. **53**(36): p. 4958-4961.

69. Wang, N., et al., *The aggregation induced emission quenching of graphene quantum dots for visualizing the dynamic invasions of cobalt (ii) into living cells.* Journal of Materials Chemistry B, 2017. **5**(31): p. 6394-6399.

70. Li, Y., et al., *Aggregation induced red shift emission of phosphorus doped carbon dots.* Rsc Advances, 2017. **7**(51): p. 32225-32228.

71. Xu, Y., et al., *Applications of carbon quantum dots in electrochemiluminescence: a mini review.* Electrochemistry Communications, 2014. **48**: p. 151-154.

72. Zhang, R., et al., *Electrochemiluminescence of nitrogen-and sulfur-doped graphene quantum dots.* Carbon, 2018. **129**: p. 45-53.

73. Lu, Q., et al., *Electrochemiluminescence resonance energy transfer between graphene quantum dots and gold nanoparticles for DNA damage detection.* Analyst, 2014. **139**(10): p. 2404-2410.

74. Wang, R., et al., *Strong Electrochemiluminescence Emission from Oxidized Multiwalled Carbon Nanotubes.* Small, 2019: p. 1901550.

75. Liang, R.-P., et al., *Electrochemiluminescence resonance energy transfer between graphene quantum dots and graphene oxide for sensitive protein kinase activity and inhibitor sensing.* Analytica chimica acta, 2016. **904**: p. 58-64.

76. Wu, L., et al., *Highly sensitive electrochemiluminescent cytosensing using carbon nanodot@ Ag hybrid material and graphene for dual signal amplification.* Chemical Communications, 2013. **49**(50): p. 5675-5677.

77. Ko, N., et al., *Graphene quantum dot-based theranostic agents for active targeting of breast cancer.* Rsc Advances, 2017. **7**(19): p. 11420-11427.

78. Bagheri, Z., et al., *Investigation the cytotoxicity and photo-induced toxicity of carbon dot on yeast cell.* Ecotoxicology and environmental safety, 2018. **161**: p. 245-250.

79. Wu, C., et al., *Insight into the cellular internalization and cytotoxicity of graphene quantum dots.* Advanced healthcare materials, 2013. **2**(12): p. 1613-1619.

80. Şenel, B., et al., *Graphene quantum dots: Synthesis, characterization, cell viability, genotoxicity for biomedical applications.* Saudi Pharmaceutical Journal, 2019.

81. Yuan, X., et al., *Cellular distribution and cytotoxicity of graphene quantum dots with different functional groups.* Nanoscale research letters, 2014. **9**(1): p. 108.

82. Fu, P.P., et al., *Mechanisms of nanotoxicity: generation of reactive oxygen species.* Journal of food and drug analysis, 2014. **22**(1): p. 64-75.

83. Meziani, M.J., et al., *Visible-light-activated bactericidal functions of carbon "Quantum" dots.* ACS applied materials & interfaces, 2016. **8**(17): p. 10761-10766.

84. Hoskins, C., A. Cuschieri, and L. Wang, *The cytotoxicity of polycationic iron oxide nanoparticles: common endpoint assays and alternative approaches for improved understanding of cellular response mechanism.* Journal of nanobiotechnology, 2012. **10**(1): p. 15.

85. Nurunnabi, M., et al., *In vivo biodistribution and toxicology of carboxylated graphene quantum dots.* Acs Nano, 2013. **7**(8): p. 6858-6867.

86. Goreham, R.V., et al., *Demonstration of the lack of cytotoxicity of unmodified and folic acid modified graphene oxide quantum dots, and their application to fluorescence lifetime imaging of HaCaT cells.* Microchimica Acta, 2018. **185**(2): p. 128.

87. Hoshyar, N., et al., *The effect of nanoparticle size on in vivo pharmacokinetics and cellular interaction.* Nanomedicine, 2016. **11**(6): p. 673-692.

88. Zhang, G., et al., *Influence of anchoring ligands and particle size on the colloidal stability and in vivo biodistribution of polyethylene glycol-coated gold nanoparticles in tumor-xenografted mice.* Biomaterials, 2009. **30**(10): p. 1928-1936.

89. Licciardello, N., et al., *Biodistribution studies of ultrasmall silicon nanoparticles and carbon dots in experimental rats and tumor mice.* Nanoscale, 2018. **10**(21): p. 9880-9891.

90. Guerrini, L., R. Alvarez-Puebla, and N. Pazos-Perez, *Surface modifications of nanoparticles for stability in biological fluids.* Materials, 2018. **11**(7): p. 1154.

91. Roy, P., et al., *Plant leaf-derived graphene quantum dots and applications for white LEDs.* New Journal of Chemistry, 2014. **38**(10): p. 4946-4951.

92. Malina, T., et al., *Carbon dots for in vivo fluorescence imaging of adipose tissue-derived mesenchymal stromal cells.* Carbon, 2019. **152**: p. 434-443.

93. Hu, X., X. An, and L. Li, *Easy synthesis of highly fluorescent carbon dots from albumin and their photoluminescent mechanism and biological imaging applications.* Materials Science and Engineering: C, 2016. **58**: p. 730-736.

94. Wang, W., et al., *Photobleaching and stabilization of carbon nanodots produced by solvothermal synthesis.* Physical Chemistry Chemical Physics, 2016. **18**(1): p. 466-475.

95. Jia, T., et al., *Mesoporous cerium oxide-coated upconversion nanoparticles for tumor-responsive chemo-photodynamic therapy and bioimaging.* Chemical Science, 2019. 10(37): p. 8618-8633.

96. Pedram, P., et al., *Cadmium sulfide quantum dots modified with the human transferrin protein siderophiline for targeted imaging of breast cancer cells.* Microchimica Acta, 2016. 183(1): p. 67-71.

97. Mazrad, Z.A.I., et al., *Target-specific induced hyaluronic acid decorated silica fluorescent nanoparticles@ polyaniline for bio-imaging guided near-infrared photothermal therapy.* Journal of Materials Chemistry B, 2017. **5**(34): p. 7099-7108.

98. Kumar, S.S.D., et al., *Cellular imaging and folate receptor targeting delivery of gum kondagogu capped gold nanoparticles in cancer cells.* International journal of biological macromolecules, 2018. **109**: p. 220-230.

99. Xia, J.-M., et al., *Folic acid modified copper nanoclusters for fluorescent imaging of cancer cells with over-expressed folate receptor.* Microchimica Acta, 2018. **185**(3): p. 205.

100. Kersting, D., et al., *From in vitro to ex vivo: Subcellular localization and uptake of graphene quantum dots into solid tumors.* Nanotechnology, 2019.

101. Yang, S.-T., et al., *Carbon dots as nontoxic and high-performance fluorescence imaging agents.* The Journal of Physical Chemistry C, 2009. **113**(42): p. 18110-18114.

102. Ge, J., et al., *Carbon dots with intrinsic theranostic properties for bioimaging, red-light-triggered photodynamic/photothermal simultaneous therapy in vitro and in vivo.* Advanced healthcare materials, 2016. **5**(6): p. 665-675.

103. Xue, B., et al., *Photoluminescent lignin hybridized carbon quantum dots composites for bioimaging applications.* International journal of biological macromolecules, 2019. **122**: p. 954-961.

104. Feng, T., et al., *Charge-convertible carbon dots for imaging-guided drug delivery with enhanced in vivo cancer therapeutic efficiency.* ACS nano, 2016. **10**(4): p. 4410-4420.

105. Siegel, R.L., K.D. Miller, and A. Jemal, *Cancer statistics, 2019.* CA: a cancer journal for clinicians, 2019. **69**(1): p. 7-34.

106. Jiang, B.P., et al., *Recent advances in carbon nanomaterials for cancer phototherapy.* Chemistry–A European Journal, 2019. **25**(16): p. 3993-4004.

107. Estanqueiro, M., et al., *Nanotechnological carriers for cancer chemotherapy: the state of the art.* Colloids and surfaces B: Biointerfaces, 2015. **126**: p. 631-648.

108. Duran, N., et al., *Nanobiotechnology of carbon dots: a review.* Journal of biomedical nanotechnology, 2016. **12**(7): p. 1323-1347.

109. Li, X., et al., *Recent Advances in Carbon Nanodots: Properties and Applications in Cancer Diagnosis and Treatment.* Journal of Analysis and Testing, 2019. **3**(1): p. 37-49.

110. Geng, B., et al., *NIR-responsive carbon dots for efficient photothermal cancer therapy at low power densities.* Carbon, 2018. **134**: p. 153-162.

111. Kam, N.W.S., et al., *Carbon nanotubes as multifunctional biological transporters and near-infrared agents for selective cancer cell destruction.* Proceedings of the National Academy of Sciences, 2005. **102**(33): p. 11600-11605.

112. Kang, E.B., et al., *pH-Selective Fluorescent Probe with Photothermal Ablation of Bacteria Based NIR Dye-Embedded Zwitterionic Carbon Dots.* Macromolecular Research, 2019: p. 1-9.

113. Zheng, M., et al., *One-pot to synthesize multifunctional carbon dots for near infrared fluorescence imaging and photothermal cancer therapy.* ACS applied materials & interfaces, 2016. **8**(36): p. 23533-23541.

114. Gao, T., et al., *Red, yellow, and blue luminescence by graphene quantum dots: syntheses, mechanism, and cellular imaging.* ACS applied materials & interfaces, 2017. **9**(29): p. 24846-24856.

115. Markovic, Z.M., et al., *Graphene quantum dots as autophagy-inducing photodynamic agents.* Biomaterials, 2012. **33**(29): p. 7084-7092.

116. Ge, J., et al., *A graphene quantum dot photodynamic therapy agent with high singlet oxygen generation.* Nature communications, 2014. **5**: p. 4596.

117. Ding, H., et al., *DNA–carbon dots function as fluorescent vehicles for drug delivery.* ACS applied materials & interfaces, 2015. **7**(12): p. 6889-6897.

118. Samantara, A.K., et al., *Good's buffer derived highly emissive carbon quantum dots: excellent biocompatible anticancer drug carrier.* Journal of Materials Chemistry B, 2016. **4**(14): p. 2412-2420.

119. Bao, W., et al., *pH- sensitive carbon quantum dots− doxorubicin nanoparticles for tumor cellular targeted drug delivery.* Polymers for Advanced Technologies, 2019. **30**(11): p. 2664-2673.

120. Wang, Z., et al., *Synthesis of strongly green-photoluminescent graphene quantum dots for drug carrier.* Colloids and Surfaces B: Biointerfaces, 2013. **112**: p. 192-196.

121. Mohammadinejad, R., et al., *Shedding light on gene therapy: carbon dots for the minimally invasive image-guided delivery of plasmids and noncoding RNAs.* Journal of advanced research, 2019. **18**: p. 81-93.

122. Jaleel, J.A., et al., *Carbon dot festooned and surface passivated graphene-reinforced chitosan construct for tumor-targeted delivery of TNF-α gene.* International journal of biological macromolecules, 2019. **127**: p. 628-636.

123. Ghosh, S., et al., *Dendrimer functionalized carbon quantum dot for selective detection of breast cancer and gene therapy.* Chemical Engineering Journal, 2019. **373**: p. 468-484.

124. Cheng, L., et al., *Polycation-b-polyzwitterion copolymer grafted luminescent carbon dots as a multifunctional platform for serum-resistant gene delivery and bioimaging.* ACS applied materials & interfaces, 2014. **6**(22): p. 20487-20497.

125. Hui, Y.Y., et al., *Carbon Nanomaterials for Bioimaging, Bioanalysis, and Therapy*. 2019: Wiley.

126. García-Mendiola, T., et al., *Carbon nanodots based biosensors for gene mutation detection.* Sensors and Actuators B: Chemical, 2018. **256**: p. 226-233.

127. Huang, Q., et al., *Pd-Au@ carbon dots nanocomposite: Facile synthesis and application as an ultrasensitive electrochemical biosensor for determination of colitoxin DNA in human serum.* Biosensors and Bioelectronics, 2017. **94**: p. 507-512.

128. Ji, H., et al., *Nitrogen-doped carbon dots as a new substrate for sensitive glucose determination.* Sensors, 2016. **16**(5): p. 630.

129. Sarkar, T., H. Bohidar, and P.P. Solanki, *Carbon dots-modified chitosan based electrochemical biosensing platform for detection of vitamin D.* International journal of biological macromolecules, 2018. **109**: p. 687-697.

130. Rezaei, B., et al., *Application of modified mesoporous boehmite (γ- AlOOH) with green synthesis carbon quantum dots for a fabrication biosensor to determine trace amounts of doxorubicin.* Luminescence, 2018. **33**(8): p. 1377-1386.

131. Huang, Q., et al., *A high performance electrochemical biosensor based on Cu 2 O–carbon dots for selective and sensitive determination of dopamine in human serum.* RSC Advances, 2015. **5**(67): p. 54102-54108.

132. Lin, L., et al., *Intrinsic peroxidase-like catalytic activity of nitrogen-doped graphene quantum dots and their application in the colorimetric detection of H2O2 and glucose.* Analytica chimica acta, 2015. **869**: p. 89-95.

133. Zhang, F., et al., *Effect of lateral size of graphene quantum dots on their properties and application.* ACS applied materials & interfaces, 2016. **8**(3): p. 2104-2110.

134. Li, Y., et al., *Nitrogen-doped graphene quantum dots with oxygen-rich functional groups.* Journal of the American Chemical Society, 2011. **134**(1): p. 15-18.

135. Sk, M.A., et al., *Revealing the tunable photoluminescence properties of graphene quantum dots.* Journal of Materials Chemistry C, 2014. **2**(34): p. 6954-6960.

136. Hu, C., et al., *One-step preparation of nitrogen-doped graphene quantum dots from oxidized debris of graphene oxide.* Journal of Materials Chemistry B, 2013. **1**(1): p. 39-42.

137. Santiago, S.R.M., et al., *Effect of nitrogen doping on the photoluminescence intensity of graphene quantum dots.* Optics letters, 2017. **42**(18): p. 3642-3645.

138. Ju, J. and W. Chen, *Synthesis of highly fluorescent nitrogen-doped graphene quantum dots for sensitive, label-free detection of Fe (III) in aqueous media.* Biosensors and bioelectronics, 2014. **58**: p. 219-225.

139. Ren, X., et al., *Synthesis of N-Doped Micropore Carbon Quantum Dots with High Quantum Yield and Dual-Wavelength Photoluminescence Emission from Biomass for Cellular Imaging.* Nanomaterials, 2019. **9**(4): p. 495.

140. Travlou, N.A., et al., *S-and N-doped carbon quantum dots: Surface chemistry dependent antibacterial activity.* Carbon, 2018. **135**. p. 104-111.

141. Eto, K., et al., *Brain hydrogen sulfide is severely decreased in Alzheimer's disease.* Biochemical and biophysical research communications, 2002. **293**(5): p. 1485-1488.

142. Zhuo, S., et al., *Living cell imaging and sensing of hydrogen sulfide using high-efficiency fluorescent Cu-doped carbon quantum dots.* New Journal of Chemistry, 2018. **42**(24): p. 19659-19664.

143. Jin, K., et al., *Preparation of highly fluorescent sulfur doped graphene quantum dots for live cell imaging.* Journal of Luminescence, 2018. **197**: p. 147-152.

144. Wang, H., et al., *Paramagnetic properties of metal- free boron- doped graphene quantum dots and their application for safe magnetic resonance imaging.* Advanced materials, 2017. **29**(11): p. 1605416.

145. Wang, G., et al., *Green preparation of lattice phosphorus doped graphene quantum dots with tunable emission wavelength for bio-imaging.* Materials Letters, 2019. **242**: p. 156-159.

146. Wang, L., et al., *Chlorine-Doped Graphene Quantum Dots with Enhanced Anti-and Pro-Oxidant Properties.* ACS applied materials & interfaces, 2019.

147. Yang, W., et al., *Carbon dots with red-shifted photoluminescence by fluorine doping for optical bio-imaging.* Carbon, 2018. **128**: p. 78-85.

148. Feng, J., et al., *Tuning the electronic and optical properties of graphene quantum dots by selective boronization.* Journal of Materials Chemistry C, 2019. **7**(2): p. 237-246.

149. Liu, R., et al., *Nitrogen and phosphorus co-doped graphene quantum dots as a nano-sensor for highly sensitive and selective imaging detection of nitrite in live cell.* Sensors and Actuators B: Chemical, 2017. **240**: p. 604-612.

150. Wang, J., et al., *Fluorine and Nitrogen Co-doped Carbon Dots Complexation with Fe (III) as a T1 Contrast Agent for Magnetic Resonance Imaging.* ACS applied materials & interfaces, 2019. **11**(20): p. 18203-18212.

151. Nafiujjaman, M., et al., *Synthesis of nitrogen-and chlorine-doped graphene quantum dots for cancer cell imaging.* Journal of nanoscience and nanotechnology, 2018. **18**(6): p. 3793-3799.

152. Kundu, S., et al., *Synthesis of N, F and S co-doped graphene quantum dots.* Nanoscale, 2015. **7**(27): p. 11515-11519.

153. Nemati, F., et al., *Fluorescence turn-on sensing of thiamine based on Arginine–functionalized graphene quantum dots (Arg-GQDs): Central composite design for process optimization.* Sensors and Actuators B: Chemical, 2018. **255**: p. 2078-2085.

154. Pirsaheb, M., et al., *Functionalized fluorescent carbon nanostructures for targeted imaging of cancer cells: a review.* Microchimica Acta, 2019. **186**(4): p. 231.

155. Dawidczyk, C.M., L.M. Russell, and P.C. Searson, *Nanomedicines for cancer therapy: state-of-the-art and limitations to pre-clinical studies that hinder future developments.* Frontiers in chemistry, 2014. **2**: p. 69.

156. Van Tam, T., S.H. Hong, and W.M. Choi, *Facile synthesis of cysteine–functionalized graphene quantum dots for a fluorescence probe for mercury ions.* RSC Advances, 2015. **5**(118): p. 97598-97603.

157. Wang, R., et al., *Amino-functionalized graphene quantum dots prepared using high-softening point asphalt and their application in Fe3+ detection.* Applied Surface Science, 2019. **467**: p. 446-455.

158. Fu, Z. and F. Cui, *Thiosemicarbazide chemical functionalized carbon dots as a fluorescent nanosensor for sensing Cu 2+ and intracellular imaging.* RSC Advances, 2016. **6**(68): p. 63681-63688.

159. Deka, M.J., A. Dutta, and D. Chowdhury, *Tuning the wettability and photoluminescence of graphene quantum dots via covalent modification.* New Journal of Chemistry, 2018. **42**(1): p. 355-362.

160. Liu, R., et al., *Aptamer and IR820 Dual‐Functionalized Carbon Dots for Targeted Cancer Therapy against Hypoxic Tumors Based on an 808 nm Laser‐Triggered Three‐Pathway Strategy.* Advanced Therapeutics, 2018. **1**(5): p. 1800041.

161. Motaghi, H., M.A. Mehrgardi, and P. Bouvet, *Carbon dots-AS1411 aptamer nanoconjugate for ultrasensitive spectrofluorometric detection of cancer cells.* Scientific reports, 2017. **7**(1): p. 10513.

162. Mewada, A., et al., *Swarming carbon dots for folic acid mediated delivery of doxorubicin and biological imaging.* Journal of Materials Chemistry B, 2014. **2**(6): p. 698-705.

163. Zhao, X., et al., *Folic acid-conjugated carbon dots as green fluorescent probes based on cellular targeting imaging for recognizing cancer cells.* RSC Advances, 2017. **7**(67): p. 42159-42167.

164. Hai, X., et al., *Folic acid encapsulated graphene quantum dots for ratiometric pH sensing and specific multicolor imaging in living cells.* Sensors and Actuators B: Chemical, 2018. **268**: p. 61-69.

165. Park, Y., et al., *Improving the functionality of carbon nanodots: doping and surface functionalization.* Journal of Materials Chemistry A, 2016. **4**(30): p. 11582-11603.

166. Zhou, Y., et al., *Polymers in carbon dots: a review.* Polymers, 2017. **9**(2): p. 67.

167. Gonçalves, H. and J.C.E. da Silva, *Fluorescent carbon dots capped with PEG 200 and mercaptosuccinic acid.* Journal of fluorescence, 2010. **20**(5): p. 1023-1028.

168. Milosavljevic, V., et al., *Microwave preparation of carbon quantum dots with different surface modification.* J Metallomics Nanotechnol, 2014. **3**: p. 16-22.

169. Chandra, A., et al., *Mitigating the cytotoxicity of graphene quantum dots and enhancing their applications in bioimaging and drug delivery.* ACS Macro Letters, 2014. **3**(10): p. 1064-1068.

170. Chong, Y., et al., *The in vitro and in vivo toxicity of graphene quantum dots.* Biomaterials, 2014. **35**(19): p. 5041-5048.

171. Yang, S.T., et al., *High- Performance Red/Near- IR Carbon Dots as Fluorescence Probes for Tumor Imaging In Vivo.* ChemistrySelect, 2018. **3**(23): p. 6374-6381.

172. Sachdev, A., I. Matai, and P. Gopinath, *Implications of surface passivation on physicochemical and bioimaging properties of carbon dots.* RSC Advances, 2014. **4**(40): p. 20915-20921.

173. Havrdova, M., et al., *Toxicity of carbon dots–Effect of surface functionalization on the cell viability, reactive oxygen species generation and cell cycle.* Carbon, 2016. **99**: p. 238-248.

174. Liu, J., et al., *Antimicrobial Activity of Zinc Oxide–Graphene Quantum Dot Nanocomposites: Enhanced Adsorption on Bacterial Cells by Cationic Capping Polymers.* ACS Sustainable Chemistry & Engineering, 2019. **7**(19): p. 16264-16273.

175. Hasanzadeh, M., et al., *Graphene quantum dots decorated with magnetic nanoparticles: Synthesis, electrodeposition, characterization and application as an electrochemical sensor towards determination of some amino acids at physiological pH.* Materials Science and Engineering: C, 2016. **68**: p. 814-830.

176. Sricharoen, P., et al., *Fe3O4/hydroxyapatite/graphene quantum dots as a novel nano-sorbent for preconcentration of copper residue in Thai food ingredients: Optimization of ultrasound-assisted magnetic solid phase extraction.* Ultrasonics sonochemistry, 2017. **37**: p. 83-93.

177. Lakshmi, N. and P. Tambe, *EMI shielding effectiveness of graphene decorated with graphene quantum dots and silver nanoparticles reinforced PVDF nanocomposites.* Composite Interfaces, 2017. **24**(9): p. 861-882.

178. Rao, H., et al., *Colorimetric and fluorometric detection of protamine by using a dual-mode probe consisting of carbon quantum dots and gold nanoparticles.* Microchimica Acta, 2017. **184**(8): p. 3017-3025.

179. Ju, J. and W. Chen, *In situ growth of surfactant-free gold nanoparticles on nitrogen-doped graphene quantum dots for electrochemical detection of hydrogen peroxide in biological environments.* Analytical chemistry, 2015. **87**(3): p. 1903-1910.

180. Xu, H., et al., *Fabrication of a nitrogen-doped graphene quantum dot from MOF-derived porous carbon and its application for highly selective fluorescence detection of Fe 3+*. Journal of Materials Chemistry C, 2015. **3**(2): p. 291-297.

181. Yang, J.-M., et al., *Fabrication of a carbon quantum dots immobilized zirconium-based metal-organic framework composite fluorescence sensor for highly sensitive detection of 4-nitrophenol.* Microporous and Mesoporous Materials, 2019. **274**: p. 149-154.

182. Wei, X., et al., *Composite ZIF-8 with CQDs for boosting visible-light-driven photocatalytic removal of NO.* Journal of Alloys and Compounds, 2019.

183. Wang, X.-M., et al., *Preparation of C-ZIF-8 composite nanoparticles.* Integrated Ferroelectrics, 2018. **188**(1): p. 130-135.

184. Ju, J., R. Zhang, and W. Chen, *Photochemical deposition of surface-clean silver nanoparticles on nitrogen-doped graphene quantum dots for sensitive colorimetric detection of glutathione.* Sensors and Actuators B: Chemical, 2016. **228**: p. 66-73.

185. Su, M., et al., *Aptamer-Based electrochemiluminescent detection of MCF-7 cancer cells based on carbon quantum dots coated mesoporous silica nanoparticles.* Electrochimica Acta, 2014. **146**: p. 262-269.

186. Nozaki, T., et al., *A nanocomposite of N-doped carbon dots with gold nanoparticles for visible light active photosensitisers.* Photochemical & Photobiological Sciences, 2019. **18**(5): p. 1235-1241.

187. Ghosh Chaudhuri, R. and S. Paria, *Core/shell nanoparticles: classes, properties, synthesis mechanisms, characterization, and applications.* Chemical reviews, 2011. **112**(4): p. 2373-2433.

188. Bhogal, S., et al., *Surface Molecularly Imprinted Carbon Dots Based Core-Shell Material for Selective Fluorescence Sensing of Ketoprofen.* Journal of fluorescence, 2019. **29**(1): p. 145-154.

189. Mehta, A., A. Mishra, and S. Basu, *Optical Detection of Thiol Drugs by Core–Shell Luminous Carbon Dots—Gold Nanoparticles System.* Plasmonics, 2018. **13**(6): p. 2239-2248.

190. Kong, R.-M., et al., *Uricase based fluorometric determination of uric acid based on the use of graphene quantum dot@ silver core-shell nanocomposites.* Microchimica Acta, 2018. **185**(1): p. 63.

191. Pei, H., et al., *Graphene oxide quantum dots@ silver core–shell nanocrystals as turn-on fluorescent nanoprobe for ultrasensitive detection of prostate specific antigen.* Biosensors and Bioelectronics, 2015. **74**: p. 909-914.

192. Ma, J.-L., et al., *Simple and cost-effective glucose detection based on carbon nanodots supported on silver nanoparticles.* Analytical chemistry, 2016. **89**(2): p. 1323-1328.

193. Deng, S., et al., *Nitrogen-doped graphene quantum dots (N-GQDs) perturb redox-sensitive system via the selective inhibition of antioxidant enzyme activities in zebrafish.* Biomaterials, 2019. **206**: p. 61-72.

194. Zhang, J.-H., et al., *Perturbation effect of reduced graphene oxide quantum dots (rGOQDs) on aryl hydrocarbon receptor (AhR) pathway in zebrafish.* Biomaterials, 2017. **133**: p. 49-59.

195. Majumder, T., et al., *S, N Co-Doped Graphene Quantum Dots Decorated C-Doped ZnO Nanotaper Photoanodes for Solar Cells Applications.* Nano, 2019. **14**(1): p. 1950012.

196. Wang, Z., et al., *Biomass-derived nitrogen doped graphene quantum dots with color-tunable emission for sensing, fluorescence ink and multicolor cell imaging.* Spectrochimica Acta Part A: Molecular and Biomolecular Spectroscopy, 2020. **227**: p. 117671.

197. Sheng, L., et al., *A highly selective and sensitive fluorescent probe for detecting Cr (VI) and cell imaging based on nitrogen-doped graphene quantum dots.* Journal of Alloys and Compounds, 2020. **820**: p. 153191.

198. Wang, H., et al., *Single-layer boron-doped graphene quantum dots for contrast-enhanced in vivo T 1-weighted MRI.* Nanoscale Horizons, 2020. **5**(3): p. 573-579.

199. Li, Y., et al., *Investigation of photo-induced electron transfer between amino-functionalized graphene quantum dots and selenium nanoparticle and it's application for sensitive fluorescent detection of copper ions.* Talanta, 2019. **197**: p. 341-347.

200. Pashazadeh- Panahi, P., M. Hasanzadeh, and R. Eivazzadeh- Keihan, *A novel optical probe based on d- penicillamine- functionalized graphene quantum dots: Preparation and application as signal amplification element to minoring of ions in human biofluid.* Journal of Molecular Recognition, 2020. **33**(5): p. e2828.

201. El-Hnayn, R., et al., *One-step synthesis of diamine-functionalized graphene quantum dots from graphene oxide and their chelating and antioxidant activities.* Nanomaterials, 2020. **10**(1): p. 104.

202. Li, S., et al., *Targeted tumour theranostics in mice via carbon quantum dots structurally mimicking large amino acids.* Nature Biomedical Engineering, 2020: p. 1-13.

203. He, Z., et al., *Click multiwalled carbon nanotubes: A novel method for preparation of carboxyl groups functionalized carbon quantum dots.* Materials Science and Engineering: C, 2020. **108**: p. 110376.

204. Zhou, X., et al., *Dopamine fluorescent sensors based on polypyrrole/graphene quantum dots core/shell hybrids.* Biosensors and Bioelectronics, 2015. **64**: p. 404-410.

205. Kim, M.C., et al., *Highly photoluminescent N-isopropylacrylamide (NIPAAM) passivated carbon dots for multicolor bioimaging applications.* European Polymer Journal, 2018. **98**: p. 191-198.

206. Lu, S., et al., *Hydrothermal synthesis of nitrogen-doped carbon dots with real-time live-cell imaging and blood–brain barrier penetration capabilities.* International journal of nanomedicine, 2016. **11**: p. 6325.

207. Gao, Q., J. Han, and Z. Ma, *Polyamidoamine dendrimers-capped carbon dots/Au nanocrystal nanocomposites and its application for electrochemical immunosensor.* Biosensors and Bioelectronics, 2013. **49**: p. 323-328.

208. Pirsaheb, M., S. Mohammadi, and A. Salimi, *Current advances of carbon dots based biosensors for tumor marker detection, cancer cells analysis and bioimaging.* TrAC Trends in Analytical Chemistry, 2019. **115**: p. 83-99.

209. Li, Y., et al., *A graphene quantum dot (GQD) nanosystem with redox-triggered cleavable PEG shell facilitating selective activation of the photosensitiser for photodynamic therapy.* RSC advances, 2016. **6**(8): p. 6516-6522.

210. Amjadi, M. and R. Jalili, *Molecularly imprinted polymer-capped nitrogen-doped graphene quantum dots as a novel chemiluminescence sensor for selective and sensitive determination of doxorubicin.* RSC advances, 2016. **6**(89): p. 86736-86743.

211. Jiang, D., et al., *A fluorescent imaging assay of cast in renal disease based on graphene quantum dots and Fe3O4 nanoparticles.* Clinica Chimica Acta, 2016. **454**: p. 94-101.

212. Teymourinia, H., M. Salavati-Niasari, and O. Amiri, *Simple synthesis of Cu2O/GQDs nanocomposite with different morphologies fabricated by tuning the synthesis parameters as novel antibacterial material.* Composites Part B: Engineering, 2019. **172**: p. 785-794.

213. Wang, F., et al., *Two-photon graphene quantum dot modified Gd 2 O 3 nanocomposites as a dual-mode MRI contrast agent and cell labelling agent.* Nanoscale, 2018. **10**(12): p. 5642-5649.

214. Javanbakht, S. and H. Namazi, *Doxorubicin loaded carboxymethyl cellulose/graphene quantum dot nanocomposite hydrogel films as a potential anticancer drug delivery system.* Materials Science and Engineering: C, 2018. **87**: p. 50-59.

215. Garg, D., et al., *A sensitive turn on fluorescent probe for detection of biothiols using MnO2@ carbon dots nanocomposites.* Spectrochimica Acta Part A: Molecular and Biomolecular Spectroscopy, 2018. **192**: p. 411-419.

216. Wang, C., et al., *Fabrication and characterization of novel cRGD modified graphene quantum dots for chemo-photothermal combination therapy.* Sensors and Actuators B: Chemical, 2020. **309**: p. 127732.

217. Kadian, S., et al., *Synthesis, characterization and investigation of synergistic antibacterial activity and cell viability of silver–sulfur doped graphene quantum dot (Ag@ S-GQDs) nanocomposites.* Journal of Materials Chemistry B, 2020. **8**(15): p. 3028-3037.

218. Huang, Q., et al., *Graphene Quantum Dots/Multiwalled Carbon Nanotubes Composite-Based Electrochemical Sensor for Detecting Dopamine Release from Living Cells.* ACS Sustainable Chemistry & Engineering, 2020. **8**(3): p. 1644-1650.

219. Gao, D., et al., *Carbon quantum dots decorated on ZnO nanoparticles: An efficient visible-light responsive antibacterial agents.* Applied Organometallic Chemistry, 2020: p. e5665.

220. Abazar, F. and A. Noorbakhsh, *Chitosan-carbon quantum dots as a new platform for highly sensitive insulin impedimetric aptasensor.* Sensors and Actuators B: Chemical, 2020. **304**: p. 127281.

# Abbreviations

**ADBA**: 9,10-anthracendipropionic acid
**AEAP**: N- β-(aminoethyl)-γaminopropyltrimethoxysilane
**af-GQD**: Amino functionalized graphene quantum dot
**AIEE**: Aggregation induced emission enhancement
**AIEQ**: Aggregation induced emission quenching
**AIRS**: Aggregation induced red-shift spectra
**ATP**: Adenosine tri phosphate
**ATRP**: Atom transfer radical polymerization
**BBB**: Blood-brain barrier
**BSA**: Bovine serum albumin
**CD**: Carbon-based quantum dot
**CFTR**: Cystic fibrosis transmembrane regulator
**C-GQD**: Graphene quantum dot synthesized with carbon nanotubes
**CK2**: Casein kinase II
**Cl-GQD-N**: Chlorine and N-doped graphene quantum dot
**CLSM**: Confocal laser scanning microscopy
**CMC**: Carboxymethyl cellulose
**CQD**: Carbon quantum dot
**CQE**: Quantum confinement effect
**CS**: Chitosan
**Cu-CQD**: Copper-doped carbon quantum dot
**Cys-GQD**: Cysteine-functionalized graphene quantum dot
**DA**: Dopamine
**DCPL**: Down-conversion photoluminescence
**DDA**: Dodecyl amine
**DMF**: Dimethyl formamide
**DMSO**: Dimethyl sulfoxide
**DOX**: Doxorubicin
**ECL**: Electrochemiluminescence
**EDA**: Ethanediamine
**FA**: Folic acid
**FA-GQD**: Folic acid encapsulated graphene quantum dot
**FA-HeLa**: Folic acid treated HeLa
**FDA**: Food and Drug Administration
**FL**: Fluorescence
**GMP**: Good Manufacturing Practice
**GO**: Graphene oxide
**$GO_{ox}$**: Glucose oxidase
**GQD**: Graphene quantum dot
**GSH**: Glutathione
**HER**: Herceptin

**HFFF**: Human foreskin fibroblast cells
**H-GQD**: Hydrothermally treated-graphene quantum dot
**HOMO**: Highest occupied molecular orbital
**HTC**: Hydrothermal carbonization
**L-CD**: Lignin hybridized carbon dot
**LDH**: Lactate dehydrogenase
**MDCL**: Madin derby kidney canine
**MIP**: Molecularly imprinted polymer
**MNP**: Magnetic nanoparticle
**MOF**: Metal-organic framework
**MPS**: Mononuclear phagocyte system
**MSN**: Mesoporous silica nanoparticle
**MSS**: Mercaptosuccinic acid
**MTT**: 3-(4,5-Dimethylthiazol-2-yl)-2,5-Diphenyltetrazolium Bromide
**MW**: Microwave
**N-CQD**: Nitrogen-doped carbon quantum dot
**N-GQD**: Nitrogen-doped graphene quantum dot
**NIPAAM**: N-Isopropylacrylamide
**NM-CQD**: Nitrogen -doped microporous carbon quantum dot
**NPs**: Nanoparticles
**NS- GQD**: Nitrogen and Sulfur-doped graphene quantum dot
**OD**: Optical density
**OFG**: Oxygen-functional group
**Ox-TMB**: Oxidized Tetramethylbenzidine
**PAMAM**: Polyamidoamine
**PDMAEMA**: Poly-[2-(dimethylamino)ethylmethacrylate]
**PEG**: Polyethylene glycol
**PL**: Photoluminescence
**PL QY**: Photoluminescence quantum yield
**PLA**: Plasma pulsed laser ablation
**PMPDSAH**: Poly[N-(3-(methacryloylamino) propyl)-N, N-Dimethyl-N-(3-sulfopropyl) ammonium hydroxide]
**PS**: Photosensitized
**PTT**: Photothermal therapy
**PVP**: Polyvinylpyrrolidone
**QD**: Quantum dot
**QY**: Quantum yield

**RES**: Reticuloendothelial system
**RGD**: Arginylglycylaspartic acid
**rGO**: Reduced graphene oxide
**Rh**: Rhodamine

| | |
|---|---|
| **ROS**: | Reactive oxygen species |
| **S-CQD**: | Sulfur-doped carbon quantum dot |
| **s-GQD**: | single-layered graphene quantum dot |
| **S-GQD**: | Sulfur-doped graphene quantum dot |
| **SLN**: | Sentinel Nodes |
| **TMB**: | Tetramethylbenzidine |
| **TNBC**: | Triple negative breast cancer |
| **TSC**: | Thiosemicarbazide |
| **TSC- CQD**: | Thiosemicarbazide doped carbon quantum dot |
| **UC NP**: | Up-conversion nanoparticle |
| **UCPL:** | Up-conversion photoluminescence |

**Declaration of interests**

☒ The authors declare that they have no known competing financial interests or personal relationships that could have appeared to influence the work reported in this paper.

☐The authors declare the following financial interests/personal relationships which may be considered as potential competing interests:

Graphical abstract

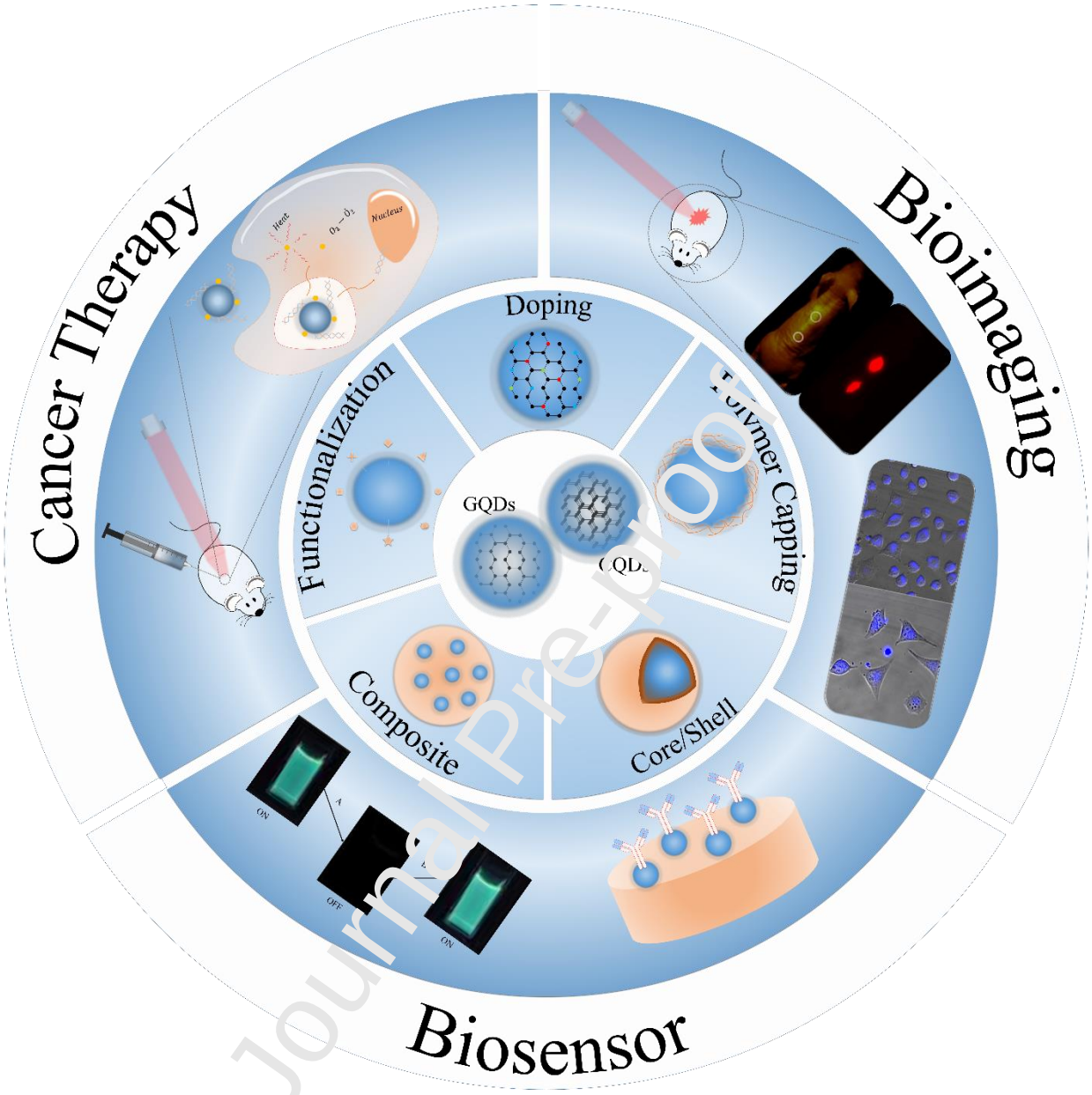

Highlights:

- Biomedical application of Carbon-based quantum dots (CDs)
- Carbon-based quantum dots synthesis techniques
- Surface modification strategies to enhance Carbon-based quantum dots characteristics
- Doping, Surface functionalization, Polymer Capping, and CDs composite-based nanomaterials as efficient surface modification techniques

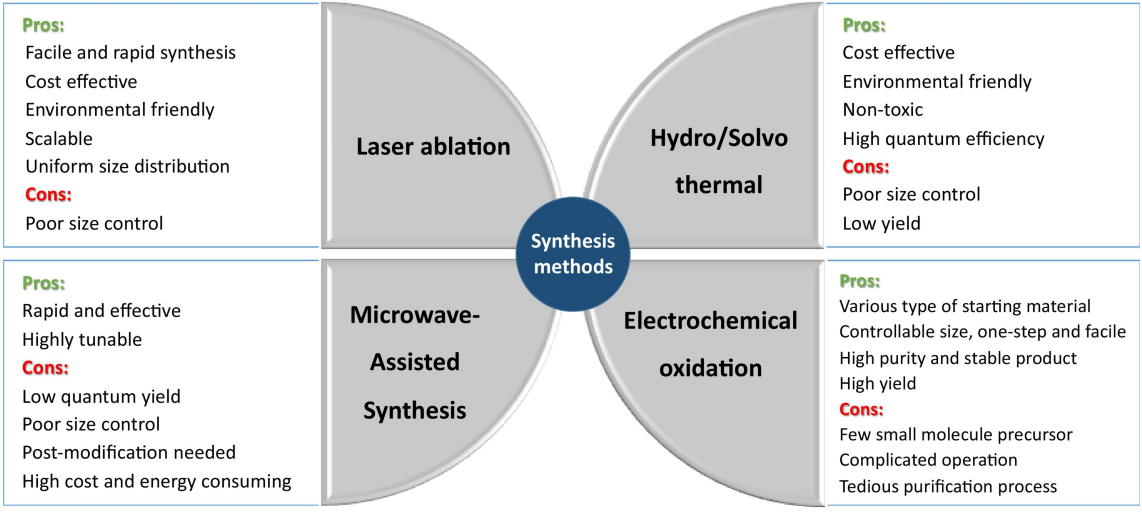
Pros:
Facile and rapid synthesis
Cost effective
Environmental friendly
Scalable
Uniform size distribution
Cons:
Poor size control
Laser ablation
Hydro/Solvo thermal
Pros:
Cost effective
Environmental friendly
Non-toxic
High quantum efficiency
Cons:
Poor size control
Low yield
Synthesis methods
Pros:
Rapid and effective
Highly tunable
Cons:
Low quantum yield
Poor size control
Post-modification needed
High cost and energy consuming
Microwave-Assisted Synthesis
Electrochemical oxidation
Pros:
Various type of starting material
Controllable size, one-step and facile
High purity and stable product
High yield
Cons:
Few small molecule precursor
Complicated operation
Tedious purification process

Figure 1

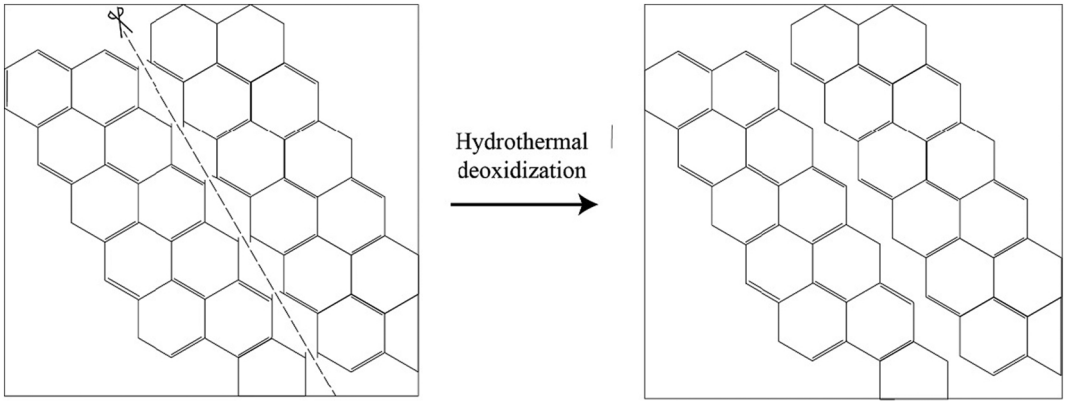


Figure 2

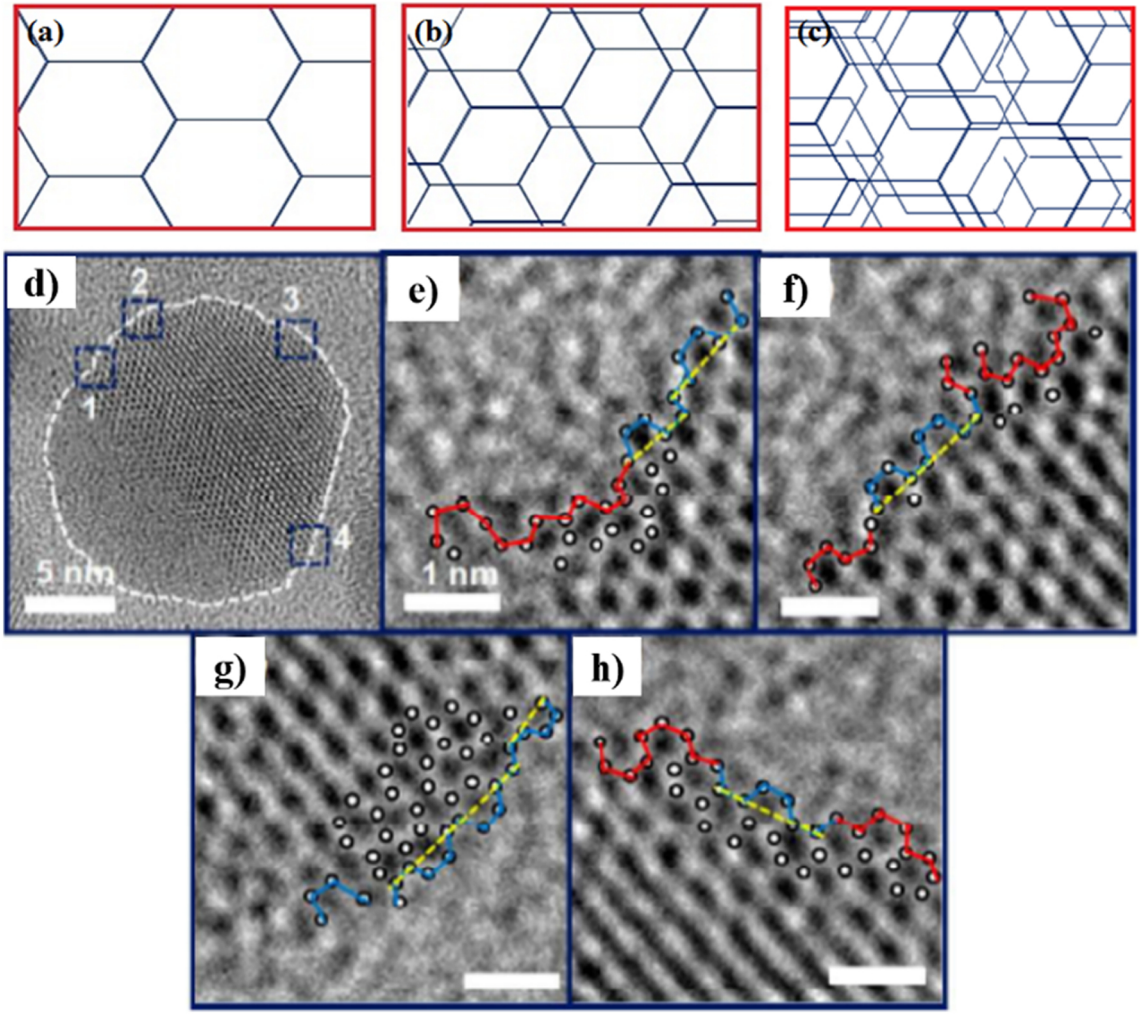


Figure 3

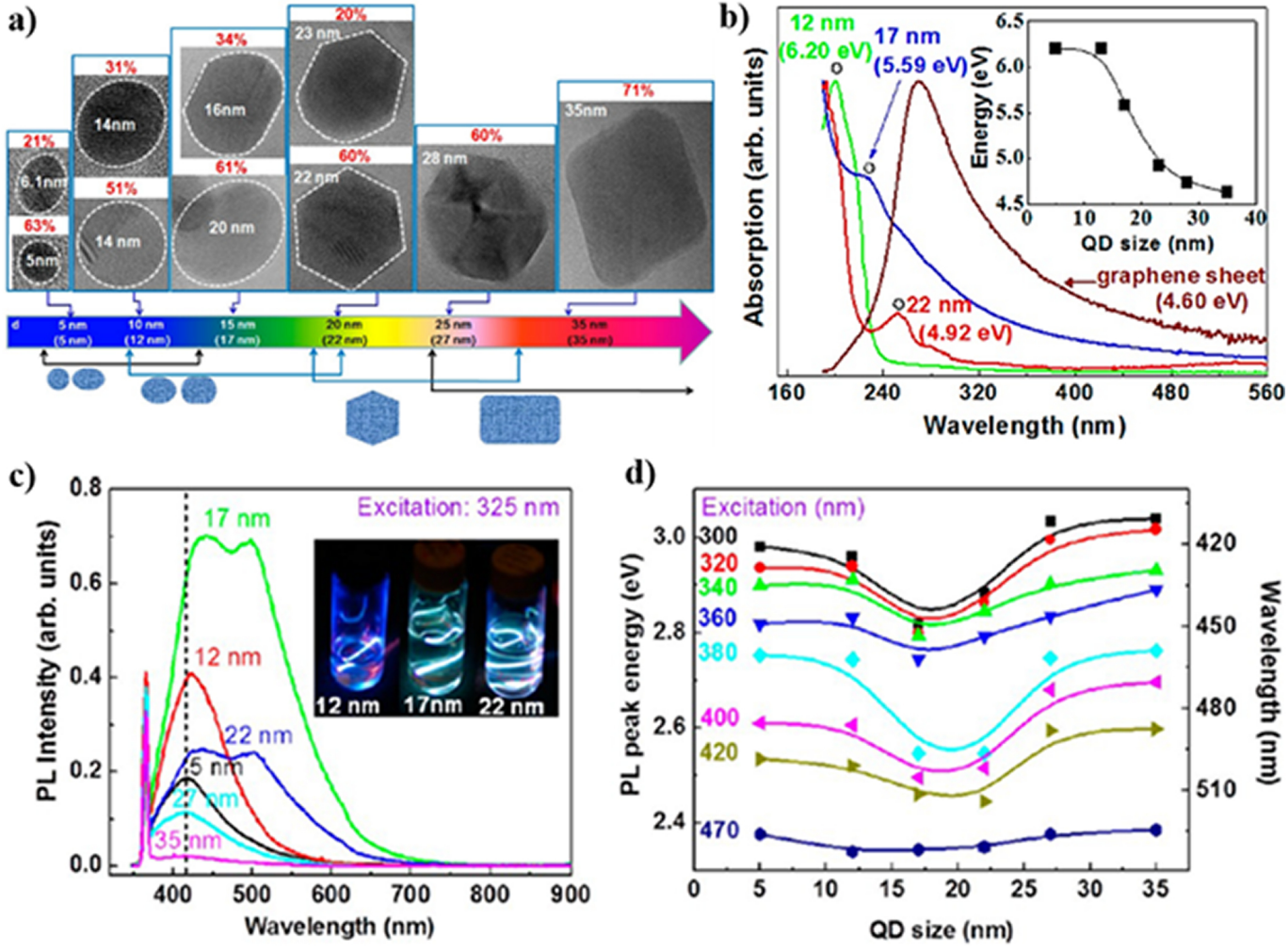
a)
21%
6.1nm
63%
5nm
31%
14nm
51%
14 nm
34%
16nm
61%
20 nm
20%
23 nm
60%
22 nm
60%
28 nm
71%
35nm
d
5 nm (5 nm)
10 nm (12 nm)
15 nm (17 nm)
20 nm (22 nm)
25 nm (27 nm)
35 nm (35 nm)
b)
12 nm (6.20 eV)
17 nm (5.59 eV)
22 nm (4.92 eV)
graphene sheet (4.60 eV)
Absorption (arb. units)
Wavelength (nm)
Energy (eV)
QD size (nm)
c)
Excitation: 325 nm
17 nm
12 nm
22 nm
5 nm
7 nm
35 nm
12 nm
17nm
22 nm
PL Intensity (arb. units)
Wavelength (nm)
d)
Excitation (nm)
300
320
340
360
380
400
420
470
PL peak energy (eV)
Wavelength (nm)
QD size (nm)

Figure 4

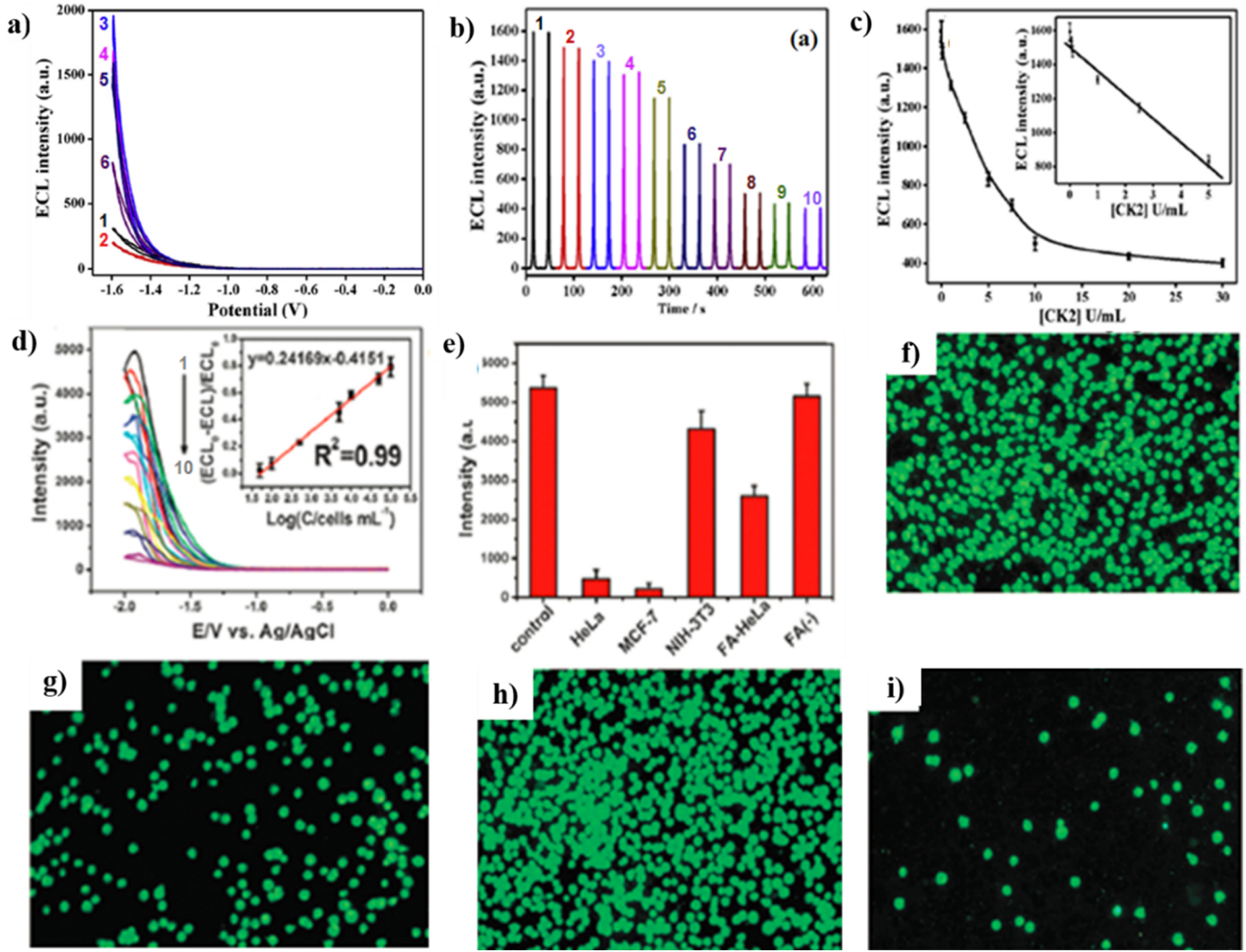
a)
ECL intensity (a.u.)
Potential (V)
b)
(a)
ECL intensity (a.u.)
Time / s
c)
ECL intensity (a.u.)
[CK2] U/mL
ECL intensity (a.u.)
[CK2] U/mL
d)
Intensity (a.u.)
E/V vs. Ag/AgCl
y=0.24169x-0.4151
R²=0.99
Log(C/cells mL⁻¹)
e)
Intensity (a.u.)
control
HeLa
MCF-7
NIH-3T3
FA-HeLa
FA(-)
f)
g)
h)
i)

Figure 5

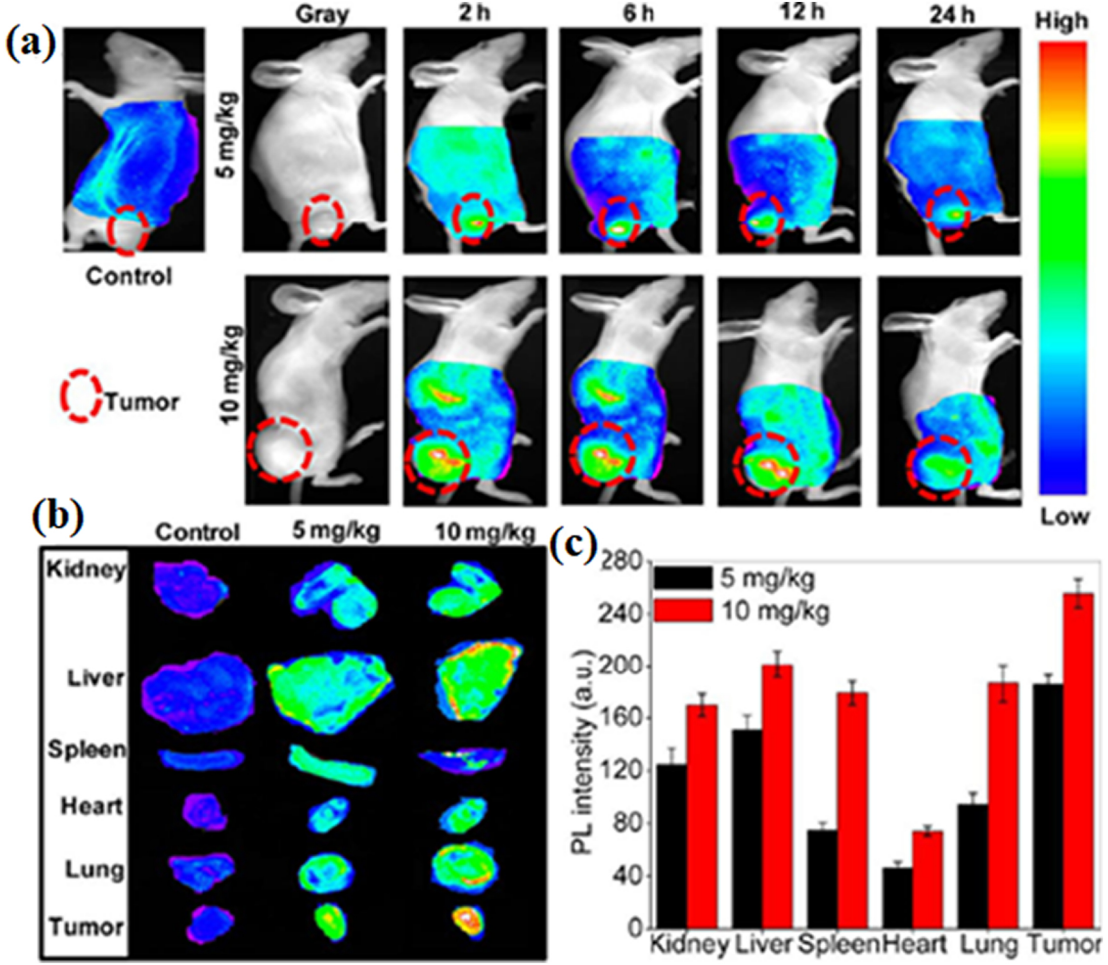
(a)
Gray
2 h
6 h
12 h
24 h
High
Low
5 mg/kg
10 mg/kg
Control
Tumor
(b)
Control
5 mg/kg
10 mg/kg
Kidney
Liver
Spleen
Heart
Lung
Tumor
(c)
5 mg/kg
10 mg/kg
PL intensity (a.u.)
0
40
80
120
160
200
240
280
Kidney
Liver
Spleen
Heart
Lung
Tumor

Figure 6

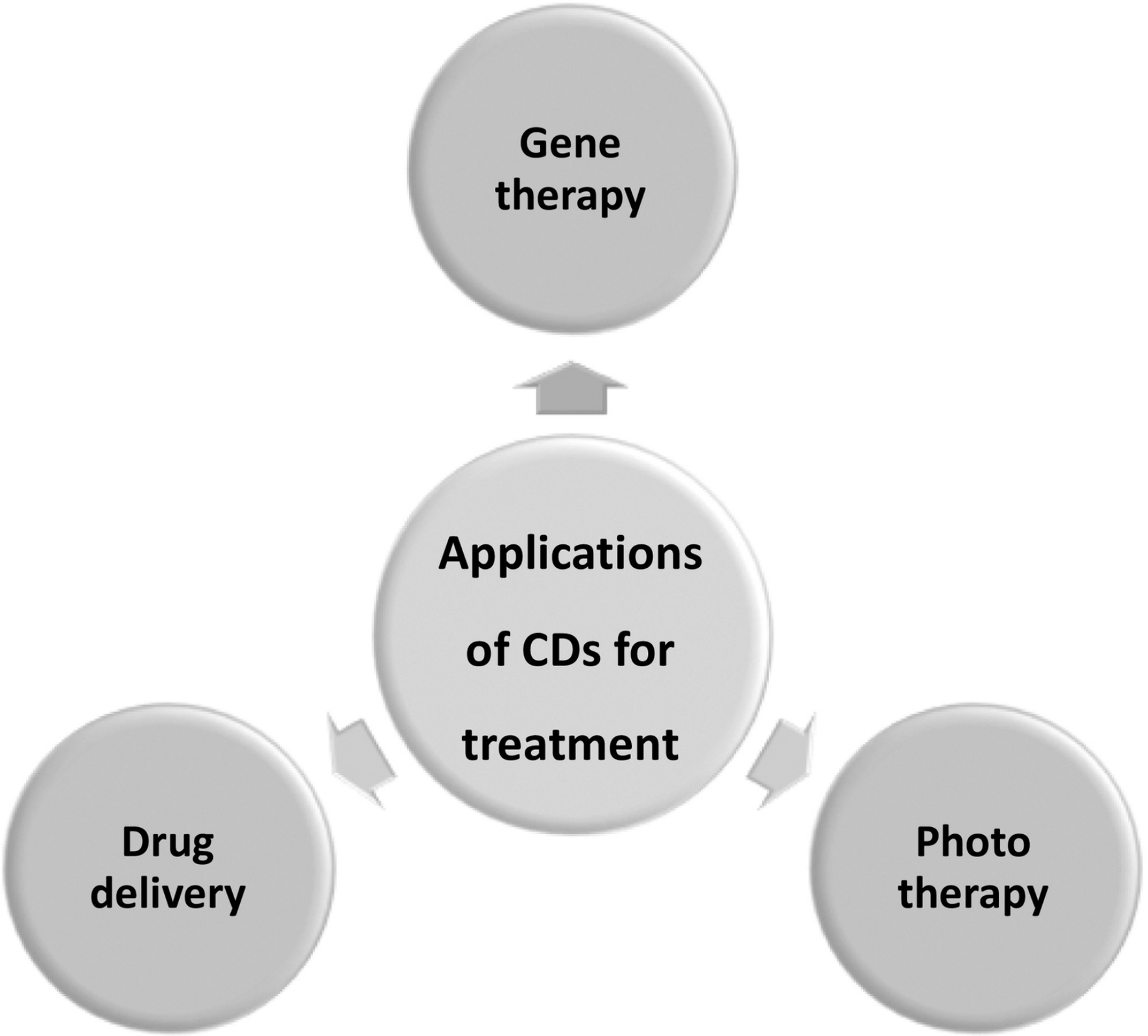
Gene therapy
Applications of CDs for treatment
Drug delivery
Photo therapy

Figure 7

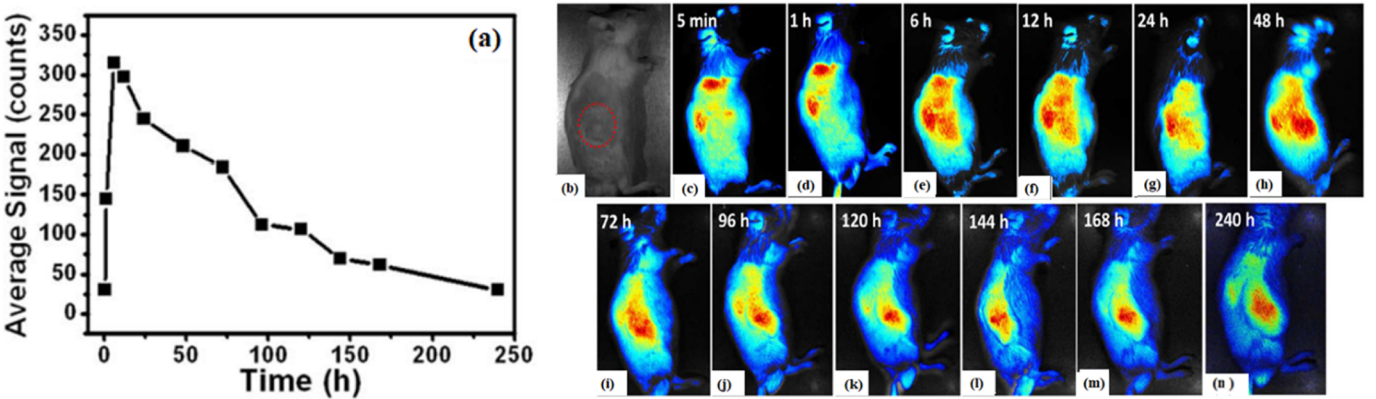
(a)
Average Signal (counts)
350
300
250
200
150
100
50
0
0
50
100
150
200
250
Time (h)
(b)
5 min
(c)
1 h
(d)
6 h
(e)
12 h
(f)
24 h
(g)
48 h
(h)
72 h
(i)
96 h
(j)
120 h
(k)
144 h
(l)
168 h
(m)
240 h
(n)

Figure 8

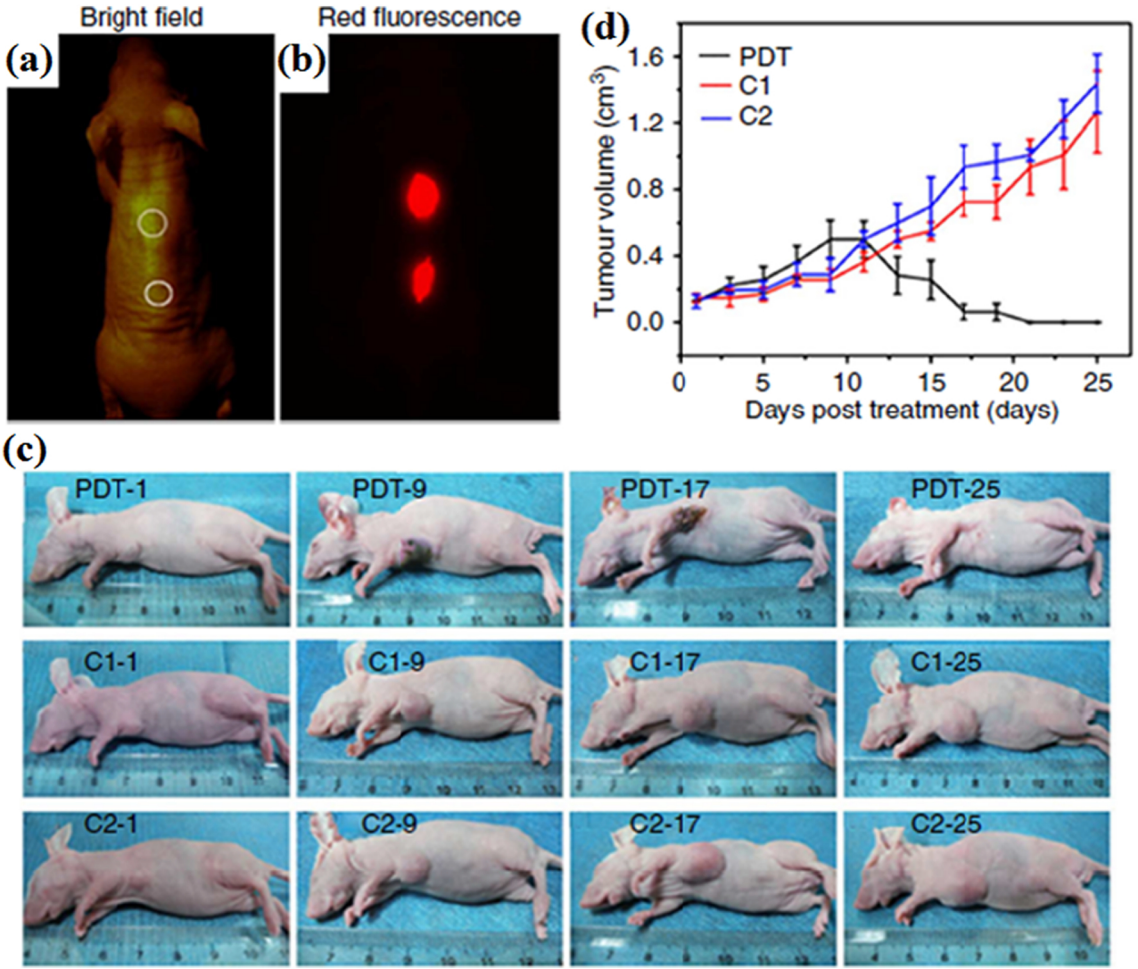
Bright field
Red fluorescence
(a)
(b)
(d)
PDT
C1
C2
Tumour volume (cm3)
1.6
1.2
0.8
0.4
0.0
0
5
10
15
20
25
Days post treatment (days)
(c)
PDT-1
PDT-9
PDT-17
PDT-25
C1-1
C1-9
C1-17
C1-25
C2-1
C2-9
C2-17
C2-25

Figure 9

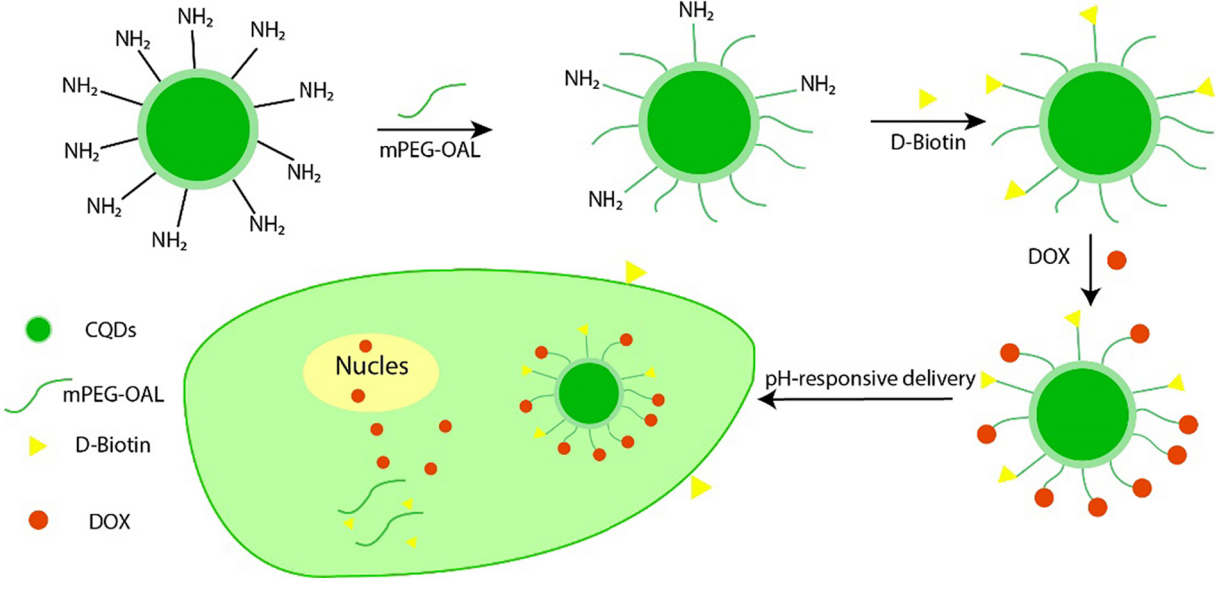
NH2
mPEG-OAL
D-Biotin
DOX
pH-responsive delivery
Nucles
CQDs
mPEG-OAL
D-Biotin
DOX

Figure 10

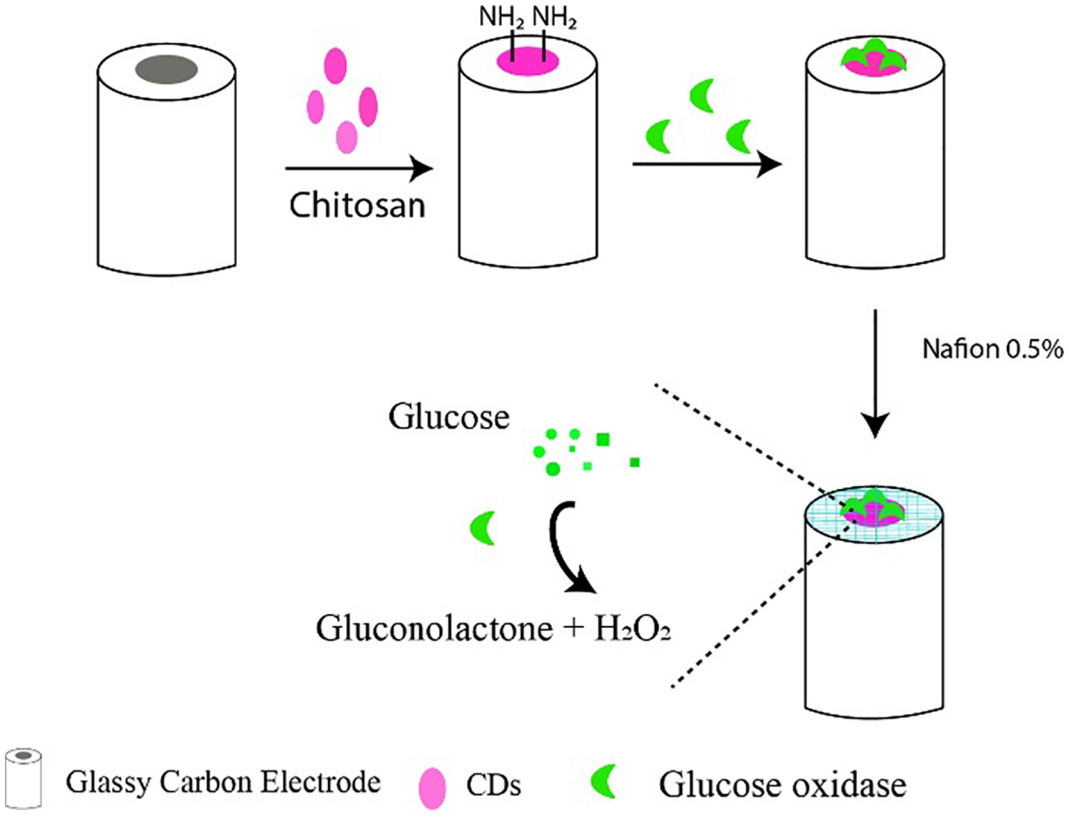
NH2 NH2
Chitosan
Nafion 0.5%
Glucose
Gluconolactone + H2O2
Glassy Carbon Electrode
CDs
Glucose oxidase

Figure 11

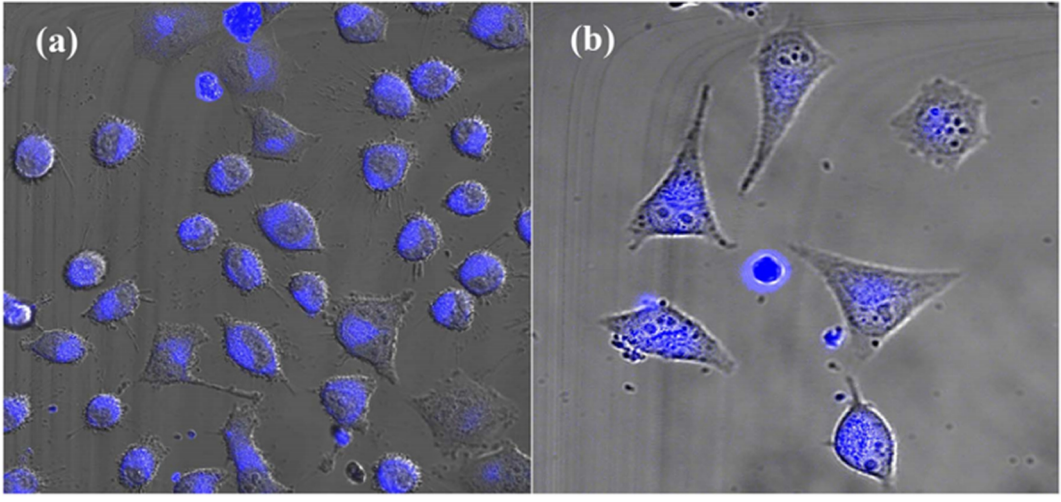


Figure 12

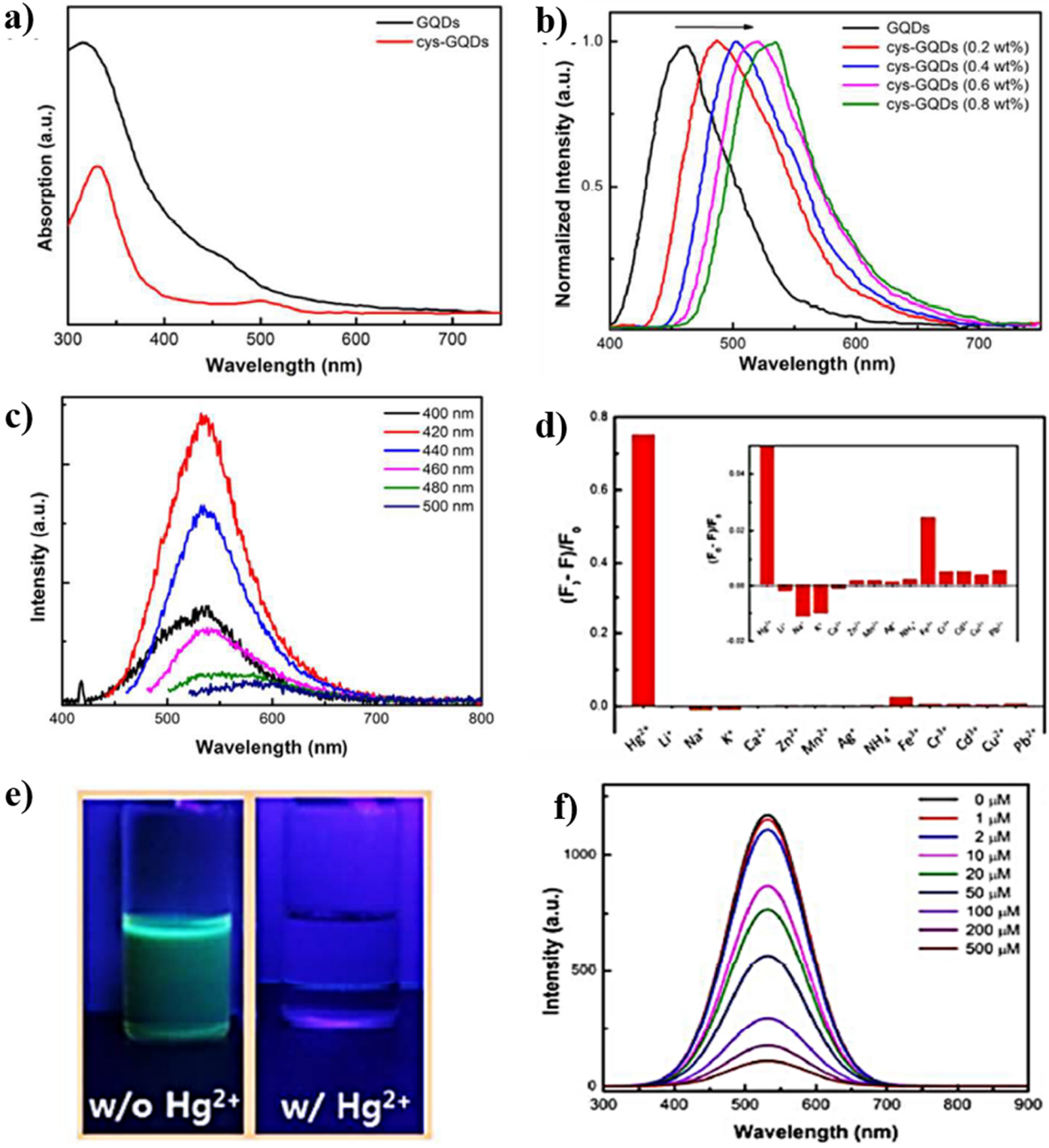
a)
GQDs
cys-GQDs
Absorption (a.u.)
300
400
500
600
700
Wavelength (nm)
b)
GQDs
cys-GQDs (0.2 wt%)
cys-GQDs (0.4 wt%)
cys-GQDs (0.6 wt%)
cys-GQDs (0.8 wt%)
Normalized Intensity (a.u.)
1.0
0.5
400
500
600
700
Wavelength (nm)
c)
400 nm
420 nm
440 nm
460 nm
480 nm
500 nm
Intensity (a.u.)
400
500
600
700
800
Wavelength (nm)
d)
(F0 - F)/F0
0.8
0.6
0.4
0.2
0.0
Hg2+
Li+
Na+
K+
Ca2+
Zn2+
Mn2+
Ag+
NH4+
Fe3+
Cr3+
Cd2+
Cu2+
Pb2+
e)
w/o Hg2+
w/ Hg2+
f)
0 μM
1 μM
2 μM
10 μM
20 μM
50 μM
100 μM
200 μM
500 μM
Intensity (a.u.)
1000
500
0
300
400
500
600
700
800
900
Wavelength (nm)

Figure 13

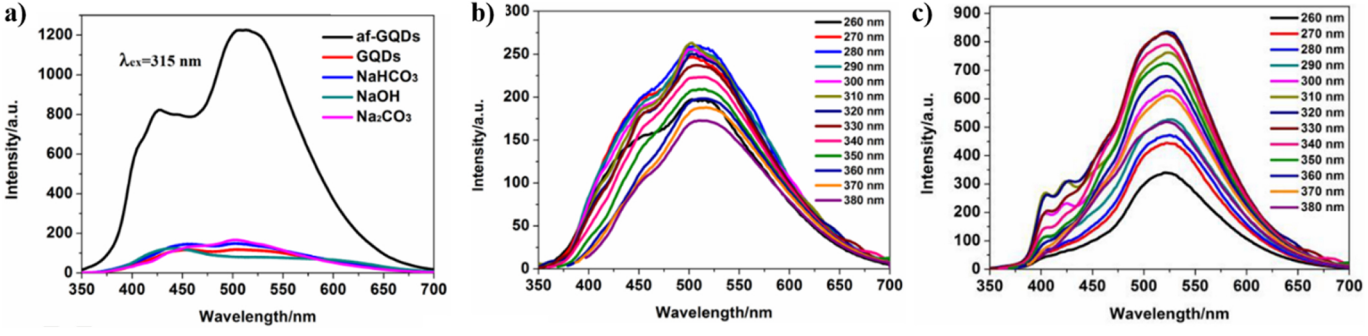
a)
λex=315 nm
af-GQDs
GQDs
NaHCO3
NaOH
Na2CO3
Intensity/a.u.
Wavelength/nm
b)
260 nm
270 nm
280 nm
290 nm
300 nm
310 nm
320 nm
330 nm
340 nm
350 nm
360 nm
370 nm
380 nm
Intensity/a.u.
Wavelength/nm
c)
260 nm
270 nm
280 nm
290 nm
300 nm
310 nm
320 nm
330 nm
340 nm
350 nm
360 nm
370 nm
380 nm
Intensity/a.u.
Wavelength/nm

Figure 14

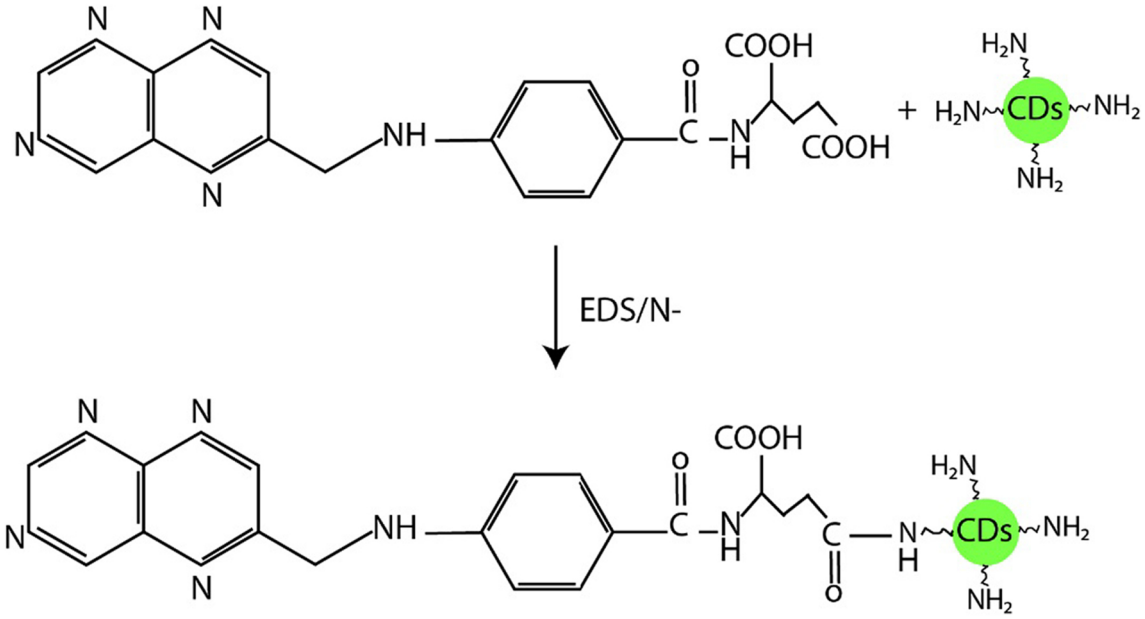
N
N
N
N
NH
COOH
O
C
N
H
COOH
+
$H_2N$
$H_2N$
CDs
$NH_2$
$NH_2$
EDS/N-
N
N
N
N
NH
COOH
O
C
N
H
C
O
N
H
$H_2N$
CDs
$NH_2$
$NH_2$

Figure 15

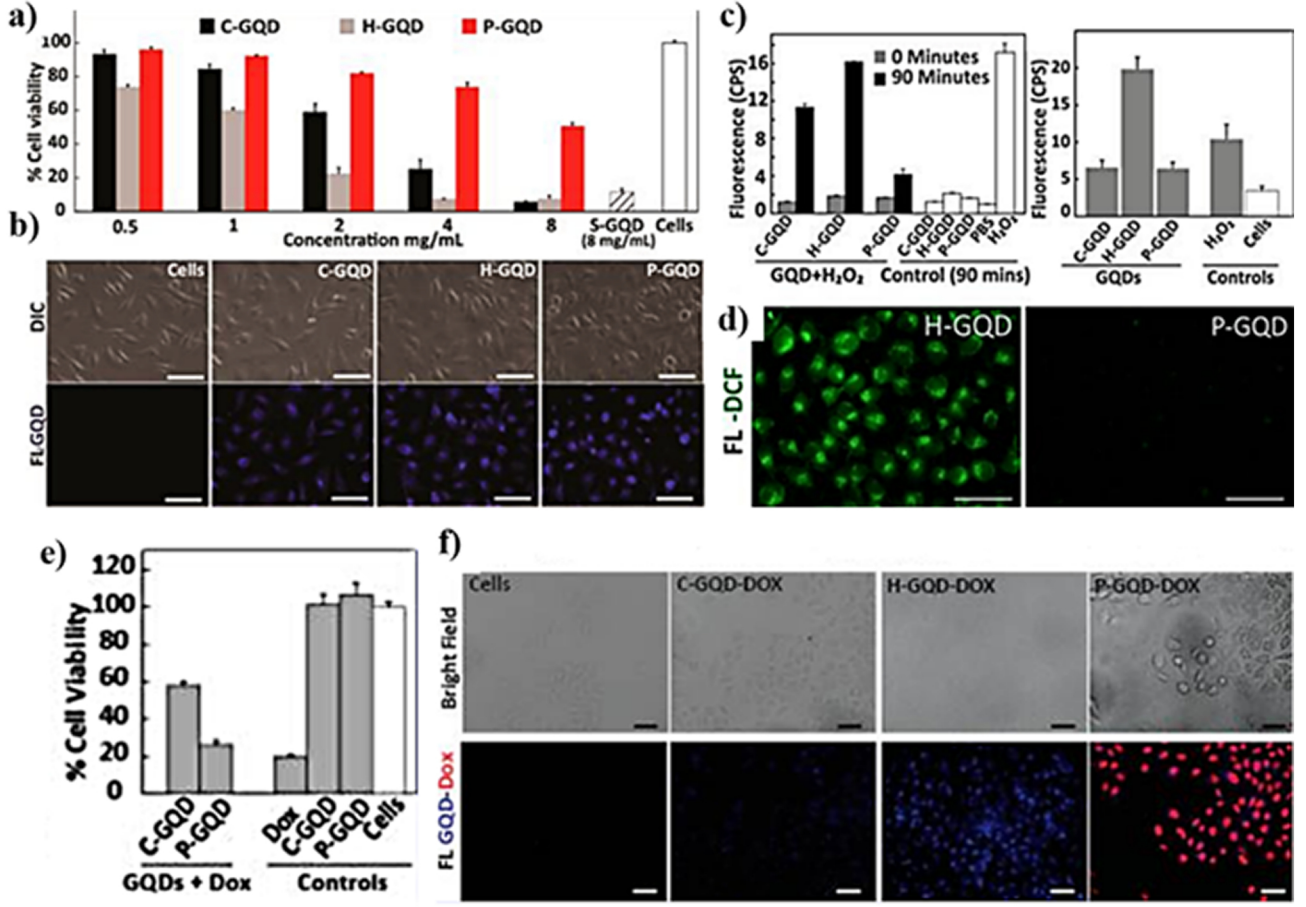
a)
C-GQD
H-GQD
P-GQD
% Cell viability
100
80
60
40
20
0
0.5
1
2
4
8
S-GQD (8 mg/mL)
Cells
Concentration mg/mL
b)
Cells
C-GQD
H-GQD
P-GQD
DIC
FLGQD
c)
0 Minutes
90 Minutes
Fluorescence (CPS)
16
12
8
4
0
C-GQD
H-GQD
P-GQD
C-GQD
H-GQD
P-GQD
PBS
H2O2
GQD+H2O2
Control (90 mins)
20
15
10
5
0
C-GQD
H-GQD
P-GQD
H2O2
Cells
GQDs
Controls
d)
H-GQD
P-GQD
FL -DCF
e)
% Cell Viability
120
100
80
60
40
20
0
C-GQD
P-GQD
Dox
C-GQD
P-GQD
Cells
GQDs + Dox
Controls
f)
Cells
C-GQD-DOX
H-GQD-DOX
P-GQD-DOX
Bright Field
FL GQD-Dox

Figure 16

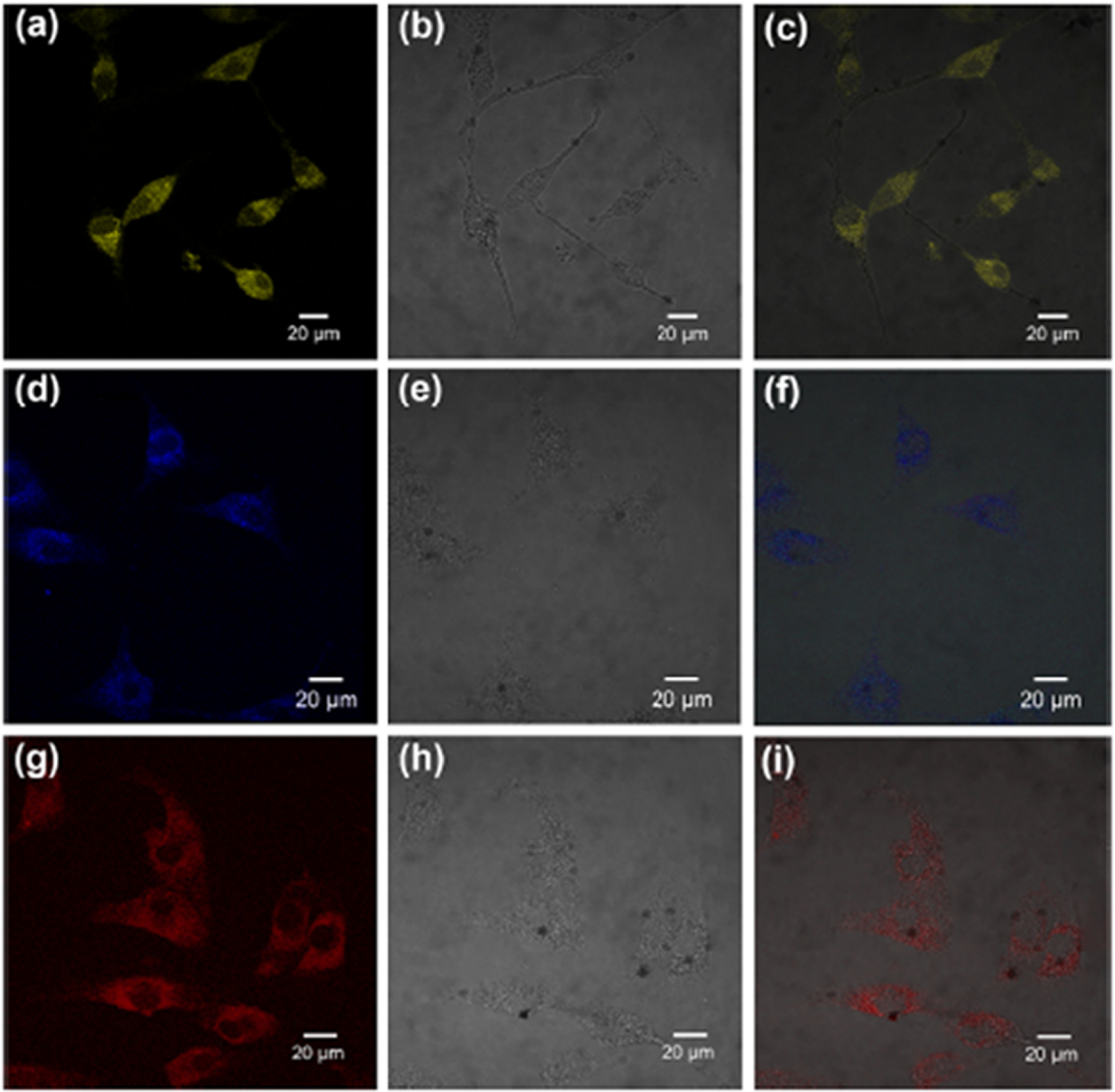


Figure 17

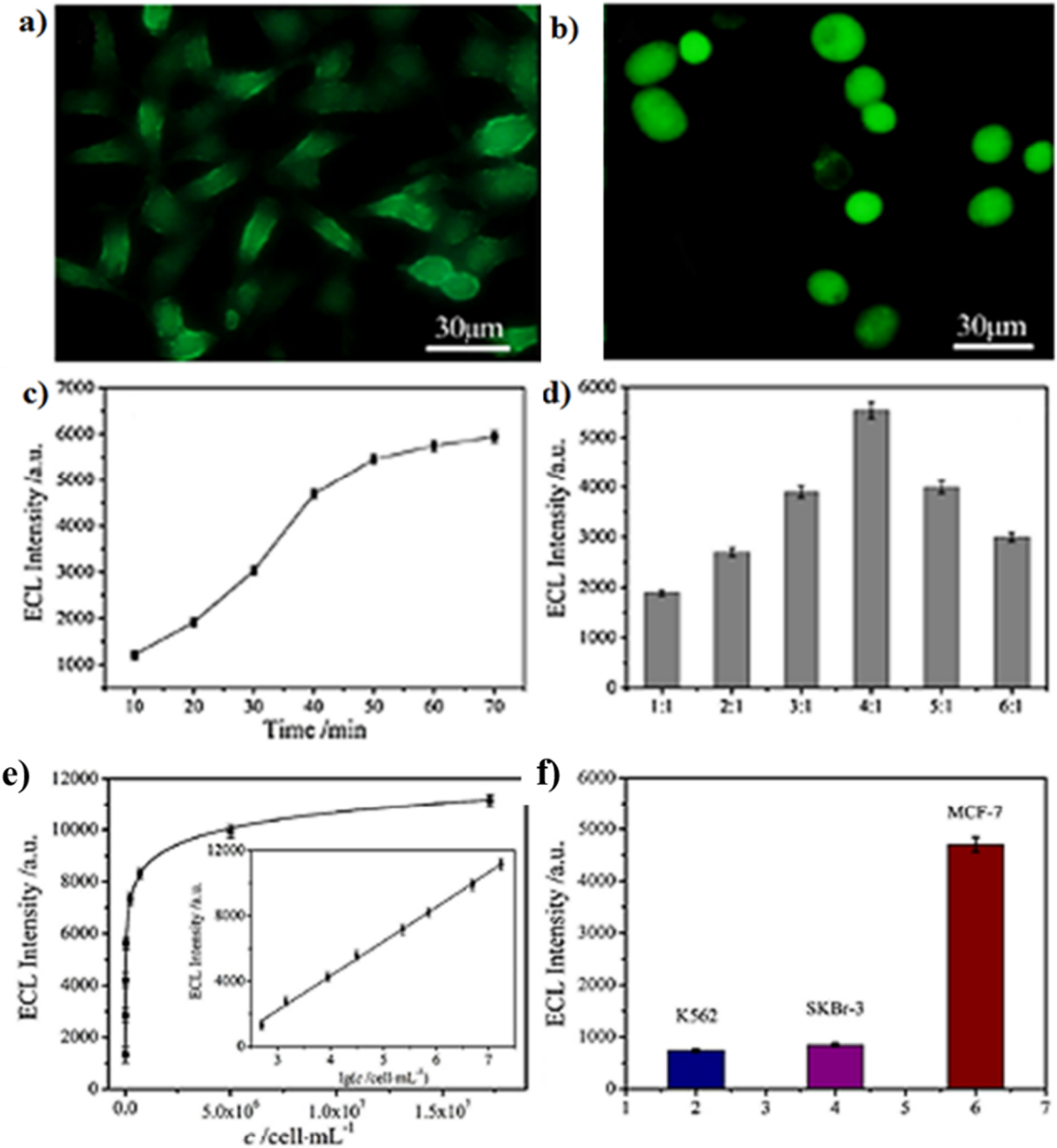
a)
30μm
b)
30μm
c)
ECL Intensity /a.u.
Time /min
d)
ECL Intensity /a.u.
1:1
2:1
3:1
4:1
5:1
6:1
e)
ECL Intensity /a.u.
c /cell·mL-1
f)
ECL Intensity /a.u.
K562
SKBr-3
MCF-7

Figure 18

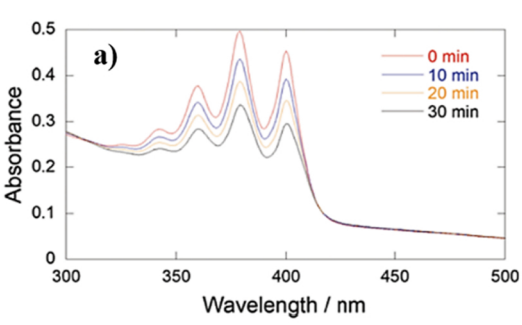
a)
0 min
10 min
20 min
30 min
Absorbance
Wavelength / nm
0.5
0.4
0.3
0.2
0.1
0
300
350
400
450
500

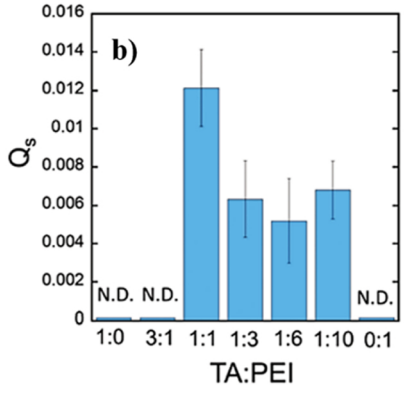
b)
$Q_s$
0.016
0.014
0.012
0.01
0.008
0.006
0.004
0.002
0
N.D.
N.D.
N.D.
1:0
3:1
1:1
1:3
1:6
1:10
0:1
TA:PEI

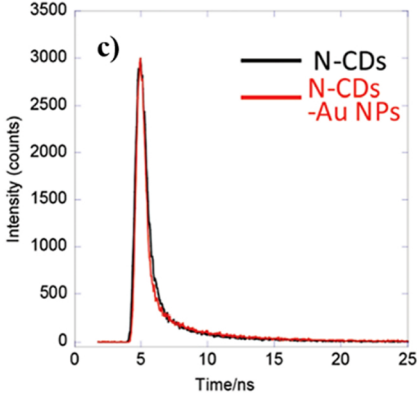
c)
N-CDs
N-CDs
-Au NPs
Intensity (counts)
Time/ns
3500
3000
2500
2000
1500
1000
500
0
0
5
10
15
20
25

Figure 19

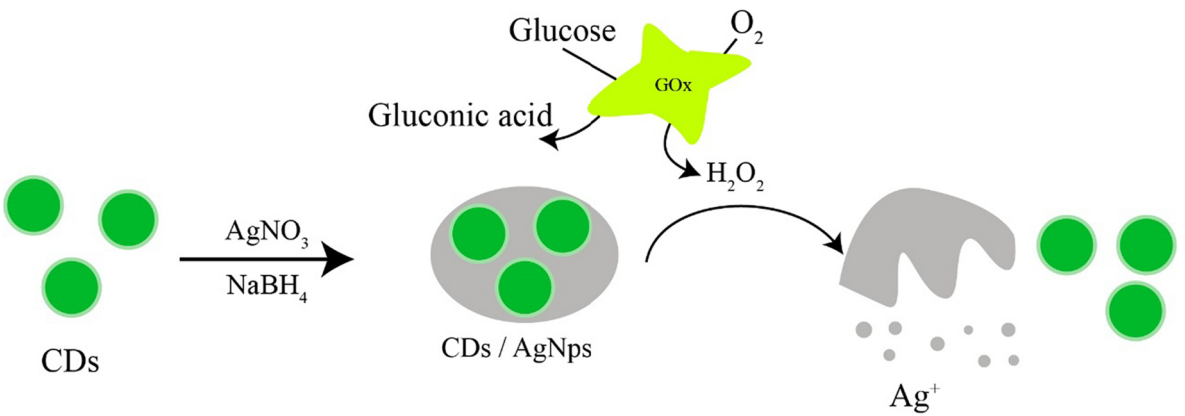
Glucose
$O_2$
GOx
Gluconic acid
$H_2O_2$
$AgNO_3$
$NaBH_4$
CDs
CDs / AgNps
$Ag^+$

Figure 20